

## **Improving the solid-liquid separation of the final tailings at the DPM Krumovgrad plant and evaluation of the process water chemistry effects on flotation (Université de Liège)**

**Auteur :** Rathnayaka Mudiyanse, Pasindu Raviranga

**Promoteur(s) :** Gaydardzhiev, Stoyan

**Faculté :** Faculté des Sciences appliquées

**Diplôme :** Master en ingénieur civil des mines et géologue, à finalité spécialisée en "geométallurgie (EMERALD)"

**Année académique :** 2019-2020

**URI/URL :** <http://hdl.handle.net/2268.2/11297>

---

### *Avertissement à l'attention des usagers :*

*Tous les documents placés en accès ouvert sur le site le site MatheO sont protégés par le droit d'auteur. Conformément aux principes énoncés par la "Budapest Open Access Initiative"(BOAI, 2002), l'utilisateur du site peut lire, télécharger, copier, transmettre, imprimer, chercher ou faire un lien vers le texte intégral de ces documents, les disséquer pour les indexer, s'en servir de données pour un logiciel, ou s'en servir à toute autre fin légale (ou prévue par la réglementation relative au droit d'auteur). Toute utilisation du document à des fins commerciales est strictement interdite.*

*Par ailleurs, l'utilisateur s'engage à respecter les droits moraux de l'auteur, principalement le droit à l'intégrité de l'oeuvre et le droit de paternité et ce dans toute utilisation que l'utilisateur entreprend. Ainsi, à titre d'exemple, lorsqu'il reproduira un document par extrait ou dans son intégralité, l'utilisateur citera de manière complète les sources telles que mentionnées ci-dessus. Toute utilisation non explicitement autorisée ci-avant (telle que par exemple, la modification du document ou son résumé) nécessite l'autorisation préalable et expresse des auteurs ou de leurs ayants droit.*

---



Université de Liège - Faculté des Sciences Appliquées

## Improving the solid-liquid separation of the final tailings at the DPM Krumovgrad plant and evaluation the process water chemistry effects on flotation

Master's Thesis submitted in partial fulfillment of the requirements for the triple Degree of  
« Master en ingénieur des mines et géologues, à finalité approfondie » de l'Université de Liège  
« Master en "Geosciences : Planètes, Ressources, Environnement » de l'Ecole Nationale  
Supérieure de Géologie de Nancy  
« Master's in Geosciences Engineering » of Luleå University of Technology  
Presented by

**Rathnayaka Mudiyanseelage Pasindu Raviranga**

The thesis is confidential - data may only be used with the written consent of the thesis  
Supervisor:

**Professor Stoyan Gaydardzhiev (ULg)**

Academic Year: 2019-2020

## Acknowledgement

First of all, I would like to thank all professors and assistants involved in the EMerald for the continuous sharing of their knowledge, experience, and commitment to the success of the program.

I would like to express my sincere gratitude to the supervisor, Professor Stoyan Gaydardzhiev, for giving me the knowledge and guiding me patiently throughout the Emerald program and the master thesis. His vast knowledge of the subject matters was indeed a great help in completing this project.

Also, abundant appreciation to Dundee Precious Metals Ltd, for the opportunity of the master thesis project and the internship. Also, I would like to thank Anitsa Nikolova, Filareta Uzunova, Iliya Uzunov, and all other staff members who helped me during my stay at DMP Krumovgrad mine.

Also, special thanks go to Ir. Mohamed Aatach, Dr. Hassan Bouzahzah, and to all staff at GeMMe Lab at the University of Liege for the given support to complete my practical works successfully. In addition, I would like to thank Mr. Pierre Jamin from the Department of Hydrology and Environment Geology for providing me the required instrument to succeed in the laboratory works.

Last but not least, my sincere gratitude goes out to my parents and family members for supporting me and encouraging me to pursue my dreams and whole Emerald classmates for lending their support in completing this wonderful journey and being such a nice family throughout the program.

Thank you all ...!!

## Abstract

This study aims to determine the optimum dosages and type of settling aids, which could improve the efficiency of solid-liquid separation, quality of recycled water, and consolidation of thickener underflow. Then, compared the flotation performance with actual process water and the flotation performance with recycled water separated under optimum condition. Furthermore, perform a mineralogical characterization to determine under which form the main minerals, and the gangue mineral phase occurs in the tailing. Then, identify the gangue, which is generating the suspended colloidal particles and their sedimentation behavior and.

The flotation tail at the DPM plant was flocculated in the presence of metal salt, ionic polyelectrolyte (PAM), and their combinations. The optimal dosage and settling aid were determined considering the turbidity of supernatant water and the initial settling rate of the fine particle. Also, the pH optimization tests were carried out using jar tests to determine the pH under which the optimum flocculation takes place. The result shows that the presence of both PAM and  $\text{Ca}(\text{OH})_2$  improved the quality of supernatant water and the initial settling than the single PAM uses in the plant. The optimum pH of the flocculation is between 5.25- 6.0 for all the tested coagulant and flocculant.

A lab-scale study was conducted under the limited condition to investigate the influence of processed water on the flotation of precious metals. These results show that the flotation performance under optimal condition is relatively lower compared to the current flotation performance might be due to precipitation of metals hydroxide on the mineral surface. However, further investigation has to be done under the actual plant flowsheet to see the actual influence.

The mineralogical characterization of tailing was done using SEM, XRD, XRF, and optical microscope. The kaolinite, orthoclase, and quartz are responsible for the generation of most fine particles in  $-20\ \mu\text{m}$  tailing fraction, which reduces the clarity of the recycled water. Also, indicate that there are some gold and electrum associated with the quartz that has lost to the tailing, and the grain size of associate minerals is above  $100\ \mu\text{m}$ , which is not a favourable size for floating. This causes the low recovery of precious metals. Also, about 12 % of identified gold grains in concentrate were associated with quartz and moderately liberated.

In conclusion, the use of a combination of coagulant and flocculant more efficient compared to the use of the only flocculant, and it reduces the daily reagent cost at the plant by approximately 95 USD. Also, finer grinding at the SAG and VertiMill™ mill would also increase the grade of precious metals in the concentrate.

## Table of content

Acknowledgment.....	i
Abstract.....	ii
Table of content.....	iii
List of figures.....	vi
List of Tables.....	ix
1 Introduction .....	1
2 Literature review.....	4
2.1 Geology and the mineralogy of the deposit .....	4
2.2 Recovering method .....	7
2.3 Integrated Mine Waste Facility (IMWF) .....	10
2.4 Dewatering of the tailing.....	12
2.4.1 The settling characteristic .....	12
2.4.2 Effect of slurry concentration on sedimentation.....	15
2.5 Coagulation and flocculation .....	16
2.5.1 Coagulation.....	16
2.5.2 Flocculation.....	21
2.6 Optimization of coagulant and flocculant dossages.....	27
2.6.1 Jar test .....	27
2.6.2 Measurement of initial settling velocity .....	29
2.7 Effect of process water chemistry on flotation .....	30
2.8 Objectives and aim of the work .....	30
3 Methodology.....	33
3.1 Sample preparation and splitting.....	33
3.2 Determination of optimum coagulant and flocculant dosages.....	35
3.3 pH optimization.....	39
3.4 Measurement of settling rate .....	41
3.5 Magotteaux Mill® calibration.....	42

3.6	Flotation trial .....	44
3.6.1	Flotation test with process water from the plant .....	45
3.6.2	Flotation trail with synthetic water .....	46
3.6.3	Simulation of thickener and flotation using recycled water. ....	47
3.7	Automated mineralogy with Scanning Electron Microscope (SEM) .....	48
4	Result and Discussion.....	49
4.1	Mineralogical Characterization .....	49
4.1.1	Optical Microscope Analysis .....	49
4.1.2	XRD result .....	52
4.1.3	Particle size distribution.....	53
4.2	Modal mineralogy and liberation of the ore, concentrate, and tails.....	54
4.2.1	Optimization of coagulant and flocculant.....	58
4.2.2	Effect of coagulant and flocculant on slurry pH.....	63
4.3	pH optimization.....	65
4.4	Settling rate result. ....	67
4.5	Process water characteristics.....	70
4.6	Flotation trials .....	71
5	Conclusions and recommendations .....	74
5.1	Conclusions .....	74
5.2	Recommendation for future work .....	75
6	EIT Chapter .....	76
6.1	Environmentally sustainable mining: The case of integrated mine waste facility (IMWF) .....	76
6.1.1	Process and life cycle of the IMWF.....	76
6.1.2	The social and environmental benefit of IMWF.....	77
6.1.3	Contribution to the circular economy .....	78
6.1.4	SWOT analysis of Ada Tepe project .....	79

6.2	An economical benefit analysis .....	81
7	Bibliography .....	<b>Error! Bookmark not defined.</b>
8	Appendices .....	85
8.1	Appendix 1: Optimization of settling aids .....	85
8.2	Appendix 2: Measurement of settling rate .....	86
8.3	Appendix 3: pH optimization.....	88
8.4	Appendix 4: Flotation trial .....	92

## List of figures

Figure 1: Geological map of Kessebiri dome and Ada Tepe deposit .....	5
Figure 2: 3D view of Ada Tepe deposit (Marchev et al., 2004) .....	6
Figure 3: Crushing and Grinding unit at DPM plant in Krumovgrad.....	8
Figure 4: Flotation and thickener unit at DPM plant in Krumovgrad.....	9
Figure 5: Before and after view of IMWF setting and geometry (H. Garrick et al. 2016).....	10
Figure 6: Left: ongoing tailing facility, right: newly prepared cell for filling .....	11
Figure 7: Effect on solid concentration on the settling rate of the mineral suspension (Besra, Sengupta, and Roy, 2000).....	15
Figure 8: Schematic picture showing destabilization and flocculation of particles (Gregory, 2013) .....	16
Figure 9: Schematic representation of the electric double layer (EDL) on a nanoparticle. Red and blue spheres represent charged species of opposite magnitude. ....	17
Figure 10: Potential energy curves for two particles approaching each other (B. Wills and Napier-Munn, 2006) .....	18
Figure 11: Effect of mono/multivalent metal concentration on the turbidity(a) and settling velocity (b) of kaolin (2018, p. 301) .....	18
Figure 12: The variation of pH (a) and zeta potential (b) coagulant concentrate (2018, p. 303) .....	19
Figure 13: Illustration of "Sweep flocculation" (Gregory, 2013).....	20
Figure 14: Chemical structures of some of common polymer flocculant.....	21
Figure 15: (a) adsorption of polymer and formation of loops available for binding (b) Polymer bridging between particles. (c) Restabilization of colloid particles; (Sharma, Dhuldhoya and Merchant, 2006) .....	22
Figure 16: Illustration of "Electrostatic patch" by highly charged cationic polyelectrolyte .....	23
Figure 17: Adsorption and flocculation by polymers. (J. Gregory, 2013).....	24
Figure 18: Effect of nonionic/anionic/cationic polymer concentration on the turbidity(a) and settling velocity (b) of kaolin.....	25
Figure 19: the variation of the zeta potential of kaolin with polymers.....	25
Figure 20: The effect of optimum dose of PAC (a) and ferric chloride (b) on the removal efficiency of turbidity. (J. Mohammed and E. Shakir, 2018) .....	26



Figure 21: The effect of optimum dose of PAC (a) and ferric chloride (b) on the removal of turbidity with combination of polyelectrolyte (J. Mohammed, and E. Shakir, 2018) .....	26
Figure 22: Standard jar test protocol.....	28
Figure 23: Schematic of the initial settling rate calculation based on the settling results of mudline height(Ji et al., 2013) .....	29
Figure 24: An overview of thickener used at DPM plant .....	35
Figure 25: Jar test set-up used for pH optimization.....	39
Figure 26: View of settling rate measurement set-up .....	41
Figure 27: Basic view of Magotteaux Mill®.....	42
Figure 28: Ball mill calibration curve .....	43
Figure 29: Flotation protocol with process water and synthetic process water .....	44
Figure 30 : Flotation protocol with thickener simulation and recycled water. ....	47
Figure 31: a) Goethite grains (light blue) and possible rutile grain oxidized from pyrite during the oxidation; b) another goethite grain shows the clear result of oxidation as pyrites grain are visible in the middle of the goethite grain. ....	49
Figure 32:a) occurrences of covellite b) native gold and c) native copper in an ore sample...50	
Figure 33:Microscopic view of flotation concentrate consists of pyrite, gold, and graphite...51	
Figure 34:Microscopic view of flotation tailing .....	51
Figure 35:XRD analysis of Ada Tepe ore sample .....	52
Figure 36: XRD analysis of concentrate sample.....	52
Figure 37: XRD analysis of tailing sample.....	52
Figure 38: The granulometry of tailing sample .....	53
Figure 39: Modal mineralogy of ore, concentrate, and two size fractions of tailing.....	54
Figure 40: SEM image of the ore sample indicate the availability of gold (left) and electrum (right) .....	55
Figure 41: SEM image of ore sample indicate the mode of occurrence of electrum and associate minerals. ....	55
Figure 42: SEM image of concentrate sample indicate the mode of occurrence of gold and electrum grains.....	56
Figure 43: Cumulative liberation curves for gold, electrum, kaolinite, Fe-oxide, orthoclase, quartz, and silver by the fraction of ore, concentrate, tailing + 20 $\mu\text{m}$ , and tailing -20 $\mu\text{m}$ ....	57
Figure 44: The effect of optimum dose of PAM on the removal of turbidity .....	58
Figure 45:The effect of optimum dose of $\text{FeSO}_4$ on the removal of turbidity .....	59
Figure 46:The effect of optimum dose of $\text{Al}_2(\text{SO}_4)_3$ on the removal of turbidity.....	59

Figure 47: The effect of optimum dose of $\text{FeCl}_3$ on the removal of turbidity. ....	60
Figure 48: Effect of combining $\text{FeSO}_4$ dose with the different doses of PAM on the turbidity. ....	60
Figure 49: Effect of combining $\text{Al}_2(\text{SO}_4)_3$ dose with the different does of PAM on the turbidity .....	61
Figure 50: Effect of combining $\text{Ca}(\text{OH})_2$ dose with the different doses of PAM.....	61
Figure 51: Graphical representation of settling aids optimization.....	62
Figure 52: Effect of coagulant and flocculant on suspension pH .....	63
Figure 53: Effect of the combination of coagulant and flocculant on suspension pH.....	63
Figure 54: Effect of slurry pH on solid-liquid separation efficiency with different coagulant and flocculant (after 10 minutes) .....	65
Figure 55:: Effect of slurry pH on solid-liquid separation efficiency with different coagulant and flocculant (after 20 minutes) .....	65
Figure 56: Summary of settling rate measurement .....	68
Figure 57: View of Sedimented Sludge with (a) 20 mg/ l(b) 24 mg/l (c) 28 mg/l (d) 32 mg/l of flocculant (PAM) .....	69
Figure 58: View of sedimented sludge with (a) 28mg/l of PAM + 500 mg/l of $\text{Ca}(\text{OH})_2$ ; (b) 28mg/l of PAM + 750 mg/l of $\text{Ca}(\text{OH})_2$ ; (c) 28mg/l of PAM +1000 mg/l of $\text{Ca}(\text{OH})_2$ .....	69
Figure 59: Height of sedimented sludge of tailing with PAM+ $\text{FeSO}_4$ , PAM+ $\text{Ca}(\text{OH})_2$ , and PAM+ $\text{Al}_2(\text{SO}_4)_3$ .....	69
Figure 60: Grade recovery relationship for the precious metals in each flotation trial .....	72
Figure 61: Comparison of grade and recovery of precious metals in five flotation trials. ....	73
Figure 62: View of sedimented sludge after pH optimization with PAM+ $\text{Ca}(\text{OH})_2$ at pH 4.63 , 4.92, 5.59, 6.17, 6.37 , 6.71 in order .....	88
Figure 63: : View of sedimented sludge after pH optimization with PAM+ $\text{FeSO}_4$ at pH 4.43 , 4.99, 5.46, 5.91, 6.35 , 6.86 in order .....	89
Figure 64: : View of sedimented sludge after pH optimization with PAM at pH 4.61 , 5.07, 5.59, 6.06, 6.45 , 6.89 in order .....	89
Figure 65: : View of sedimented sludge after pH optimization with $\text{FeSO}_4$ at pH 4.67 , 4.91, 5.47, 5.97, 6.61 , 7.15 in order .....	90
Figure 66: View of sedimented sludge after pH optimization with $\text{Al}_2(\text{SO}_4)_3$ at pH 4.45 , 5.07, 5.45, 6.01, 6.61 , 7.15 in order .....	91
Figure 67: View of sedimented sludge after pH optimization with PAM+ $\text{Al}_2(\text{SO}_4)_3$ at pH 4.69 , 5.12, 5.59, 5.83, 6.51 , 7.01 in order .....	92

## List of tables

Table 1: Operational parameters of Magotteaux Mill®.....	42
Table 2:The reagent and dosages used in flotation trial .....	45
Table 3: The chemical used for synthetic water preparation .....	46
Table 4: Summary of settling aids optimization. ....	62
Table 5: Initial settling rates of flocs with different coagulant, flocculant and their combination.....	67
Table 6: Chemical analysis of Process water, Tailing thickener overflow, and concentrate thickener overflow. ....	70
Table 7: Grade and Recovery of Au and Ag from the performed flotation trial .....	71
Table 8: Daily operational cost comparison between two methods. ....	81
Table 9:Jar test result using PAM as a flocculant.....	85
Table 10: Jar test result using $\text{FeSO}_4$ as a coagulant .....	85
Table 11: Jar test result using $\text{Al}_2(\text{SO}_4)_3$ as a coagulant .....	85
Table 12: Jar test result Using $\text{FeCl}_3$ as a coagulant.....	85
Table 13: Jar test result using combination of PAM and $\text{Al}_2(\text{SO}_4)_3$ .....	85
Table 14: Jar test result using combination of PAM and $\text{FeSO}_4$ .....	86
Table 15: Jar test result using combination of PAM and $\text{Ca}(\text{OH})_2$ .....	86
Table 16: Mudline height measurement result.....	86
Table 17: pH optimization result with PAM+ $\text{Ca}(\text{OH})_2$ .....	88
Table 18:pH optimization result with PAM+ $\text{FeSO}_4$ .....	88
Table 19: pH optimization result with PAM.....	89
Table 20:pH optimization result with $\text{FeSO}_4$ .....	90
Table 21:pH optimization result with $\text{Al}_2(\text{SO}_4)_3$ .....	90
Table 22:pH optimization result with PAM+ $\text{Al}_2(\text{SO}_4)_3$ .....	91

# 1 Introduction

Mining activity has significantly increased due to worldwide demand for mineral resources, which has been created by high population growth and their needs (Reichl et al., 2016). Simultaneously, the environmental risk associated with the mining activity has become a growing challenge for all of the companies within the sector. As per the European Union (EU) sources, waste from mining and processing of mineral resources is considered as one of the largest waste streams in the EU (European Commission, 2020). It means that mining and milling activities are very often disruptive to the environment and, for a long time, without evaluation of impacts. Therefore, nowadays, the regulation and concerns about environmental impact and remediation of mining activities are strict, and the Environment Impact Assessment (EIA) procedure to identify the potential effect and damages caused by developments in the environment and society is essential before the commencement of any project. The social demand has increased over the years for the sustainable development of all of the activities related to mining, including the management of waste products during each phase of the mining process, including exploration, processing, transport, and treatment of residual (Fernando and Carvalho., 2017). The waste generated by the mining industry is topsoil, overburden, waste rock, temporary stockpile, and mostly the tailing from the process. Therefore, these wastes must be strategically treated and managed to integrate economic efficiency and social demand for environmental sustainability.

Dundee Precious Metals (DPM) flotation plant located in Krumovgrad, Bulgaria, currently processes more than 0.85 million of ore per year to recover gold and silver using stage flotation reactor (SFR) technique. In the flotation plant, a large amount of tailing (average of 100 t/h), which consists of slurries in the form of water, ultrafine clay particles, and inorganic ions are pumped into a thickener where solid/liquid separation takes place. The separation mainly occurs by sedimentation where the coarse fraction of solids quickly settles while fine fraction takes a long time to settle, which ultimately reduces the efficiency of the separation (Yin Zhi-gang et al. .2018). The thickened material is then pumped into an Integrated Mine Waste Facility (IMWF), while recycled water returns to the processing plant. Due to the shortage of freshwater and environment and social issues for disposal of tailing, much attention on high efficiency/high clarity of solid-liquid separation of tailing has been paid by mining companies worldwide using a variety of methods and techniques throughout the decades. The high efficiency of solid-liquid separation increases the quality of the recycled water, which is re-used for processing and reduces technical and economic difficulties in handling, dispose, and

water removal of final tailing. Nowadays, mineral processing is considered as one of the most intensive water-consuming processes (Boujounoui et al.,2015)

In the DPM plant, the situation is more challenging due to the generation of a large number of ultrafine particles, which cause dewatering problems, including low settling rate, poor supernatant clarity, low consolidation rate of thickened material in Integrated Mine Waste Facility (IMWF). As a result, the company faces two major problems. The first is that the time to construct a new tailing cell over the bottom cell as it takes a long time to reach the required consolidation condition in the bottom cell. The second is that the low quality of recycled water, which can negatively affect on floatation process, thereby decrease the grade and recovery in concentrate. Therefore, in industrial applications, the pre-agglomeration of colloidal particles is required to make sure that all the fine particles are settled.

The Integrated Mine Waste Facility (IMWF) of DMP Krumovgrad is an innovative design that is being built using both waste rock and thickener underflow. The waste rock is used to provide the structural basis of the facility with a honeycomb structure of tailings cells that fill the valley. The facility design incorporates a basal drainage system, capturing flow to the base of the two main valleys and directing water to contact water capture sumps at the toe of the facility. The objective of the design is to reduce the footprint both of the overall mine site and the waste facilities, in comparison to two separate facilities, and to allow the IMWF to be sited in an area of very steep, rocky terrain. The waste rock will provide strength for design stability and allow infiltrating rainwater and tailings drain-down water from consolidation to drain freely. However, the IMWF is sited in a steep valley close to a sensitive alluvial aquifer used for drinking water supply and an upland river, rendering the site setting highly sensitive in respect to the potential risks posed to surface water and groundwater quality.

This study describes the approach which was used at DPM Krumovgrad to determine the optimum dosages and type of settling aids, which could improve the efficiency of solid-liquid separation, quality of recycled water, and consolidation rate of thickened material. Then, a comparison of current flotation performance and the performance after using recycled water which has been separated under optimum condition obtained by the experiments. Finally, to correlate the mineralogical characteristics of the ore body and the setting behavior of the fine particles in the tailing was an objective. In addition to that, investigation of the effect of clay mineral on gold flotation was reviewed. The set of jar tests and lab-scale flotation tests were mainly carried out to determine the optimum condition and effect of water chemistry on

flotation performance. The mineralogical characterization of tailing was done using SEM, XRD, XRF, and optical microscope. The particle size distribution was analyzed by DMP external laboratory in Thessaloniki, Greece.

## 2 Literature review

### 2.1 Geology and the mineralogy of the deposit

The Ada Tepe is a typical low-sulfidation epithermal gold deposit, unusual in that it is hosted mostly in Maastrichtian-Paleocene sedimentary rocks and does not show a direct relationship to local magmatic activities. A regionally extended low-angle normal fault separates the consolidated sedimentary formation and underlying metamorphic rocks with dips of 10°-15° to the north-northeast (Figure 1). This detachment was named as Tockachka detachment fault (TDM) in a Ph.D. thesis by Bonev in 1996. The hanging wall mostly consists of conglomerates, sandstone, breccia, argillaceous limestone, and metamorphic blocks within the area. The total thickness of the sedimentary formation is around 350m along the Kal-djic river, near the Shavar village. As mentioned above, the TDM is the major domain structure along the western slope of Ada Tepe hill, which has been identified as a contact between Paleozoic metamorphic rocks and Maastrichtian-Paleocene sedimentary rocks of the Shavaro Formation. According to the result of the outcrop and drill core sampling campaign, the occurrence of 0.5 m to 20 m thick massive silicification zone(wall) has been identified just above the detachment fault. Beneath the detachment fault, a 10-20 cm thick layer of tectonic clay, Gneiss, magmatic, marble, and the amphibolite of the metamorphic basement has been identified.

The wide-angle, NW-SE oriented fault cuts the southwestern slope of the Ada Tepe, forming a small half-graben filled with sedimentary rocks of the older Maastrichtian-Paleocene syndetachment. Younger Priabonian-Oligocene sedimentary rocks overlay them in the eastern part. Besides that, several E-W and N-S oriented sub-vertical faults separated by a zone of silicification, occurs to the south, east, and west of the deposit. These faults have coincided with the major direction of the mineralized veins in the sedimentary covers and can be interpreted as feeder structures for the mineralizing fluids (P. Marchev et al. 2004)

The gold mineralization of the deposit occurs primarily in two zones; a massive, tabular body located just above the detachment fault, and the open space along east-west oriented sub-vertical listric fault consisting of breccia-conglomerate. The tabular massive is formed as a result of multiple periods of silicification and veining events. In the beginning, the original rock above the detachment fault has been replaced by massive white to light grey silica. And it is surrounded by carbonate cutting and quartz veins, which were commonly veined by sub-vertical banded veins or brecciated and cemented by calcite, sugary quartz or pyrite.

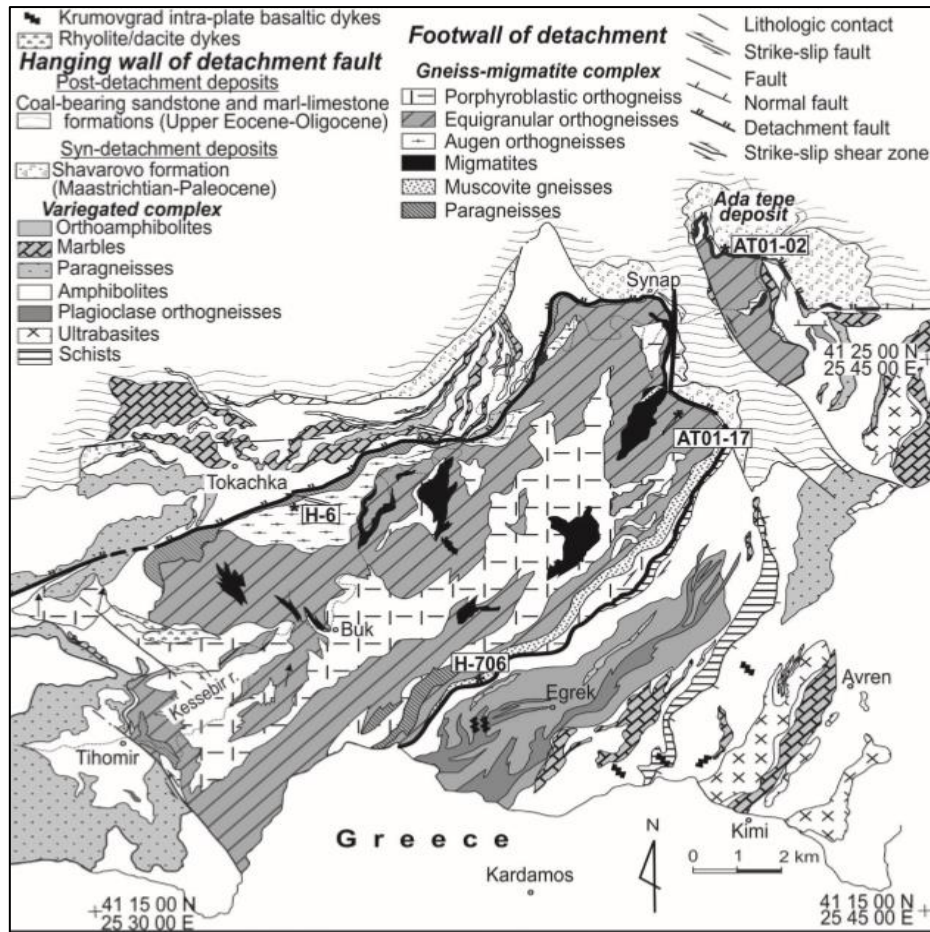


Figure 1: Geological map of Kessebir dome and Ada Tepe deposit

The mineralogy of the Ada Tepe deposit is a simple, consisting mainly of electrum with the trace of galena, gold-silver tellurides. Gangue mineral consists of silica polymorphs (microcrystalline, fine-grained, sugary quartz, and opaline silica), various carbonates such as calcite, dolomite, ankerite, and siderite. The composition of the electrum is 73-76%, Au. The mineralization of banded vein above the wall has further classified into four stages based on the relationship of quartz and carbonate veins, mineralogy, texture, and gold grades (P. Marchev et al. 2004)



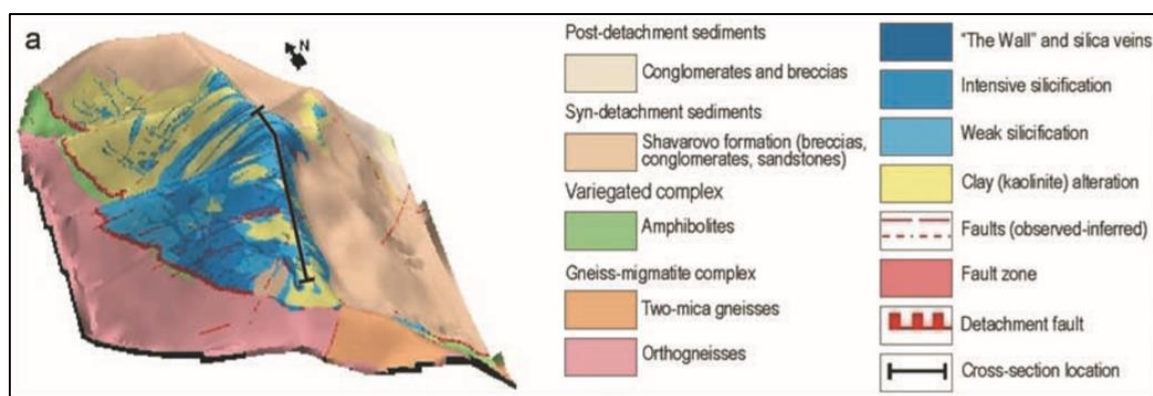


Figure 2: 3D view of AdaTepe deposit (Marchev et al., 2004)

The earliest stage was the deposition of microcrystalline to fine-grained grayish to white massive or banded quartz with rare pyrite and adularia, which has filled in the host rocks near the margin of the vein or rock fragments in the wall replacing the existing minerals. The second stage mineralization consists of a millimeter-scale band of opaline or microcrystalline where an electrum rich band commonly occurs toward the bottom of the bands and some electrum along the boundary of the first and third stages. The size of electrum grains ranges from less than 1 to 20  $\mu\text{m}$ . A deposition of sugary quartz followed by a band of quartz and bladed calcite, and finally by massive calcite with a small amount of quartz, is the main characteristic of the third stage. The last stage mineralization consists of pinkish ankerite-dolomite and siderite, which was formed by the precipitation of massive pyrite in some parts of the deposit. (P. Marchev *et al.* 2004)

Most of the pyrite within the uppermost of the deposit has been converted into limonite identified as goethite and kaolinite due to the oxidation by the supergene process. The depth of the oxidation zone varied upon the intensity and the direction of the faults because these faults and fractures acted as a conduit for surface water to reach the impermeable silicified zone, forming the oxidized zone above the wall. However, there is no oxidation in the wall due to extensive silicification. The alteration of the deposit consists of chlorite, calcite, kaolinite, and subordinate albite, pyrite, and ankerite-dolomite (P. Marchev et al. 2004).

## 2.2 Recovering method

The Processing plant of DMP Krumovgrad has been designed with the treatment rate of nominal 0.85 to 1.1 Mtpa of the mixture of the siliceous wall and the brecciated Upper Zone ore with an average feed grade of 4.5g/t Au. The flowsheet mainly consists of primary crusher, Semi-Autogenous Grinding (SAG) mill, ball mill, and fine grinding VertiMill™ mill followed by different stages of froth flotation to produce Au and Ag bearing concentrate for shipment to a smelter. The tailing is thickened to a paste of 55-56 wt% and disposed in the Integrated Mine Waste Facility (IMWF) along with waste rock from the mine.

Primary crushing is done using a primary jaw crusher to reduce the particle size +200 up to P80 of 125mm. Both crushed and screened material (-200 mm) before the primary crushing stage are collected into a coarse ore bin with a capacity of 4400 tones before it is transferred to the SAG Mill grinding.

SAG Mill circuit is operated in open circuit mode. The material from the coarse ore bin is transferred to the mill with additional water supply to maintain the slurry density of 65 wt.% in the mill. The amount of water that needs to be added is calculated based on the moisture content of feed material measured on the belt scale reading. The SAG mill overflow discharges through a trommel, which has a 12mm opening where fine product passes to the SAG Mill classification cyclone feed. At the same time, the +12 mm material contains a “critical size” pebble that is processed through SAG Mill recycle cone crusher that discharge ground material back to SAG Mill feeds for additional attrition. The tramped steel in an oversize fraction is removed using an overhead belt magnet before it is transferred to the pebble crusher. The SAG Mill classification cyclones are designed to make a size separation with an overflow product size P80 of 150µm. The SAG Mill classification cyclone overflow passes onto the VertiMill™ feed trash screen through a metallurgical sampler and a size sampler and into the VertiMill™ cyclone feed sump. The VertiMill™ cyclone is designed to make a size separation product P80 of 30µm as a requirement of the flotation process. The VertiMill™ cyclone underflow is sent through two VertiMill™ mills, and the discharge product is mixed in the VertiMill™ cyclone feed sump for re-classification. The flotation reagent sodium silicate and copper sulfate are mixed inside the VertiMill™ mill. (Bennett *et al.*, 2014). The flowsheet of the crushing and grinding unit at the DPM plant is shown in Figure 3.

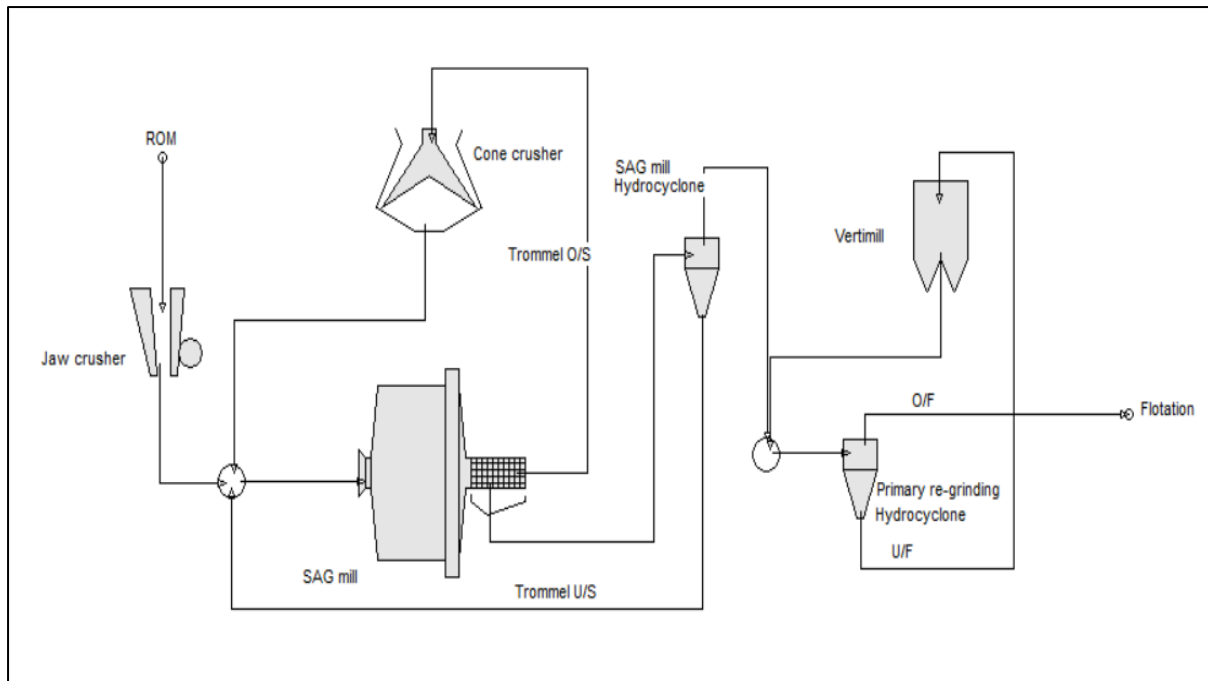


Figure 3: Crushing and Grinding unit at DPM plant in Krumovgrad

The VertiMill™ overflow passes through an on-line particle size analyzer to determine the PSD of flotation feeds. Then, it flows into a rougher conditioning tank where flotation collector; Potassium Amyl Xanthate (PAX); and activator (Aeroflot 208) are mixed with the slurry followed by addition of frother; Methyl Isobutyl Carbinol (MIBC). The conditioning tank is agitated at an appropriate speed. The conditioned slurry flows into each cell with a 70 cubic meter volume. The total nominal residence time in the rougher bank is 35 minutes. Froth concentrate is sent for regrind classifier circuit consisting of cyclone cluster and tertiary grinding unit where the overflow of cyclone containing fine material (P80 of 15µm) flows to cleaner flotation bank consisting of 2 tank flotation cells and underflow is re-grind using VertiMill™ mill with the 2mm of grinding media to achieve the target product size (White et al. 2014)

The overflow slurry of a re-grind classifier is mixed with more PAX and MIBC before the cleaner flotation stage and flows to the cleaner flotation tank. The concentrate of cleaner flotation is sent to concentrate thickener followed by filtration, bagging, and shipment as final product grade of 200g/t Au. The tailing from the cleaner flotation flows to a cleaner-scavenger flotation bank consisting of 5 flotation tank cells where tailing flows back to the rougher flotation stage and concentrate flows to the final cleaner stage flotation bank consists of 4 tanks of flotation cells. The concentrate of the final cleaner stage is sent to concentrate thickener

The discharge tailing from the scavenger flotation bank is pumped to a deep cone thickener where it will be thickened up to 62 wt.% of solids, and the underflow is pumped out to the IMWF. The thickener overflow water is returned to the reclaim water tank in the concentrator. Settling aid: flocculant will be prepared with a concentration of 0.04% and stocked in a storage tank. Later, the stock solution is mixed with thickener feed before it is transferred to the cone thickener. Current dosages of flocculant are varied from 74 g/t to 117 g/t depending on the concentration of clay particles in the slurry (White *et al.* 2014).

### 2.3 Integrated Mine Waste Facility (IMWF)

The IMWF is constructed of a series of waste rock cells within two valleys incorporate with basal underdrain system for bleed or surface water collection that will lead to two separate sumps (North and South). Drain water from north and south parts of the IMWF will report to either sump. Water from the south sump pump will discharge into the north sump. Water from the north sump pump will report to the main collection sump. The IMWF received both waste rock and thickened tailing where waste rock is used to build the cell structure, and thickened tailing is used to fill the cell. Once a cell of one valley is filled, thickened tailing is directed to the newly prepared cell of other valley and leave the north cell for about 25 days to achieve a required consolidation strength. After consolidation is achieved, the next cell is built on top of the consolidated bottom cell using mine waste before the ongoing north cell is filled to redirect the tailing to a new build top cell. Likewise, two valleys are filled alternatively step by step upward. Therefore, the consolidation rate of the thickened tailing is one of the critical factors to be considered as it could improve the efficiency in terms of time consumption and maintenance cost. The objective of the design is to reduce the footprint of both of the overall mine site and the waste facilities. (H. Garrick et al. 2016) and by the end of mine closure, it has to look like a part of the mountain as shown in Figure 5

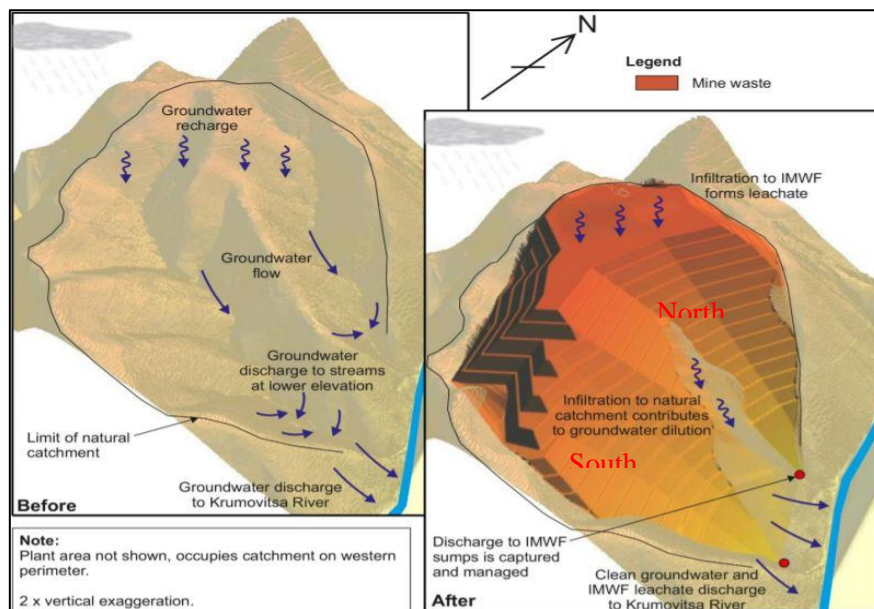


Figure 5: Before and after view of IMWF setting and geometry (H. Garrick et al. 2016)



Figure 6: Left: ongoing tailing facility, right: newly prepared cell for filling

## 2.4 Dewatering of the tailing

Dewatering of tailings is a crucial factor in the mineral processing industry due to two main reasons; it increases the solid percentage of tailing that is being transferred to the final tailing reservoir, thus reducing the space requirement as well as the stability of the reservoir. Also, supernatant water from the dewatering process can be used in the extraction process to reduce freshwater intake. Even though the dewatering process of concentrate is a combination of three main dewatering methods consisting of sedimentation, filtration, and thermal drying as concentration must deliver relatively dry concentrate for shipment. The dewatering of tailing is mostly done by gravity sedimentation. However, sedimentation is highly effective when there is a large density difference between liquid and solid (B. Wills and Napier-Munn, 2006, p. 378). The main parameters to be considered in sedimentation are turbidity of supernatant water and settling rate of suspended particles

The thickener is widely used in the processing industry for sedimentation of suspension particles and the sedimentation of slurry mainly depends on several primary properties. They are particle size and distribution, shape, density, solid/liquid ratio surface, pH, and presence of chemical additives (Besra, Sengupta, and Roy, 2000).

### 2.4.1 The settling characteristic

The settling rate of particles is mainly governed by Stokes' or Newton's laws, depending on the particle size (Stokes' law < 50  $\mu\text{m}$  and Newton's law > 0.5 mm) and density of the particles and it has been explained with several mathematical expression as shown in following paragraphs (B. Wills and Napier-Munn, 2006)

For these studies, the main assumption is that all particles are spherical with diameter  $d$  and density  $D_s$ , which fall under gravity in a viscous fluid of density  $D_f$  under free-settling conditions, i.e. ideally in a fluid of infinite extent. The particle is acted upon by three forces: a gravitational force acting downwards, an upward buoyant force due to the displaced fluid, and a drag force  $D$  acting upwards. The equation of motion of the particle is

$$mg - m'g - D = \frac{m}{g} \frac{dv}{dt} \quad (1)$$

where  $m$  is the mass of the particle,  $m'$  is the mass of the displaced fluid,  $v$  is the particle velocity, and  $g$  is the acceleration due to gravity. When the terminal velocity is reached,

$\frac{dv}{dt} = 0$ , and hence

$D = (m - m')g$ . Therefore

$$D = \left(\frac{\pi}{6}\right)gd^3(D_s - D_f) \quad (2)$$

where  $d$  is the diameter in the case of a sphere, and for other shapes, this gives equivalent stokes diameter. Stokes assumed the drag force on a spherical particle to be entirely due to viscous resistance and deduced the expression

$$D = 3\pi d\eta v \quad (3)$$

where  $\eta$  is the fluid viscosity, and  $v$  is the terminal velocity, Hence, substituting in equation 2

$$3\pi d\eta v = \left(\frac{\pi}{6}\right)gd^3(D_s - D_f)$$

and

$$v = \frac{gd^2(D_s - D_f)}{18\eta} \quad (4)$$

This expression is known as Stokes' law. Newton assumed that the drag force was entirely due to turbulent resistance, and deduced:

$$D = 0.055\pi * d^2 * V^2 * D_f \quad (5)$$

Substituting in equation 2 gives

$$v = \sqrt{\frac{3gd(D_s - D_f)}{D_f}} \quad (6)$$

This is Newton's law for turbulent resistance. Furthermore, Stokes' law (4) for a particular fluid can be simplified to

$$V = k_1 d^2 (D_s - D_f) \quad (7)$$

and Newton's law (6) can be simplified to

$$V = k_2 \sqrt{d(D_s - D_f)} \quad (8)$$

where  $k_1$  and  $k_2$  are constants, and  $(D_s - D_f)$  is known as the effective density of a particle of density  $D_s$  in a fluid of density  $D_f$ . Both laws show that the settling velocity of a particle in a fluid is directly proportional to particle size and density. However, actual particle settling velocities will be lower than those predicted by Eq. (6) due to non-spherical particle shapes and, at increasing particle concentrations, hindrance effects from the neighboring particle. Stoke's law is widely used as a basic approximation to describe particle settling in stagnant media, such as tailings impoundments. (C. Wang et al. 2014).



According to Stock's law, gravity sedimentation is usually ineffective and destabilization of the suspended solids by aggregation is often necessary at first. Then, natural accelerated settling will occur after particle aggregation, followed by the densification of the settled solid sediments. At the industrial level, the settling rate is improved by mechanical mixing, combined with the coagulation and flocculation using coagulant and flocculant to reduce the interaction energy barrier, which is described under subtopic 2.6.1.

#### 2.4.2 Effect of slurry concentration on sedimentation

Some past studies by Besra, Sengupta, & Roy (2000) have investigated the effect of solid concentrate on settling rates of kaolinite, quartz, and calcite. According to the result presented in Figure 7. It is observed that the settling rate is higher for low concentration solid compared to those at high solid concentrate.

As the number of suspended solids increases, there occurs a marked decrease in settling rate up to a certain initial solid concentration, after which the decrease is gradual. The decrease in the settling rate with solid concentration is more pronounced in the case of kaolin and calcite compared to quartz. Such a decrease in the settling rate is attributed to the interference by surrounding particles. A previous study (T.Tadros, 2011) has explained how solid concentration can alter the rheological properties of the slurry, which strongly depends on the net interaction between particles.

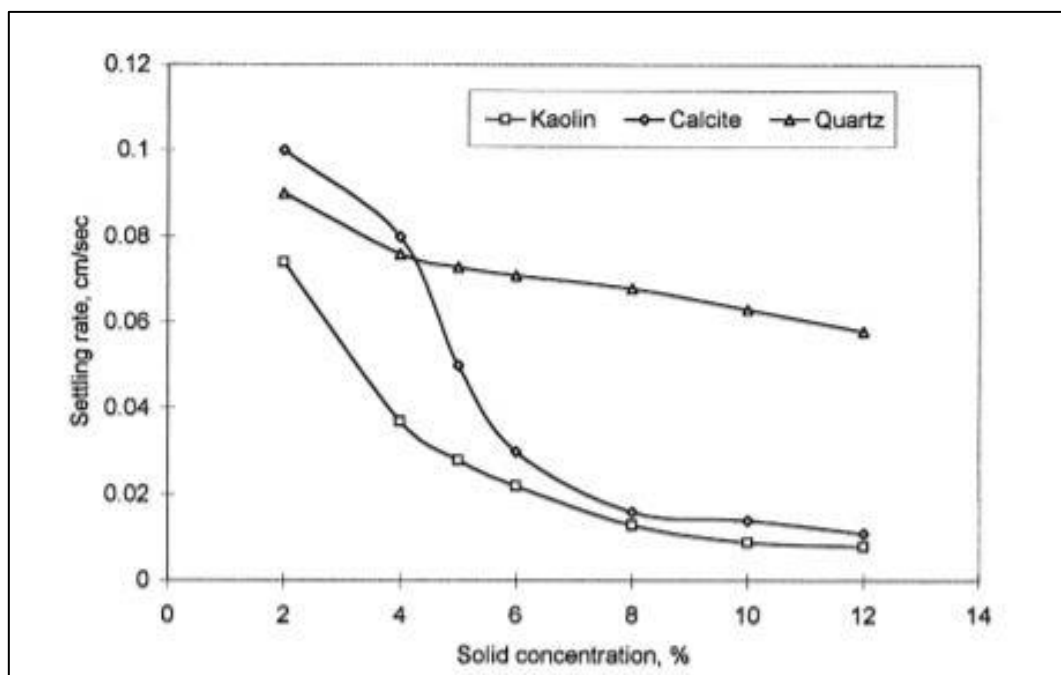


Figure 7: Effect on solid concentration on the settling rate of the mineral suspension (Besra, Sengupta, and Roy, 2000)

## 2.5 Coagulation and flocculation

In an aqueous system, interparticle repulsion is the most common reason for fine particle (Colloidal) stability, but other types of interaction are also important. With stable suspension, no agglomeration occurred until the suspension has been destabilized so that repulsion between particles is reduced and attachment becomes possible. Even though the destabilization can be achieved by a physical method such as heating or cooling, in practical situations, a chemical change is required. A change in pH also causes destabilization (J.Gregory, 2013). There are two main steps in the typical agglomeration process; (a) destabilization (neutralization) are, (b) attachment, as shown in Figure 8. These two steps occur in successive steps called coagulation and flocculation, which allow particles to collide each other and growth of flocs (Mukheled and Al-Sameraiy. 2017).

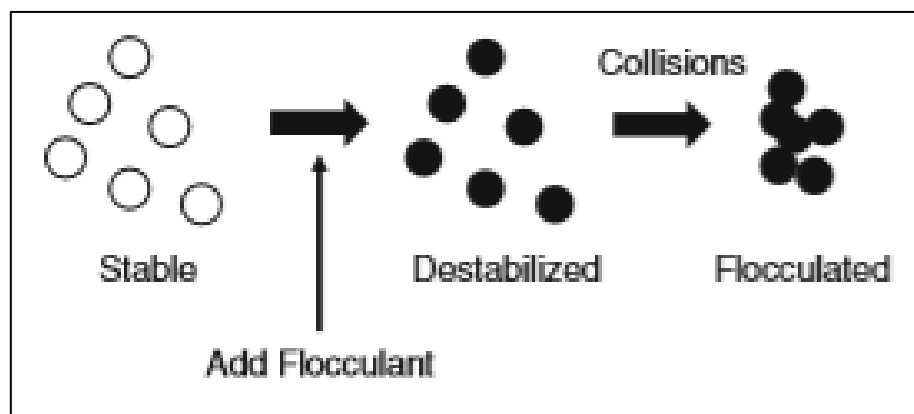


Figure 8: Schematic picture showing destabilization and flocculation of particles (Gregory, 2013)

### 2.5.1 Coagulation

The coagulation is neutralization of suspended particles with an electrolyte having an opposite charge to the particles. All suspended particles have mutual attraction forces, known as London- Van der Waals' forces, which are effective only at very close range. Generally, the attraction due to these forces is prevented by a repulsive force caused by the overlap of electric double layers surrounding the neighboring particles, thus preventing the agglomeration. These double-layer forces are both material and solution dependent (electrolyte type, concentrate, and pH) (C.Wang et al., 2014) These repulsive forces not only prevent agglomeration of particles but also settling behavior by keeping them in motion. Figure 9 shows a general model of the electrical double layer at the surface of a particle (N. Moss. 1978). It shows the formation of the bound layer of positive ions due to the attractive force of negatively charged ions on the particle surface and the diffuse layer of counter ions decreasing in concentration with

increasing distance until the solution equilibrium concentration is achieved. When a particle moves in the liquid, there is a shear between the bound layer, which also moves with the particle. The potential at the plane of shear is known as the zeta potential. The magnitude of the zeta potential depends on the surface potential and the concentration and charge of the counter-ions. The repulsive forces between two particles can be reduced, decreasing the surface potential of the fine solid, and it can attain a surface potential through a different mechanism in an aqueous environment. Especially, by isomorphous substitution, where structural cations such as  $\text{Si}^{4+}$  and  $\text{Al}^{3+}$  are replaced by dissolved cations of equal or lower valence (e.g.,  $\text{K}^+$ ,  $\text{Mg}^{2+}$ , and  $\text{Al}^{3+}$ ) which ultimately results in a net negative charge on the basal surface changing the zeta potential. (C. Wang et al. 2014).

Since the zeta potential of particles is a function of both pH and coagulant concentration of the suspension and the pH at which coagulation occurs is one of the most important parameters for proper coagulation. Therefore, the optimum pH value at which the optimum coagulation takes place must be determined before industrial uses.

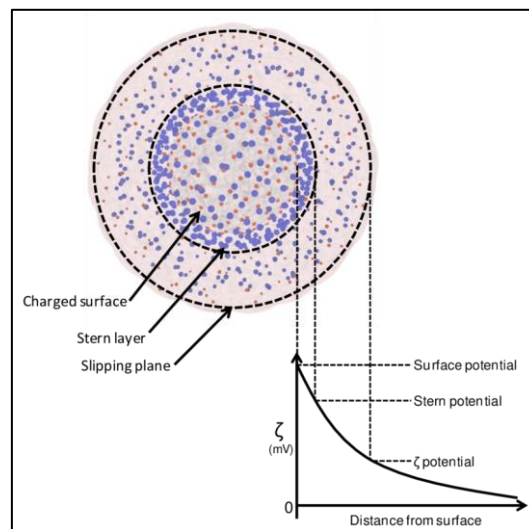


Figure 9: Schematic representation of the electric double layer (EDL) on a nanoparticle. Red and blue spheres represent charged species of opposite magnitude.

The magnitude of the repulsive and attractive force acting on two suspended particles concerning the distance between particles is shown in Figure 10 for two spheres experiencing van der Waals and double-layer interaction. According to the graph, when two suspended particles are approaching each other, an energy barrier to the primary minimum, which corresponds to a strong increase in aggregation, can be observed. In addition, secondary energy minimum can also be observed before the energy barrier, which results in weak and reversible aggregation.

The magnitude of the energy barrier is directly correspondent to the stability of the dispersion in an aqueous environment.

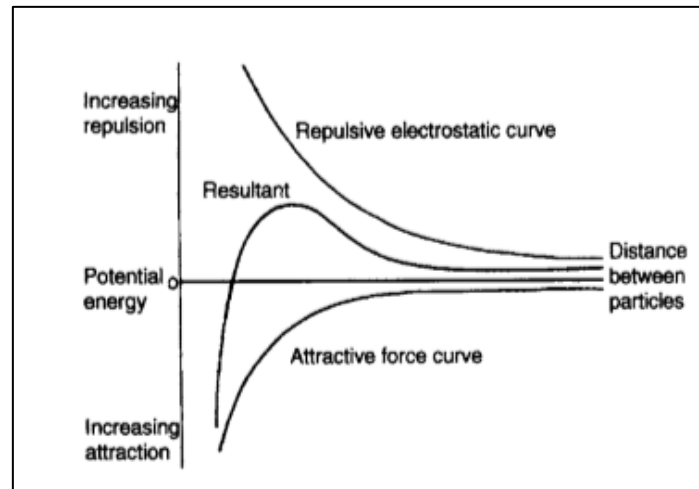


Figure 10: Potential energy curves for two particles approaching each other (B. Wills and Napier-Munn, 2006)

The salt of a multivalent cation such as aluminum sulfate, ferric sulfate, aluminum chloride, ferric chloride, calcium chloride which contain Al(III), Fe(III), and Ca(II) have been used as coagulation aid for a long time (Sharma, 2006; Chen Wang, 2014). Another recent study about the effect of coagulant on dewatering has experimentally shown (Önel, Gocer, and Taner, 2018) that the efficiency of sedimentation with trivalent coagulant has better performance. In contrast, the univalent coagulant has the worst performance in terms of turbidity as well as for the settling rate, as presented in Figure 11.

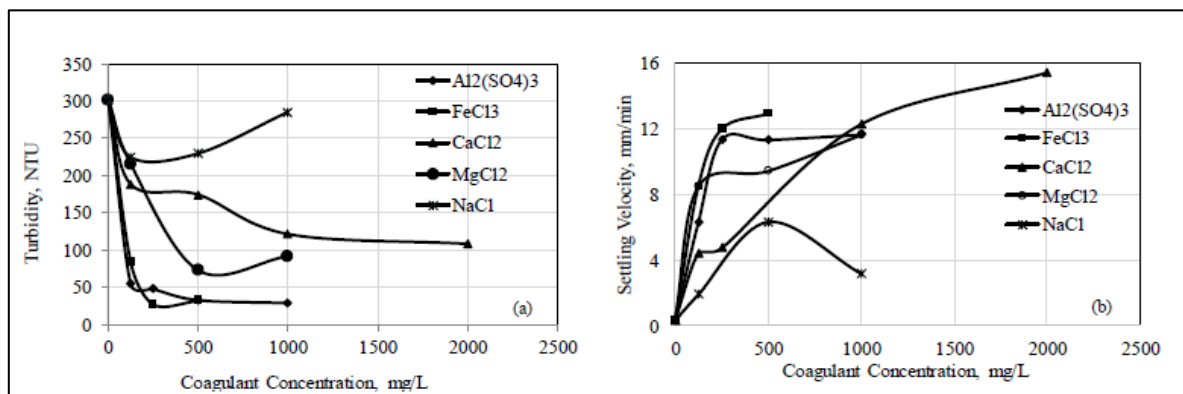


Figure 11: Effect of mono/multivalent metal concentration on the turbidity(a) and settling velocity (b) of kaolin (2018, p. 301)

Lime, or Sulphuric acid, depending on the surface charge of the particles, can also be used to cause coagulation (B. Wills and Napier-Munn, 2006). Most effective coagulation occurs when

the pH of the suspension is in the Isoelectric point (IEP), where the surface charge of the particles is zero in relation to the suspending medium (Besra, Sengupta, and Roy, 2000).

In the same study by (Önel, Gocer, and Taner, 2018) has been mentioned the range of IEP of kaolin which is a quite common mineral of the tailing at DPM processing plant. According to those studies, the pH at IEP of the Si-OH and Al-OH edge sites is between pH 5.0–7.0, and that of octahedral alumina sheets is between pH 6.0–8.0. According to these IEPs, at high pH, the number of positively charged sites on kaolin surfaces should be low to exist in negligible quantities. IEP value of kaolin was determined as 4.2. Also, this study implies few facts discussed regarding the depression of pH with the addition of alum and ferric coagulant (Figure 12(a)), and the effect of coagulant concentrate on zeta potential (Figure 12(b)). It shows that di- and trivalent cation bring zeta potential of clays closer to zero more than monovalent cations.

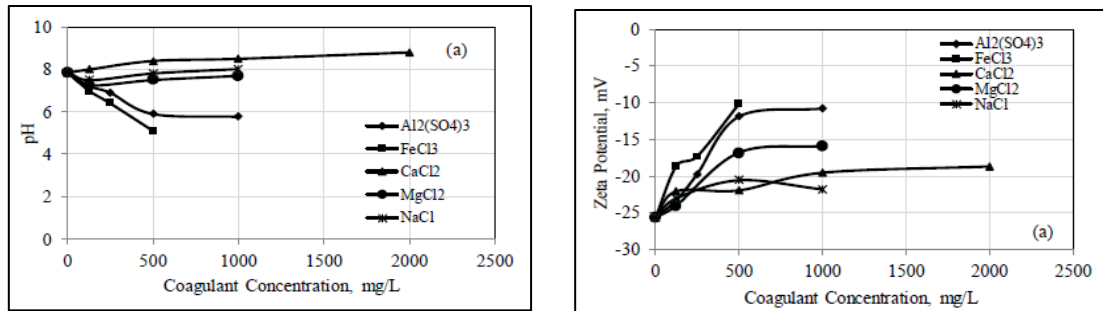


Figure 12: The variation of pH (a) and zeta potential (b) coagulant concentrate (2018, p. 303)

However, the higher dosage of coagulant causes charge reversal of suspension, thus preventing agglomeration of the particle due to repulsion forces. Therefore, the determination of optimum dosages along with optimum pH values is essential before industrial uses. Furthermore, coagulation can be classified into four distinct zones, according to coagulant dosages.

Zone 1: very low dosages where particles are still negative and stable; Zone 2: Dosage sufficient to give charge neutralization and coagulation; Zone 3: Higher dosage giving charge reversal and re-stabilization; Zone 4: still higher dosage giving hydroxide precipitation and sweep flocculation. (J. Gregory, 2013)

Sweep flocculation can be explained most likely as growing hydroxide precipitate incorporation with impurity particles and thereby removal from the suspension (Figure 13). This happens when the dosages of coagulants are above the solubility of the amorphous hydroxide under a suitable condition. This method always gives faster agglomeration than charge neutralization and large strong flocs. The collision rate of those precipitated particles is

high due to the increase in effective particle volume concentration hence increasing the agglomeration rate of the particles. This is the predominant reason why sweep flocculation is so much more effective than charge neutralization. The flocs produced under “sweep” conditions are also rather stronger and hence grow larger for the same shear conditions. However, hydroxide flocs are still rather weak compared to those formed by polymeric flocculants (J. Gregory, 2013).

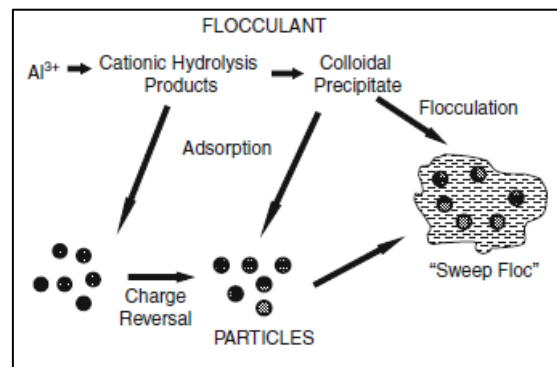


Figure 13: Illustration of “Sweep flocculation” (Gregory, 2013)

In addition, there are disadvantages of the use of coagulants such as:

- (i) Extremely sensitive to pH
- (ii) The high amount of coagulant is required for effective solid-liquid separation of the dispersion and produces a lot of sludge
- (iii) They do not coagulate very fine particles

Another disadvantage of relying on charge neutralization is that, for low particle concentrations, the collision rate is low. Hence, the aggregation rate will be low and long times may be needed to give sufficiently large aggregates (flocs). Neutralizing surface charge by small adsorbed species does nothing to enhance the collision rate, although, of course, the collision efficiency can be greatly enhanced (J. Gregory 2013).

### 2.5.2 Flocculation

To resolve the above issues, an organic polymer with great abilities to flocculate even under small quantities were developed and have been used over three decades. Flocculation forms much more open, strong agglomerates than those resulting from coagulation and relies upon molecules of reagent acting as bridges between separate suspended particles. Usually, flocculation is used after the coagulation process to produce larger visible floc with an additional collision of coagulated particles.

The polymers can be classified into three main categories based on their charge type as nonionic, anionic, or cationic polymers. These polymers can differ from each other with different chemical structure, molecular weight, and, in the case of polyelectrolytes, differences in charge density. Some of the common flocculants are:

- Nonionic: polyethylene oxide (PEO), polyacrylamide (PAM), polyvinyl alcohol (PVA), and polyvinylpyrrolidone (PVP)
- Anionic: hydrolyzed polyacrylamide (APAM), polyacrylic acid (PAA), and polyvinyl sulfate
- Cationic: poly-diallyl dimethyl ammonium chloride (PDADMAC), cationic polyacrylamide (CPAM), polyethyleneimine (PEI), epichlorohydrin-dimethylamine (ECH/DMA), cationic starch, and chitosan. The structures of some of these polymers are shown in Figure 14.

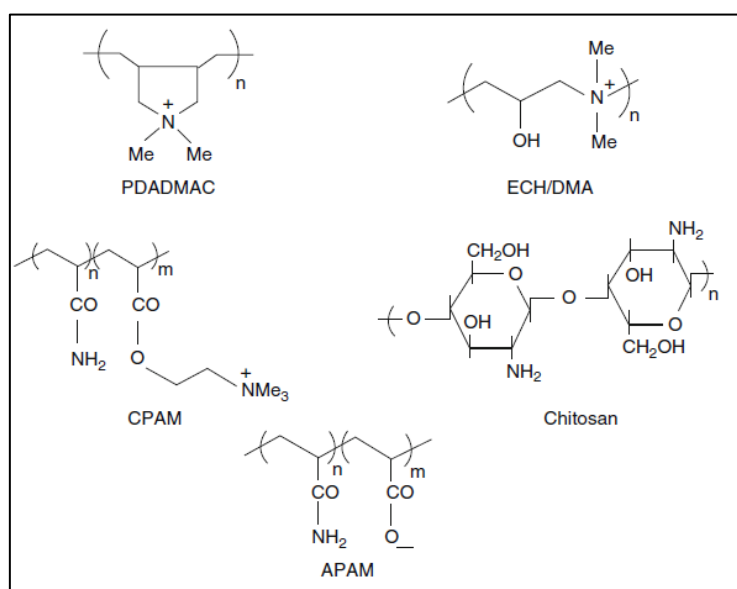


Figure 14: Chemical structures of some of common polymer flocculant

The most important mechanism for the high efficiency of polymeric or polyelectrolyte flocculant are (a) polymer bridging; (b) electro static patch.



Paper written by J.Gregory, (2013) has described the destabilization of colloidal particles according to the bridging theory, which was developed by previous studies. Destabilization by bridging occurs when segments of a polymer chain adsorb on more than one particle, thereby bridging the particles together. When a sufficient amount of polymer molecule comes into contact with a colloidal particle, some of the reactive groups on the polymer adsorb at the particle surface, leaving other portions of the molecule extending into the solution (Figure 15(a)). The polymer will adsorb on the surface in a series of loops (segments extending into the solution) and trains (segments adsorbed on the surface). If a second particle with vacant adsorption sites contacts these extended loops and tails, an attachment can occur (Figure 15(b)). A particle–polymer–particle aggregate is formed in which the polymer serves as a bridge even if they are charged and repel each other. This effect is originally known as “sensitization. Effective bridging requires that adsorbed polymers extend far enough from the particle surface to attach to other particles and that some free surface is available for adsorption of the extended segments. With excess polymer, the particles are re-stabilized by surface saturation and can be sterically stabilized as shown in Figure 15 (c).

From this description, the length of the polymer chain is crucial for effective bridging to occur. It also follows that a linear (i.e., non-branched) polymer would be the most effective. Longer the chain (high molecular weight), the greater the chances of interacting with more than one particle (A. Mierczynska-Vasilev et al. 2013). The most important thing is the size of polymer in solution, i.e., hydrodynamic volume rather than merely the molecular weight. Bridging is a preferred mechanism for applications of non-ionic polymers with molecular weights of more than 1 million.

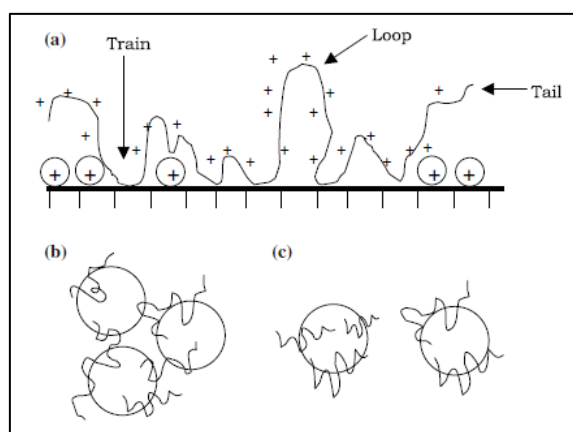


Figure 15: (a) adsorption of polymer and formation of loops available for binding (b) Polymer bridging between particles. (c) Restabilization of colloid particles; (Sharma, Dhuldhoya and Merchant, 2006)

For polyelectrolytes (polymer contains ionizable groups such as carboxyl, amino, sulphonic), the charge density is also an important variable for effective flocculation because highly charged chains are tended to adopt a more expanded structure. However, highly charged polymer and particle with the same charge (anionic polyelectrolyte with negative particles) might lead to less effective flocculation. Therefore, optimum charge density is also needed for effective flocculation. Also, the ionic strength of polyelectrolyte plays a significant role in bridging action because increasing salt concentration would reduce chain expansion. Also, the repulsion action of particles depends on ionic strength.

The second type of polymer flocculation, described as an electrostatic mechanism or patch model, involves the uneven distribution of charges resulting from the adsorption of discrete patches of polymer on the surface. A highly charged cationic polymer is adsorbed on a negative particle surface in a flat conformation or vice versa. That is to say, most of the charged groups are closed to the surface of the particle, as illustrated in Figure 16. This promotes flocculation by first reducing the overall negative charge on the particle, thus reducing interparticle repulsion. This effect is called charge neutralization and is associated with reduced electrophoretic mobility. In addition, the areas of polymer adsorption can have a net positive charge because of the high charge density of the polymer. The positive regions are also attracted to negative regions on other particles, which is called hetero coagulation. The tenacious floc that results is very resistant to redispersion. Polymeric inorganic materials may also adsorb on surfaces and cause flocculation by a similar mechanism. Patch model flocculation mechanism is a preferred mechanism for applications of low molecular weight polyelectrolytes with high charge density. (J. Gregory, 2013).

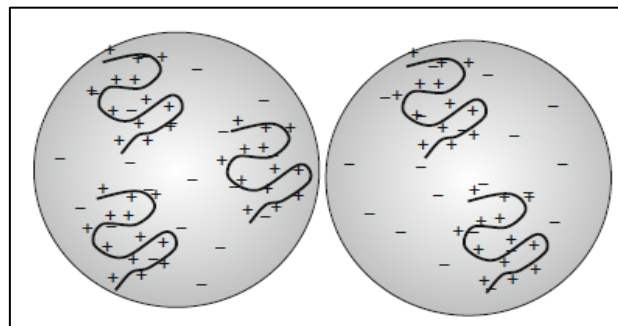


Figure 16: Illustration of "Electro static patch" by highly charged cationic polyelectrolyte

The kinetic aspect of the flocculation process by polymer has been summarized by Gregory as below and illustrated in Figure 17.

- (a) Collisions of particles and polymer molecules, giving attachment
- (b) Relaxation of adsorbed chains to give an equilibrium conformation
- (c) Collisions of particles to form a floc
- (d) Breakage of floc

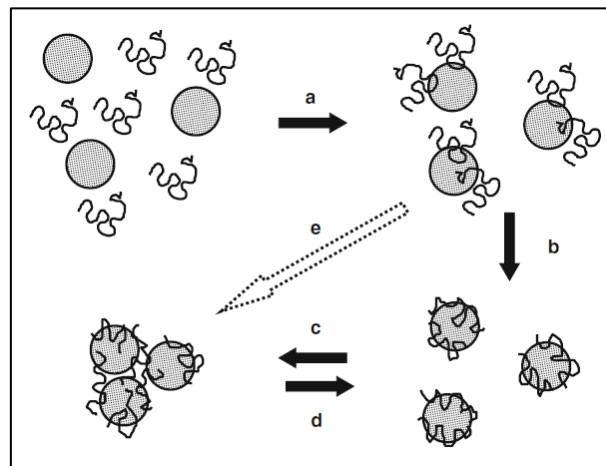


Figure 17: Adsorption and flocculation by polymers. (J. Gregory, 2013)

Since most of the particles in water or industrial suspensions are negatively charged, cationic polyelectrolyte might be the most effective flocculant for particle neutralization and the bridging process. However, a past study by (Önel, Gocer, and Taner, 2018) has shown Figure ) that the flocculation of negatively charged industrial suspension can sometimes more effective (in term of turbidity and settling velocity) with high molecular anionic polyelectrolyte, at a lower concentration, compared to cationic polyelectrolyte. Even though they change the zeta potential of particles into even more negative value, as shown in Figure . In this case, the polymer bridging mechanism plays the main role. Figure shows the behavior of anionic polyelectrolyte (A150), cationic polymer (C521), and non-ionic polymer (N100). A150 has both lower residual turbidity and higher settling velocity with less concentration.

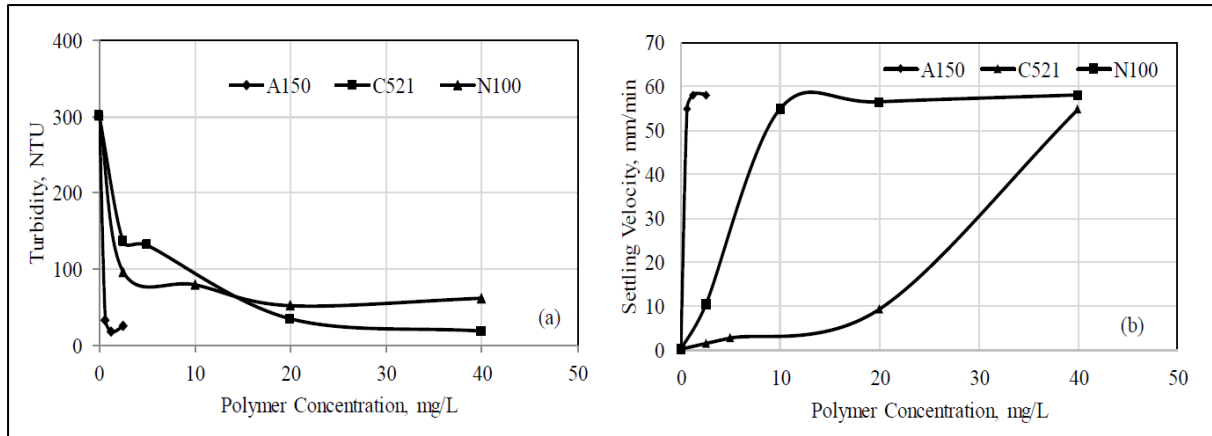


Figure 18: Effect of nonionic/anionic/cationic polymer concentration on the turbidity (a) and settling velocity (b) of kaolin

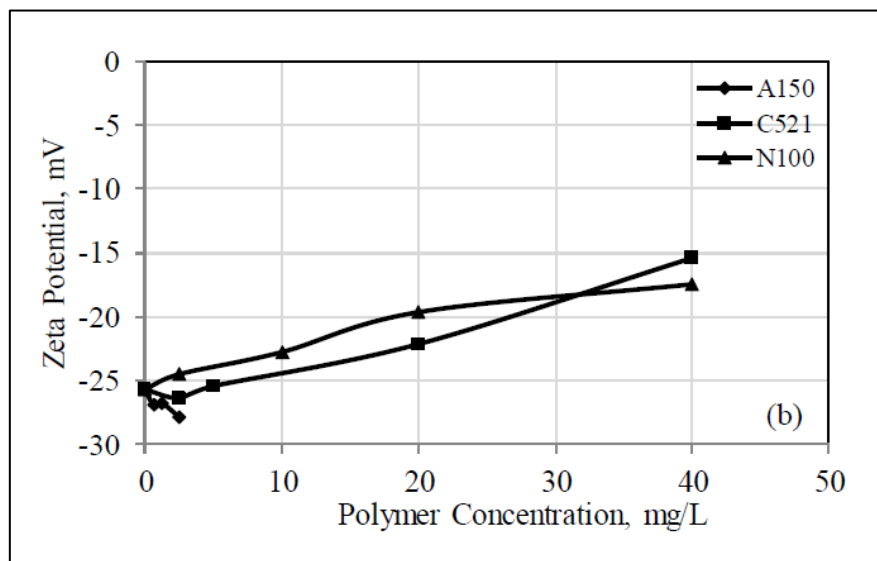


Figure 19: the variation of the zeta potential of kaolin with polymers

Apart from using individual coagulant or flocculant, some previous studies have shown efficient sedimentation with a combination of both coagulant (metallic salt) and polymer flocculant. The study has been carried out using Poly-aluminum chloride (PAC) ( $\text{Al}_2(\text{OH})_3\text{Cl}_3$ ) and Ferric Chloride ( $\text{FeCl}_3 \cdot 6\text{H}_2\text{O}$ ) as a coagulant and cationic polymer (CHIMEC5268) as a flocculant and the result are presented below.

Figure 20 (a) and (b) show the particle removal efficiency with PAC and  $\text{FeCl}_3 \cdot 6\text{H}_2\text{O}$ . Figure 21 (a) and (b) show the particle removal efficiency with a combination of both coagulant and polyelectrolyte (PE). Observing the results, it can be observed the removal efficiency of PAC with PE has been increased to 99.61%. In comparison, the removal efficiency of ferric chloride with PE has been increased to 99.64%, which quite high value compared to the performance of coagulant alone. It has also reduced the required coagulant dosage to achieve optimum removal efficiency. (J. Mohammed and E. Shakir, 2018)

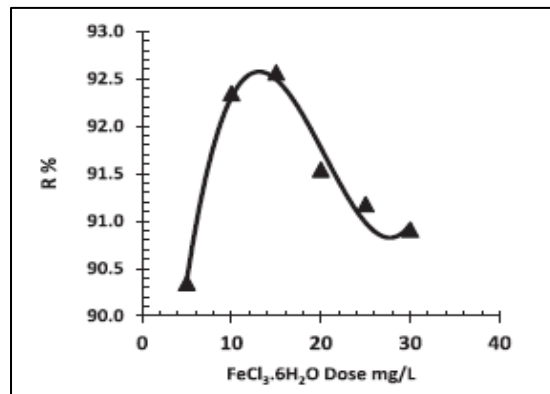
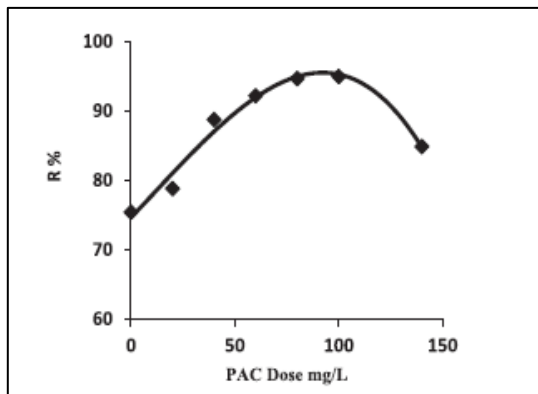


Figure 20: The effect of optimum dose of PAC (a) and ferric chloride (b) on the removal efficiency of turbidity. (J. Mohammed and E. Shakir, 2018)

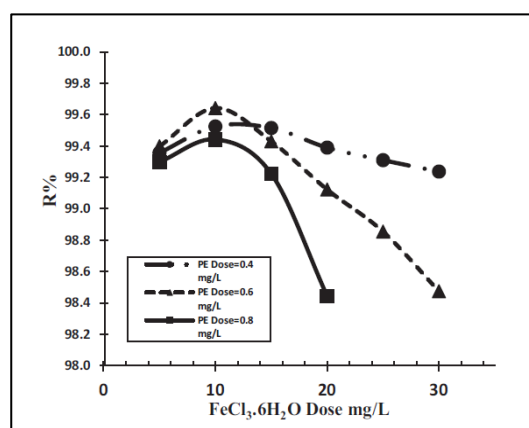
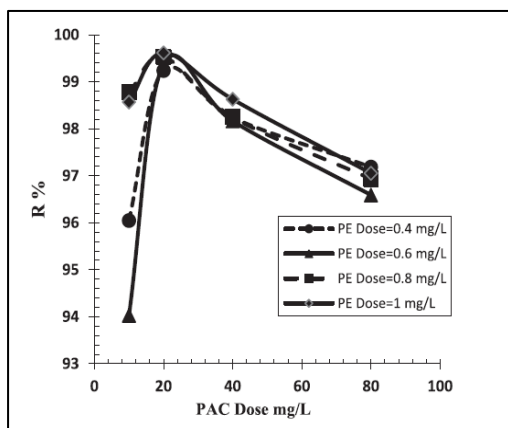


Figure 21: The effect of optimum dose of PAC (a) and ferric chloride (b) on the removal of turbidity with combination of polyelectrolyte (J. Mohammed, and E. Shakir, 2018)

## 2.6 Optimization of coagulant and flocculant dosages

### 2.6.1 Jar test

Jar testing has been recognized as the most suitable tool for simulating coagulation, flocculation, and sedimentation at a large-scale water treatment throughout several decades. By performing a jar test, alternative treatment dosages and strategies can be tried without alternating the performance of the full-scale plant as it sufficiently duplicates the behavior of full-scale plant at bench scale. Still, there are some issues while duplicating the most advanced physical treatment processes. (American Water Works Association, 2011)

As per American Water Works Association, the jar test can be used to perform several tests to evaluate the optimum dosage of coagulant and flocculant, to choose the alternative coagulants, add polymeric coagulant aids, and suitable mixing intensities and time.

This method uses a set of beakers and magnetic stirrer or equivalent (Figure 22) to stirrer the suspension after the addition of flocculant or coagulant under rapid mixing and flocculation stages and then allowing flocs to settle for a certain time at rest. For a typical jar test, the rapid mixing time of 30-60 seconds can be used, with an agitating speed of 100-300 rpm and typical flocculation times are approximately 15-20 min, with an agitating speed of 30-50 rpm (American Water Works Association, 2011). The efficiency of particle removal of supernatant is assessed by measuring the residual turbidity after specified settling time as required. The turbidity is usually measured by a nephelometric technique where results are given in the Nephelometric Turbidity Unit (NTU), which measures scattered light from the sample at a 90-degree angle from the incident light. Still, Formazin Attenuation Unit (FAU) can also be used. This type of measurement usually done in a spectrometer or colorimeter by measuring transmitted light through the sample at an angle of 180 degrees to the incident angle. However, FAU unit is not considered as valid units by most laboratory agencies.

These results can be presented as residual turbidity or the efficiency of turbidity removal (R%) formula as:

$$R\% = \frac{(C_o - C)}{C} * 100$$

C<sub>o</sub>: initial turbidity, C final turbidity

Typically, six jars are agitated simultaneously, with different amount of coagulant or flocculant, Optimum flocculation dosages can be determined as the one which gives minimum

residual turbidity. In addition, the optimum pH value can be determined using the same apparatus and procedure with different pH values and constant coagulant dosages at each jar.



Figure 22: Standard jar test protocol

### 2.6.2 Measurement of initial settling velocity

Several research studies have reported measurement techniques of particle settling rate in their studies. One recent study about the effect of solution salinity on settling of mineral tailings by polymer flocculants has described (Ji et al., 2013) the following steps of settling rate measurement. First, the sample must be homogenized by high-speed agitation. Then, the samples are transferred to a standard 250 mL baffle beaker on balance and then agitated under 600 rpm for 2 minutes. After that, the desired amount of coagulant or flocculant (polymer) is mixed for one minute under a lower agitation speed of 300 rpm to achieve a uniform mixture and avoid breaking the flocs. The agitation was stopped immediately after the addition of the desired amount of settling aids. Finally, the slurry was transferred into a 100 ml graduated cylinder. The cylinder was inverted five times and the so-called mudline was monitored as a function of settling time. The initial settling rate (ISR) was calculated from the initial slope of the mudline height ( $h$ ) versus settling time ( $t$ ) as shown in Figure 23.

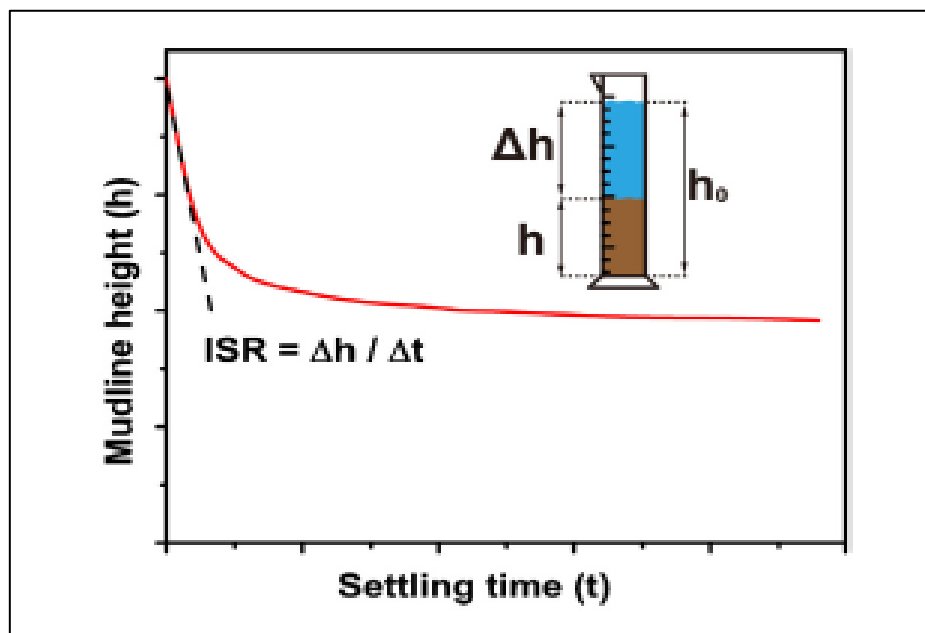


Figure 23: Schematic of the initial settling rate calculation based on the settling results of mudline height (Ji et al., 2013)



## 2.7 Effect of process water chemistry on flotation

Several previous studies have investigated the effect of recycled water quality on the flotation performance of various ore types as it lowers the primary water requirement to the system as well as reduce the amount of discharge to the tailing (Muzenda, and Edison, 2010). Due to the insufficient time to decompose these dissolved ions, suspended solids, and flotation reagent in thickener or tailing tank, it can severely affect the flotation performance in both positive and negative ways. The typical residual available in recycled water is colloidal material (silicate, clays, precipitated metal hydroxides), ions of base metals,  $\text{SO}_4^{2-}$ ,  $\text{Cl}^-$ ,  $\text{F}^-$ ,  $\text{Mg}^{2+}$ ,  $\text{Ca}^{2+}$ ,  $\text{Na}^+$ ,  $\text{K}^+$ , sulfide, thiosalts, collectors, frothers, activators, depressants (Bıçak et al., 2012; Corin & Manono, 2020). But  $\text{Ca}^{2+}$ ,  $\text{Mg}^{2+}$ ,  $\text{Fe}^{2+}$ , and  $(\text{SO}_4)^{2-}$  are the most discussed cations and anions in previous studies due to precipitation of particularly calcium sulfate, magnesium carbonate, iron hydroxide which contaminate the mineral surface. (Muzenda, and Edison, 2010). Also, colloids which contain a varying concentration of Si, S, Cu, and Ni increase the surface area for reagents to attach as well as form non-selective and hydrophobic coat on gangue mineral which causes grade loss and loss of separation efficiency (Saari, Jansson, and Musuku, 2020)

Low decomposition of flotation reagent at the plant increases in grade due to the presence of residual reagent, which enhances the flotation of valuable minerals as shown in a study carried out with Platinum Group Metals (PGM). On the other hand, a high total dissolved solids (TDS) level can decrease the recovery metals. Generally, increasing the TDS level increases the Specific Gravity (SG) of the slurry thus, if the SG of the plant is maintained constant while that of water is increased, it will decrease the solid throughput along the process. (Muzenda, and Edison, 2010).

The case study carried out at Hajar Mine, Morocco, has discussed the influence of water quality on the flotation performance of complex sulfide ore (Boujounoui *et al.* 2015). It has shown that an increment of 7 to 14 mg/l of  $\text{Cu}^{2+}$  concentration has a positive effect on the recovery of Pb, Cu, Zn, and Fe. Also, it shows that  $\text{Cu}^{2+}$  concentration affects the selectivity of galena over chalcopyrite, sphalerite, and pyrrhotite. The positive effect of high  $\text{Cu}^{2+}$  concentration on the recovery of the mineral mentioned above is due to the adsorption of  $\text{Cu}^{2+}$ ,  $\text{Cu}(\text{OH})_2$ , and  $\text{Cu}(\text{OH})_3$  on the surfaces of these minerals as discussed in studies by (Prestidge, 1997; D.Fornasiero, and J. Ralston. 2006). However,  $\text{Cu}^{2+}$  has a depression effect of sphalerite at low concentration. The possible reason for this depression effect might be due to the weak absorption of copper onto the sphalerite surface due to competition with  $\text{Cu}^{2+}$  for adsorption sites (M. Deng, Q. Liu, and Z. Xu, 2013).

The same study (Boujounoui *et al.*, 2015) has shown the negative effect of  $\text{Zn}^{2+}$  concentration on the recovery of galena. At low concentration (0-20 mg/L), the negative effect is high on the galena, chalcopyrite, sphalerite, and pyrrhotite. Still, it will become positive at  $\text{Zn}^{2+}$  concentration from 20 to 40 mg/l except for galena. However, another study was carried out at the Woodlawn has shown that the presence of  $\text{Zn}^{2+}$  over 200 mg/l has a negative effect on the recovery of sphalerite caused by the presence of the colloidal oxide on the surface of the mineral (S. Williams, and J. Phelan, 1985)

Furthermore, it has been shown that the high concentration of  $\text{Ca}^{2+}$  (1200-2000mg/L) has a depressing effect on sphalerite and no significant effect on other minerals (Boujounoui *et al.*, 2015), (Ikumapayi *et al.*, 2012) while high concentration (100-200 mg/L) of  $\text{Mg}^{2+}$  has a negative effect on galena, chalcopyrite, and sphalerite recoveries but no any effect on pyrrhotite due to formation of hydrophilic layers such as  $\text{CaCO}_3$  on the surface in an alkaline condition which prevents the adsorption between collector and mineral surface (Boujounoui *et al.*, 2015) or it may activate non-sulfide gangue which eventually reduces the concentrate recovery while increasing the concentrate grade. (Muzenda, and Edison, 2010).

The high concentration of  $\text{SO}_4^{2-}$ ,  $\text{SO}_3^{2-}$  from 200 to 1500 mg/l have a depressing effect on the recovery of galena, chalcopyrite, and sphalerite due to the formation of heavy metal sulfite which hinders collector adsorption (Ikumapayi *et al.*, 2012), (Muzenda, and Edison, 2010).

The influence of water chemistry on gold flotation has been rarely studied because the gold is mostly recovered as a by-product of metal sulfide which is considered as gold carrier minerals and contains trace to a low amount of gold (Dunne, 2005). If the gold is associated with other sulfide minerals, the water chemistry of recycled water will influence the recovery of gold as same as its influence on sulfide minerals as discussed in previous paragraphs.

Also, a study carried out by (Bustamante-Rúa *et al.*, 2018) has discussed that the native gold which is an alloy of non-specific composition and natural occurrence that contains 80-99% gold, 1-15% silver and between 0-5% copper is naturally hydrophilic. Still, it can form hydrophobic surfaces that are sufficient for flotation if a monolayer of carbonaceous contaminants is absorbed from air or solution (Bustamante-Rúa *et al.*, 2018). The same study has shown the requirement of surface activation of native gold if it is associated with coated pyrite. In this case, sodium carbonate, copper sulfate (which precipitate calcium and heavy metal ions), sodium sulfide, sulfur dioxide, and base metal salt can be used as an activator. The metallic ions of base metals are adsorbed on the surface of the mineral particles to modify their superficial chemical property, thus act as an activator. Therefore, the availability of metallic ions such as  $\text{Cu}^{2+}$ ,  $\text{Zn}^{2+}$  can be favorable for high recovery and selectivity over pyrite.

## 2.8 Objectives and aim of the work

In conclusion, past studies have shown that the optimum dosages of coagulant or flocculant must be determined before being used for solid-liquid separation of final tailing in the thickener. Both under dosage and overdosage of coagulant or flocculant can reduce the solid-liquid separation efficiency due to insufficient amount which is required for agglomeration mechanisms such as surface neutralization or bridging. According to the literature review, the jar test is a widely used method the optimization. In the jar test, different dosages, and type of metal salt as a coagulant and anionic or cationic polyacrylamide as flocculant are used. The main parameter to be considered in this test is the turbidity of supernatant water. In addition, measurement of the initial settling rate of the sedimentation bed is also another test which has been using along with the jar test. Finally, the optimal condition can be determined considering both turbidity and initial settling rate. Also, determination of the optimum pH where the high-efficiency solid-liquid separation takes place must be done as the efficiency of flocculation and coagulation is pH-dependent. Therefore, the methodology of this study mainly focuses on jar tests, measurement of settling rate, and pH optimization to fulfill the objective of the study.

Also, several studies have been done to investigate the effect of water chemistry on flotation performance. Since the recycled water is reused in the plant, the study of change of water chemistry with the addition of coagulant and flocculant must be investigated. According to the literature review,  $\text{Ca}^{2+}$ ,  $\text{Mg}^{2+}$ ,  $\text{Fe}^{2+}$ , and  $(\text{SO}_4)^{2-}$  are the most discussed cations and anions in previous studies due to precipitation of particularly calcium sulfate, magnesium carbonate, iron hydroxide which contaminate the mineral surface. However, the addition of a coagulant such as  $\text{Ca}(\text{OH})_2$ ,  $\text{FeCl}_3$ , and  $\text{FeSO}_4$  could change the water chemistry of the recycled water. Therefore, laboratory scale flotation trials with actual process water, synthetic process water, and recycled water are included to compare the result between each case.

Also, the importance of mineralogical analysis of an ore, concentrate, and tailing has been discussed in number of papers. The fine particle reduces the efficiency of solid-liquid separation of the tailing due to the negligible settling rate and stability of the suspension. Therefore, identification of the gangue minerals that generate a high percentage of finer particles is essential to suggest a method to reduce the fines generation, thus improve the solid-liquid separation efficiency. Hence, the analysis of modal mineralogy, SEM images, and liberation curves is included in the methodology.

## 3 Methodology

### 3.1 Sample preparation and splitting

Sample preparation of any experiment is one of the essential factors as it must be a representative sample of bulk material. In this thesis project, sampling was done mainly for three different purposes. They are the samples required for mineralogical characterization, jar test, and flotation trial. The samples required for jar tests were directly collected from scavenger tailing stream at DPM plant at four times in 30 minutes intervals to get a most representative sample. A 50 L of tailing sample of 20% solid were shipped to the University of Liege for further tests (Settling rate measurement and pH optimization) while other samples were used to carry out jar test.

The sample preparation for XRD, optical microscopy and SEM were done using the first sample batch, which was initially shipped from the DPM plant. These samples consist of 5 kg of ore, 3 kg of concentrate, and 3 kg of tailing. For each sample, the cone and quartering method was used, followed by riffle sampling with instruments available at the University of Liege and 30 grams of two samples were collected from each fraction. Finally, samples were sent for XRD and making polished sections.

Another batch of ore sample was prepared for the flotation trial. First of all, the solid density of the ore sample was determined to be able to calculate the amount of material required for each flotation trial based on the actual pulp density of the flotation slurry at the DPM plant and the volume of flotation cell available at the laboratory. According to Will's mineral processing technology (B. Wills and Napier-Munn, 2006, pp. 51-52), the following steps followed for the calculation.

- Weight the dried measuring cylinder on a precision analytical balance, and recorded the weight, M1 (37,57g).
- Add 10 g of sample to measuring cylinder and recorded the weight, M2 (5,91 g).
- Add deionized water to the bottle is filled up to 100ml and recorded the weight, M3 (143,62).
- Then, the sample is washed out of the measuring cylinder and recorded the weight, M4. After refilling the measuring cylinder with deionized water up to 100 ml (134,04 g). The solid density is given by equation 9 in  $\text{kg/m}^3$  where  $D_f$  is the density of fluid used and the solid density of the sample is  $3004.18 \text{ kg/m}^3$ . The solid density of samples was  $3004,18 \text{ kg/m}^3$  ( $3\text{g/cm}^3$ ).

$$\frac{M2-M1}{(M4-M1)-(M3-M2)} \times Df \text{ kg/m}^3 \quad (9)$$

After that, the amount of material to be used for flotation trial was calculated considering 32 % w/w of slurry density and maximum volume of the cell as the following equation where Ms, Ml, ds, and dl represent the mass of the solid, mass of liquid, the density of solid, and density of water, representatively. After calculation, 1780 g of sample was required for each flotation trail.

$$\frac{Ms}{Ms+Ml} = 0.32 \quad \text{and} \quad Vt = \frac{Ms}{ds} + \frac{Ml}{dl}$$

Once the calculation was done, about 19kg of the remaining ore sample was crushed in a jaw crusher followed by 2mm screening to achieve maximum feed size of Magotteaux Mill® for grinding. The oversize material was crushed again using roller crusher until all of the materials were below 2 mm. after that, the sample was split 29 times in two by two pyramidic ways using riffle sampler until each fraction reached about 600 g. Then, three samples were mixed to get about 1800 g samples. Finally, 9 sample bags of 1780 g were prepared.

### 3.2 Determination of optimum coagulant and flocculant dosages

Dosages optimization was carried out using scavenger tailing samples, which were collected four times at 30-minute intervals to obtain representative samples. This sample contains about 20 % wt and the 7.9 pH. The process and the sketch of the thickener, which is used at the DPM plant, are shown in Figure 24.

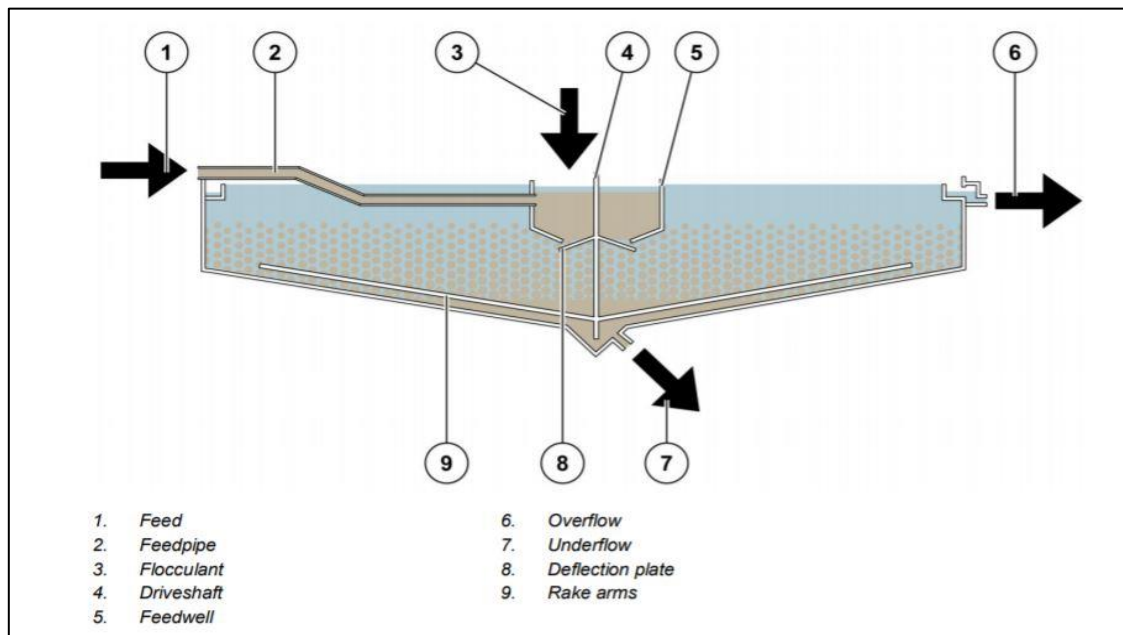


Figure 24: An overview of thickener used at DPM plant

- Feed slurry enters the feed well via the feed pipe.
- Flocculant (Magnaflow® 155 anionic Polyacrylamide (PAM)) is added to the feed slurry at optimal locations in the feed pipe and/or in the feed well.
- The feed is diluted with water in the vaned feed well to aid with flocculant mixing. The water is drawn from the overflow using directional autodilts.
- Vanes in the feed well promote mixing of the flocculated feed slurry and allow an acceptable residence time.
- With the mixing energy dissipated, the feed exits the feed well and is injected through the deflector cone and across the top of a deep fluidized bed.
- The particles then settle to the bottom of the thickener, while the clear water rises to the top.
- The clear water at the top can spill over a notched weir into a launder located around the circumference of the thickener.

The purpose of the jar test is to determine optimum solid-liquid separation using flocculant and coagulant, as discussed in the literature review. For that,  $\text{Al}_2(\text{SO}_4)_3$ ,  $\text{FeCl}_3$ ,  $\text{FeSO}_4$ , and  $\text{Ca}(\text{OH})_2$  were used as a coagulant. Magnafloc® 155 anionic Polyacrylamide (PAM) was used as a flocculant. The Magnafloc® 155 PAM is the only settling aid that is currently used at DMP Krumovgrad tailing thickener. The first bench-scale jar test was done using PAM to find out optimum dosage should be used in the plant. Then, the next sets of jar tests were carried out to determine optimum dosages of each coagulant and combination of both coagulant and flocculant on their setting and clarity of the process water. Due to the limitation of available equipment at the laboratory, the initial protocol was changed. And 200 ml of tailing samples were used instead of 500 ml in each beaker at the DPM laboratory in Krumovgrad.

Before the experiments, current flocculant dosages at the DPM plant were converted to milligrams per liter of slurry for the ease of use at the laboratory level. The minimum and the maximum dosages used in the thickener were calculated, considering the following data obtained from the processing plant.

- Average volumetric flow rate - 350 m<sup>3</sup>/h,
- Average solid flowrate - 100t/h,
- Current flocculant dosages - 74 g/t to 117 g/t maximum

The range of dosages is between 21.1mg/l to 33.35 mg/l. However, in the plant, the dosage within the range is adjusted only based on visual inspection of the thickener overflow turbidity. When the turbidity is high, the flocculant dosage is increased to the maximum amount without considering an optimum amount.

The next step is to prepare a stock flocculant solution with the same concentration as used in the plant. It was prepared by adding 0.2g of PAM to 500 ml of distilled water and mixing at 700 rpm for 30 minutes to obtain 0.04% of flocculant concentration. The addition of 1ml of stock solution to the 200 ml beaker increases the dosage by 2 mg/l.

Once the stock solution was ready, the tailing sample was stirred for 15 minutes at 750 rpm in order to obtain a well-dispersed suspension. Then, 200 ml of tailing was introduced to each beaker. After that, a different amount of PAM ( 8, 10, 12,13, 14 ml) was added to five beakers respectively to achieve the different dosages (16, 20, 24, 28, 32 mg/l) followed by 1 minute of manual stirring which is the recommended rapid mixing time in the cone thickener tank in the site. After stirring, flocculated samples were left 20 minutes to settle, the flocs and two

supernatant water samples were collected in 10-minute intervals. The turbidity value was measured in FAU units using a Spectroquant® NOVA 60 photometer. The pH of each beaker was measured after adding reagent.

The next jar test was carried out using Iron (ii) Sulfate as a coagulant. 1 % of the stock solution was prepared by adding 1 gram of  $\text{FeSO}_4$  into 100 ml of distilled water and stirred for 20 minutes. The addition of 0.1 ml of this solution into 200 ml results in 5 mg/l increment. According to information in previous papers, the optimum dosages of metal salt as a coagulant is mostly below 500 mg/l. Therefore, the dosages were selected in 20 mg/l intervals starting from 20 mg/l (e.g.: 20, 40, 60, 80, ...) until the optimum result is achieved. The first beaker of each test was kept as a reference without coagulant. After adding the coagulant to each beaker, the slurries were stirred manually for 1 minute and allowed samples to settle down for 20 minutes. Finally, supernatant water samples were taken from each beaker after 10 and 20 minutes and turbidity was measured in FAU units.

Likewise, the next test was carried out with Aluminium sulfate hydrate. A 1% of stock solution was prepared by dissolving 1 gram of  $\text{Al}_2(\text{SO}_4)_3$  in 100 ml distilled water. The addition of 0.1 ml of this solution into 200 ml results in 5 mg/l increment. The same procedure was carried out as the previous process.

The same procedure was followed using Ferrous (II) chloride solution with 45% active ingredient and a specific gravity of 1.48 g/cm<sup>3</sup>. The coagulant was added directly using a micropipette to get the dosages of 100 mg/l to 220 mg/l in an interval of 20 mg/l, followed by 1 minute of manual stirring. The supernatant water samples were collected at 10 and 20 minutes and turbidity were measured.

Once the optimum dosages were determined from the above tests, another set of jar tests was carried out with a combination of PAM and other metal salt based on the optimum dosages obtained from previous tests with individually settling aids. The reason to use a combination of flocculant and coagulant is that some past studies have shown that the combination of coagulant and flocculant is more effective than the use of coagulant or flocculant alone. It reduces the turbidity of supernatant water as well as the amount of flocculant required to obtain the same result with flocculant alone.

The first combination was PAM and  $\text{Al}_2(\text{SO}_4)_3$ . Four beakers were filled with 200 ml tailing and manually stirred for 1 minute with four different coagulant dosages (160, 180, 200 mg/l), including the optimum dosage obtained from  $\text{Al}_2(\text{SO}_4)_3$  alone. Then, 10 ml of PAM (0.04%)



was added to get a dosage of 20 mg/l and stirred for one minute. After that, the turbidity of the supernatant water was measured after 10 minutes. The same procedure followed with the same dosages of  $\text{Al}_2(\text{SO}_4)_3$  with 24 mg/l and 28 mg/l flocculant dosages.

Likewise, another 2-jar test was carried out with a combination of  $\text{FeSO}_4$  and  $\text{Ca}(\text{OH})_2$  with PAM. The optimum dosages of  $\text{FeSO}_4$  used were 140,160,180 mg/l along with 20, 24,28 mg/l PAM. The optimum dosages of  $\text{Ca}(\text{OH})_2$  used were 500 ,750 ,1000 mg/l along with 20, 24,28 mg/l PAM.

### 3.3 pH optimization

The pH of the tailing slurry also influences the efficiency of the coagulation of the colloidal particle. Therefore, pH optimization is also another important test to be done along with coagulant and flocculant optimization. In this experiment, jar tests were done with different pH of slurry with the optimum dosage of each coagulant and flocculant obtained before. Conc.  $\text{H}_2\text{SO}_4$  and NaOH were used as the main pH regulators. Only four sets of jar tests were done at a time due to the limitation of agitators.

Firstly, the scavenger tailing shipped from the DPM plant was stirred at 700 rpm in a 25 L container to make a homogeneous slurry. Then, a 500 ml sample was measured using a measuring cylinder and poured into a 1 L beaker. After that, the sample was stirred at 300 rpm for 2 minutes and the pH was recorded. The same procedure was followed while mixing a known number of  $\text{H}_2\text{SO}_4$  drops into the slurry to get a rough idea of how many drops need to be added to get a certain pH ( about 4.5, 5, 5.5, 6, 6.5, 7) and recorded. The pH optimization protocol is shown in Figure 25.

Firstly, a pH optimization test was performed with the optimum dosage of the combination of PAM and  $\text{Al}_2(\text{SO}_4)_3$ . Prior to the test, 0.04 % of PAM and 1% of  $\text{Al}_2(\text{SO}_4)_3$  were prepared. The first four sets of beakers were then filled with 500 ml of scavenger tailing and stirred well. The pH of the beakers was adjusted in ascending order ( close to 4.5, 5, 5.5, 6 ) by adding  $\text{H}_2\text{SO}_4$  drops.



Figure 25: Jar test set-up used for pH optimization

After this, 9 ml of  $\text{Al}_2(\text{SO}_4)_3$  was added to set the dosage of 180 mg/l and stirred a minute before adding 35 ml of PAM to set the dosage of 28 mg/l. Then, these four beakers were left

to settle. Finally, supernatant water of each beaker was collected using a syringe after 10 and 20 minutes, and turbidity was measured in NTU. In the meantime, another two samples were tested with pH close to 6.5 and 7.

The second jar test was performed with the optimum dosage of PAM and  $\text{Ca(OH)}_2$ . The same PAM solution and 5 % of  $\text{Ca(OH)}_2$  was used. Firstly, four beakers were filled with 500 ml of scavenger tailing and stirred for 2 minutes at 300 rpm before adding  $\text{H}_2\text{SO}_4$  as the previous test. Then, 6.5 ml of  $\text{Ca(OH)}_2$  was added to all beakers to set the dosage of 750 mg/l and stirred for a minute. After that, 30 ml of PAM was added to set the dosage of 24 mg/l and left to settle after one minute of stirring. The turbidity of supernatant water was recorded after 10 and 20 minutes.

The third jar test was performed with the optimum dosage of PAM and  $\text{FeSO}_4$ . The same PAM solution and 1 % of  $\text{FeSO}_4$  were used. Firstly, four beakers were filled with 500 ml of scavenger tailing and stirred for 2 minutes before adding  $\text{H}_2\text{SO}_4$  as in the previous test. Then, 8 ml of  $\text{FeSO}_4$  was added to all beakers to set the dosage of 160 mg/l and stirred for a minute. After that, 35 ml of PAM was added to set the dosage of 28 mg/l and left to settle after one minute of stirring. The turbidity of the supernatant water was recorded after 10 and 20 minutes.

Likewise, another three tests were performed with PAM,  $\text{FeSO}_4$ , and  $\text{Al}_2(\text{SO}_4)_3$  alone. The same procedure was followed as a previous test with the same concentration of each solution. The optimum dosages of PAM,  $\text{FeSO}_4$ , and  $\text{Al}_2(\text{SO}_4)_3$  were 32 mg/l, 160 mg/l, and 180 mg/l, respectively. The pH optimization with  $\text{FeCl}_3$  and  $\text{Ca(OH)}_2$  alone was not performed considering low efficiency according to coagulant optimization result.

### 3.4 Measurement of settling rate

The same scavenger tailing sample was used for the test. The purpose of this test is to determine the initial settling rate of the floc with a different combination of flocculant and coagulant. The tailing sample was transferred into 500 ml beaker and stirred at 600 rpm for 2 minutes, followed by 1 minute of agitation at 300 rpm while adding 40 ml of 1% PAM to set the optimum dosage of 32 mg/l. Then, the sample was transferred to a 1000 ml measuring cylinder. The cylinder was inverted upside down five times and left for settling. Finally, mudline was monitored as a function of settling time up to 60 minutes at different time intervals ( 1, 3, 5, 10, 15, 20, 30, 45, 60 min). For the convenience, graduated marks were read and later converted to into height considering the length between adjacent marks. The initial settling rates (ISR) were then calculated from the initial slope of the mudline height (mm) versus settling time (minutes). Likewise, the same procedure was followed with optimum dosages of a combination of PAM,  $\text{Ca(OH)}_2$ ,  $\text{FeSO}_4$ , and  $\text{Al}_2(\text{SO}_4)_3$ . Lab set-up of setting rate measurement is shown in Figure 26 below.

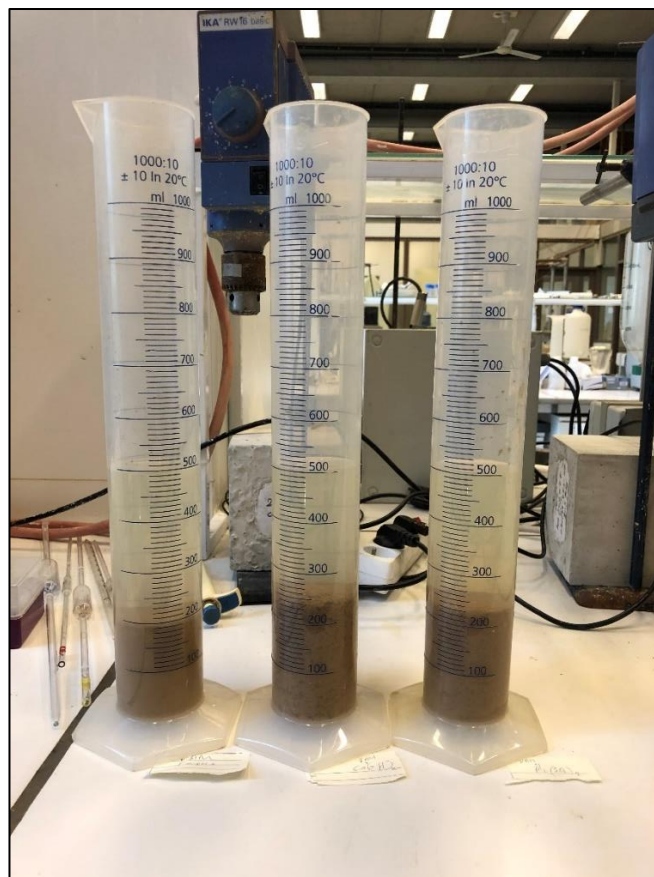


Figure 26: View of settling rate measurement set-up

### 3.5 Magotteaux Mill® calibration.

Lab scale ball mill named Magotteaux Mill® was used for grinding to achieve a P80 (30  $\mu\text{m}$ ) at the rougher feed to have the same granulometry as those in the plant. The mill has a dimension of 1300x680x1620 mm with a chamber volume of 25 liters. The unit can measure and control pulp chemistry (pH), pulp potential (Eh), temperature, dissolved oxygen (DO), and conductivity. Essentially, the grinding cylinder is presented as two separate chambers, grinding chamber and measuring chamber, respectively, which is separated by a screening device (Figure 27). The measuring chamber consists of DO, pH, Eh, and temperature probes. Through an opening of the mill's chamber cover additional pipelines coming from the peristaltic pump, lime dosing pump, and gas pipelines are entering in the measuring chamber. Grinding media used is steel balls with an average diameter of 30 mm.

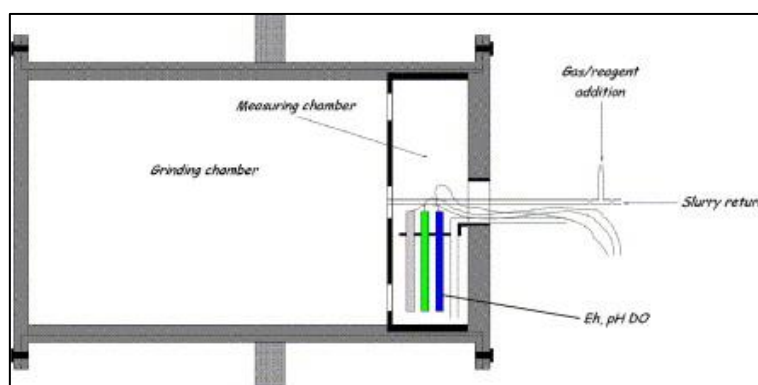


Figure 27: Basic view of Magotteaux Mill®

For the calibration, three grinding tests were performed with different grinding times and all other parameters were kept constant since the main objective of this calibration was to obtain P80, 30  $\mu\text{m}$ . The parameters are listed in Table 1 below.

Table 1: Operational parameters of Magotteaux Mill®

Operational parameter		
Feed Mass (g)	1780	
Solid %	50	
Forged steel (kg)	20	
	Mixing operation	Grinding operation
Grinding time (min)	2	10, 20 ,40
Grinding Speed (rpm)	10	60

Before starting each grinding test, the grinding media was cleaned to avoid oxidation on the ball's surface which could affect the flotation performance. After that, approximately 1 kg of fine quartz sand with 1 liter of water introduced to the mill and ground for about 5 minutes at

a mill speed of 60 rpm. This mill was cleaned only once, as the same type of material was used for the next two tests. After cleaning, 1780 g of material and 1780 mL of water was introduced to the mill chamber followed by 40 minutes of grinding. The same procedure was followed for the other two tests with a grinding time of 20 and 10 minutes. Conditioning with  $\text{Na}_2\text{SiO}_3$  and  $\text{CuSO}_4$  was not done in the calibration stage as it does not influence for size reduction.

After each grinding test, all the ground material was collected to the flotation cell and homogenized using an agitator. Then, about 300 ml of the representative sample was collected without disturbing homogeneity of the slurry and sieved using 38  $\mu\text{m}$  sieve due to the unavailability of 30  $\mu\text{m}$  sieve at the laboratory. Both +38  $\mu\text{m}$  and -38  $\mu\text{m}$  sample were placed in the dryer overnight and measured the weight to find out percentage oversize and undersize. Then, grinding time vs. passing % of under 38 $\mu\text{m}$  fraction was plotted as Figure 28 below.

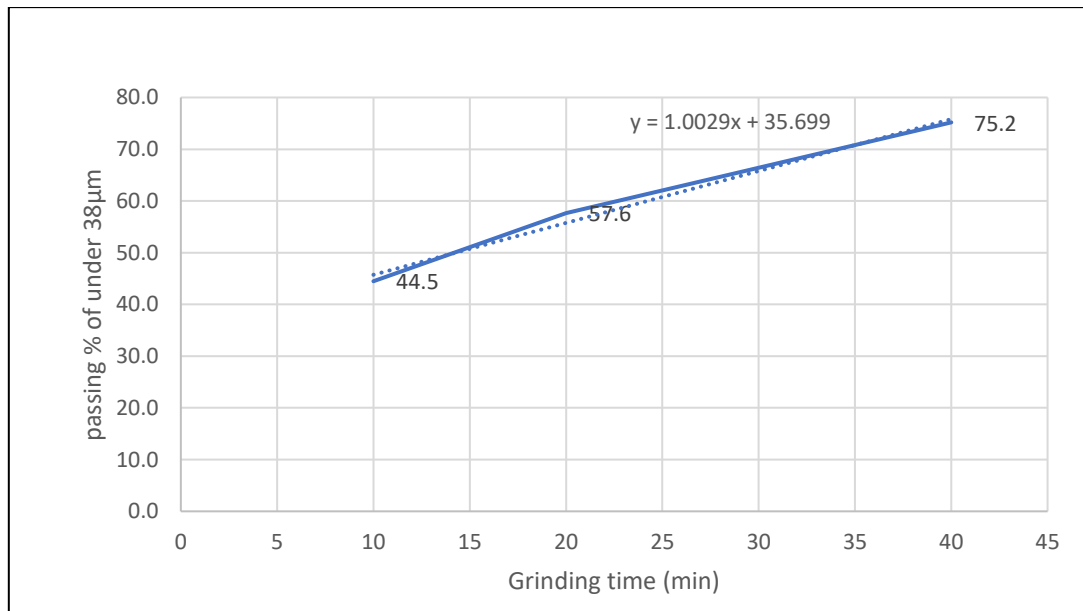


Figure 28: Ball mill calibration curve

Assuming that 90 % of the pass-through 38 $\mu\text{m}$  would give the P80 of about 30 $\mu\text{m}$ , the grinding time to obtain the desired P80 was calculated using slope  $y = 1,0029 + 35.699$  and the required grinding time is 55 minutes.

### 3.6 Flotation trial

A Magotteaux bottom driven cell was used for the batch flotation trials. The machine consists of a body with a PID controller for adjusting the rotor velocity, an air valve to control the amount of air entering the cell, and a variety of flotation cells with a volume of 1.5, 2.5, and 5 liters. In these trials, only 5 liters cell was used. The flotation cell is equipped with a bottom driven rotor with 20 blades. All the cells were rectangular and built from translucent material. The level of the pulp can be easier to monitor and control in this type of cell. The number of stator blades is 16 for every flotation cell volume, sitting around the stator plate with blades pointing the impeller. The PID controller can control the rotor speed for 300 to 1300 rpm. The purpose of these flotation trials was to compare the performance of flotation trials with purified process water using flocculant (PAM) as the actual plant condition and purified water using optimum dosage, which was determined by jar test. The process water collected from the plant was used for flotation test 1 and flotation test 2. Figure 29 below shows the protocol of the first four flotation tests which consists of milling and rougher flotation followed by filtration to recover the water from the tailing which was later used for thickener water simulation.

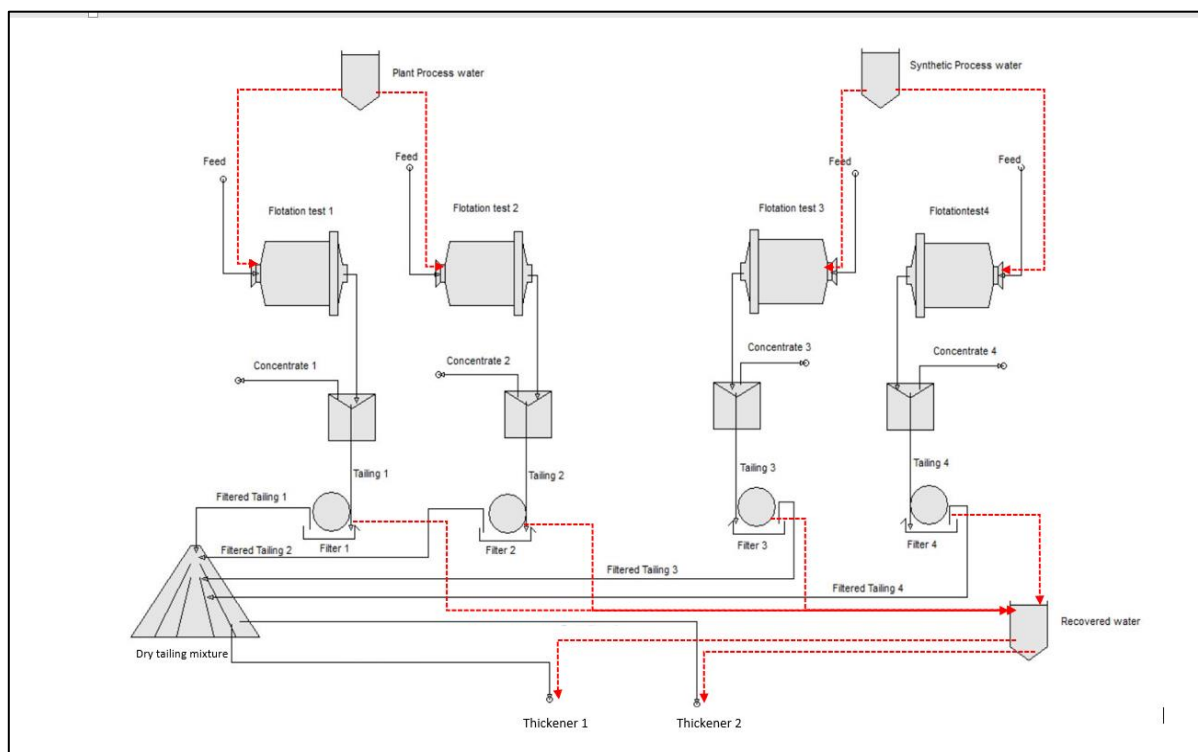


Figure 29: Flotation protocol with process water and synthetic process water

### 3.6.1 Flotation test with process water from the plant

First of all, Magotteaux Mill® and grinding media were cleaned properly. Then, grinding media and 1780g of samples were introduced to the ball mill. After that, 1800 ml of process water was measured in measuring cylinder, and 333mg of CuSO<sub>4</sub> (120 g/t) and 0.2 ml of Na<sub>2</sub>SiO<sub>4</sub> (11.5 g/t) were properly mixed to the water. These chemicals were added in the ball mill to simulate the exact condition in the DPM plant with the same dosages mentioned above. After introducing the water, grinding was done for 55 minutes while keeping all other parameters constant, as listed in

Table 1 above. In the meantime, flotation reagents, 2 % Potassium Amyl Xanthate (PAX), Aero flot 208, and methyl isobutyl carbinol (MIBC) were prepared. The flotation reagent used, and dosages are listed in Table 2 below.

Table 2: The reagent and dosages used in flotation trial

Type	Reagent	Concentrate	Dosage uses in Plant (g/t)	Amount per 1780 g
Dispersion	CuSO <sub>4</sub> (solid)		120	333 mg
	Sodium silicate (liquid)	100%	11.5	0.2 ml
Collector	PAX (Potassium Amyl Xanthate ) (l)	2%	250-300	25 ml
Activators	Aero flot 208 (liquid)	100%	30	0.5 ml
Frothers	MIBC (liquid)	100%	30-50	54.3-89 mg

After 55 minutes, the mill was stopped, the lid and the screen were removed carefully and cleaned with the same process water. Mill charge was discharged directly into a 5 l flotation cell by using a screen provided by Magotteaux to separate grinding balls from the grinding product. When cleaning, a minimum amount of water was used to ensure that the slurry level does not exceed 4.4 l limit. The reason not to use total volume is to prevent slurry from overflowing and the amount of feed requires for each trial was also calculated considering this limit.

Once cleaning is done, the water level was checked and adjusted adding some process water. Then, the flotation cell was placed on the flotation and agitated for 1 minute at 800 rpm. After that, PAX and Aero float was added to the slurry and agitated for another 1 minute before adding MIBC. Finally, the air was released, allowing the flotation process to begin. The airflow rate was adjusted in such a way to prevent pulp transferring from the cell to the tray. The froth was collected at a constant rate from the top of the pulp. The depth of scraping was constant (30 mm) utilizing the scraping device, scraping was performed every 10 seconds for 15 minutes



after releasing the air. The froth was collected in a pre-weighed tray. The scraper was washed with water after each scraping. End of the test, the concentrate was dried in a laboratory dryer at a temperature of 50°C. The tailing was left overnight for settling. The next day, supernatant water was filtered and collected for further trials. Remaining tailing and filtrate were dried in a dryer. After drying, the weight of each fraction was recorded, and 30 g of concentrate was prepared to be sent to the DPM laboratory for precious metal analysis. The second test was also done with the same condition with the same parameters. Filtered water was collected to the same water bucket which was placed in a cold room.

### 3.6.2 Flotation trail with synthetic water

The third and fourth tests were carried out using synthetic water which was prepared considering concentrate of ions base metals concentrate on process water collected from DPM plant. According to literature, the most influencing ions on flotation are  $\text{SO}_4^{2-}$ ,  $\text{Cl}^-$ ,  $\text{Mg}^{2+}$ ,  $\text{Ca}^{2+}$ ,  $\text{K}^+$ . The type of chemical and the amount used for synthetic water are listed in Table 3 below. After adding each chemical at a time, 10 liters of deionized water were stirred thoroughly for about an hour. ICP analysis was done to verify the concentration of each ion.

Table 3: The chemical used for synthetic water preparation

Ion	Concentration in process water (mg/l)	Chemical	Amount per 10 L (mg)
Potassium (K)	55.4±11.1	K <sub>2</sub> SO <sub>4</sub>	1234.5
Calcium (Ca)	36.9±7.4	CaSO <sub>4</sub>	1585
Magnesium (Mg)	12.4±2.5	MgSO <sub>4</sub>	1257.1
Chloride (Cl <sup>-</sup> )	27.5±2.8	NaCl	453.4
Sulfate (SO <sub>4</sub> <sup>-2</sup> )	264±13	Na <sub>2</sub> SO <sub>4</sub>	865.8

During these two tests, the same procedure was followed with the same parameters. Filtered water from both tailings was collected and placed inside the cold room. The purpose of these two tests was to compare the effect on flotation performance with and without remaining flotation reagent in process water and collect a sufficient amount of tailing sample and recycled water for the next steps.

### 3.6.3 Simulation of thickener and flotation using recycled water.

The next step of the flotation protocol is shown in Figure 30 below. The purpose of thickener simulation is to prepare process water that was purified using the same type and dosages of flocculant as in real plant and prepare process water which was purified using optimum type and dosages of flocculant determined by the jar test. Then, investigate the flotation performance to see if the new combination is suitable to be tested in the real plant. Before this, all the dry tailing samples from the previous tests were mixed to get a homogeneous product and 1200 g of samples were introduced into 10 l bucket. After that, 4.5 liters of recycled water was introduced to the bucket and stirred well to obtain about 20 % w/w tailing slurry to simulate real plant condition. pH was adjusted to 7,9 as in the plant. Two samples were prepared like that. The final volume of both samples is about 5 l. Then, one sample was thickened by adding 400 ml of PAM (0.04%) in thickener 1, while thickener was thickened by adding 75 ml of  $\text{Ca(OH)}_2$  (750 mg/l) and 300 ml of PAM (24 mg/l). After these coagulation and flocculation processes, two samples were left settle for 20 minutes and supernatant water was collected separately. Finally, flotation trials 5 and 6 were carried out with the recycled water from thickener one and thickener two, respectively. All other conditions and parameters were kept constant. Once all the tests were completed, two samples of feed and samples from each concentrate were sent to the DPM laboratory for precious metals analysis.

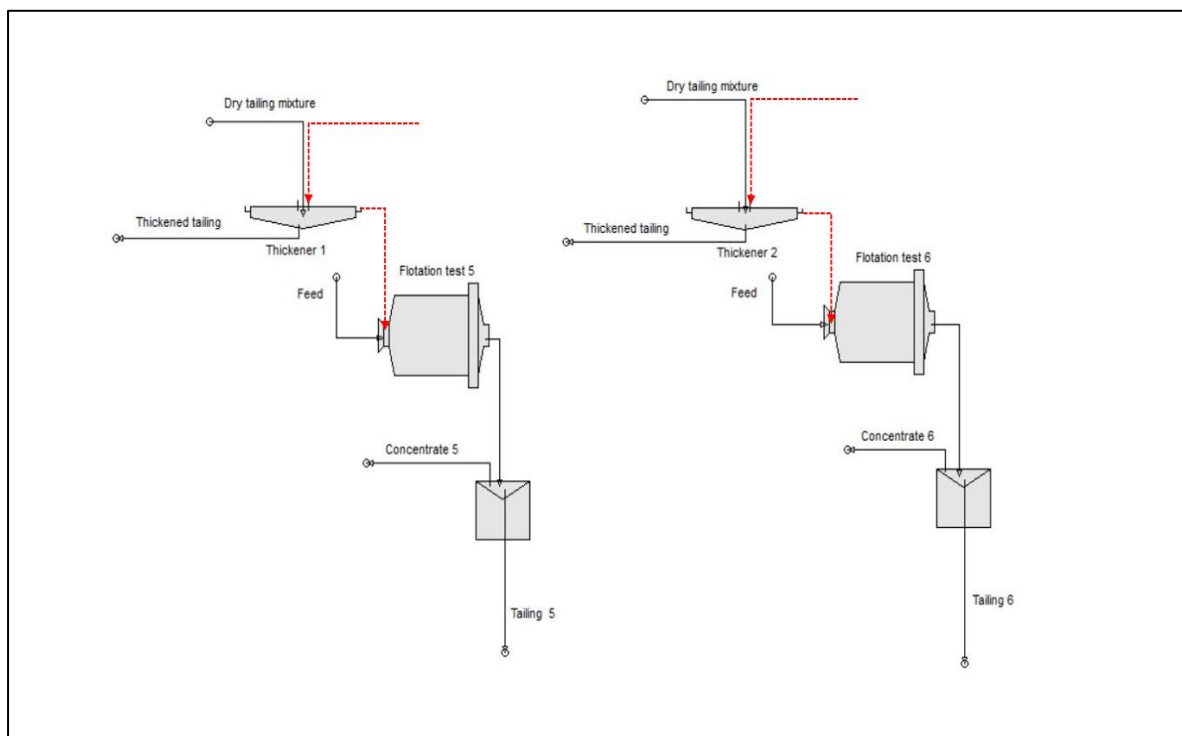


Figure 30 : Flotation protocol with thickener simulation and recycled water.

### 3.7 Automated mineralogy with Scanning Electron Microscope (SEM)

The University of Liège has a new generation ZEISS Sigma 300 scanning electron microscope and mineral analyzer. The instrument is equipped with two Bruker xFlash 6|30 X-ray detectors for analysis by energy-dispersive X-ray spectroscopy (EDS). The system also provides further texture related information like grain size, a mineral associated, liberation degree, and Bright Phase Search (BPS). When analyzing a sample, an electron beam examines the surface of the polished section, resulting in the production of x-ray and backscatter electron (BSE), collected by a detector that transfers the output to load software which converts and evaluate the received data to a user-friendly interface. The name of the software is Mineralogic Mining V1.03. In this study, modal analysis and liberation analysis was carried out to identify the available minerals and BPS mode was used for searching gold and silver which provide BSE contrast against gangue minerals. The operating conditions were an acceleration voltage of 20 kV and a current of 20 nA; the working distance has been adjusted to 8.5mm; the analysis mode was the Mapping mode giving a complete analysis of the sample

## 4 Result and Discussion

### 4.1 Mineralogical Characterization

The main objective of the mineralogical characterization is to evaluate the mode of occurrence and liberation degree of gold and gangue minerals in various samples from the testing. Also, to investigate the associate minerals of native and electrum as to evaluate the performance of flotation.

The samples (Ore, concentrate, tailings) obtained from DPM-Krumovgrad were analyzed using reflected light optical microscopy, X-ray diffraction, and automated mineralogy analysis. The chemical reconciliation after the SEM analysis was done using X-ray fluorescence. Furthermore, -20 $\mu$ m fraction of the tailing sample was separated using available micro sieve at the DPM laboratory. The automated mineralogical analysis was performed to identify the available minerals in the fine fraction that influence the efficiency of the sedimentation.

#### 4.1.1 Optical Microscope Analysis

The two samples from each ore, concentrate, and tailing was analyzed to identify the available minerals and their phases. The ore sample predominantly consists of goethite and pyrite as shown in Figure 31 (a) and (b). Most of the pyrite has been converted to goethite or rutile during the oxidation process. This can be easily concluded by observing the occurrence of pyrite in the middle of goethite grain or possible rutile grains. Apart from that, covellite, native gold, and native copper grains were identified and shown in Figure 32. The availability of Cu has been verified by the XRF result (42.2ppm). The size of identified gold was about 15-20 $\mu$ m and goethite grains have a wide range from ultrafine grains up to 100 $\mu$ m.

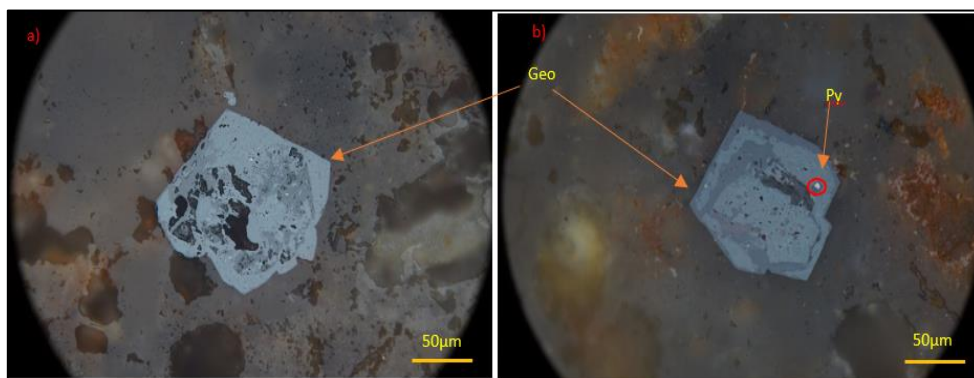


Figure 31: a) Goethite grains (light blue) and possible rutile grain oxidized from pyrite during the oxidation; b) another goethite grain shows the clear result of oxidation as pyrites grain are visible in the middle of the goethite grain.

According to literature (P. Marchev. 2004) about the Ada Tepe deposit, the mineralogy of the deposit is simple, mainly, gold occurs as electrum with 73-76% Au and rest Ag. The main gangue minerals consist of silica polymorphs which are microcrystalline, fine-grained, sugary quartz, and opaline silica. Also, carbonates (calcite, dolomite siderite, and ankerite) and adularia. Chlorite, calcite, kaolinite, and subordinate albite, pyrite, and ankerite-dolomite are also available due to the hydrothermal alteration.

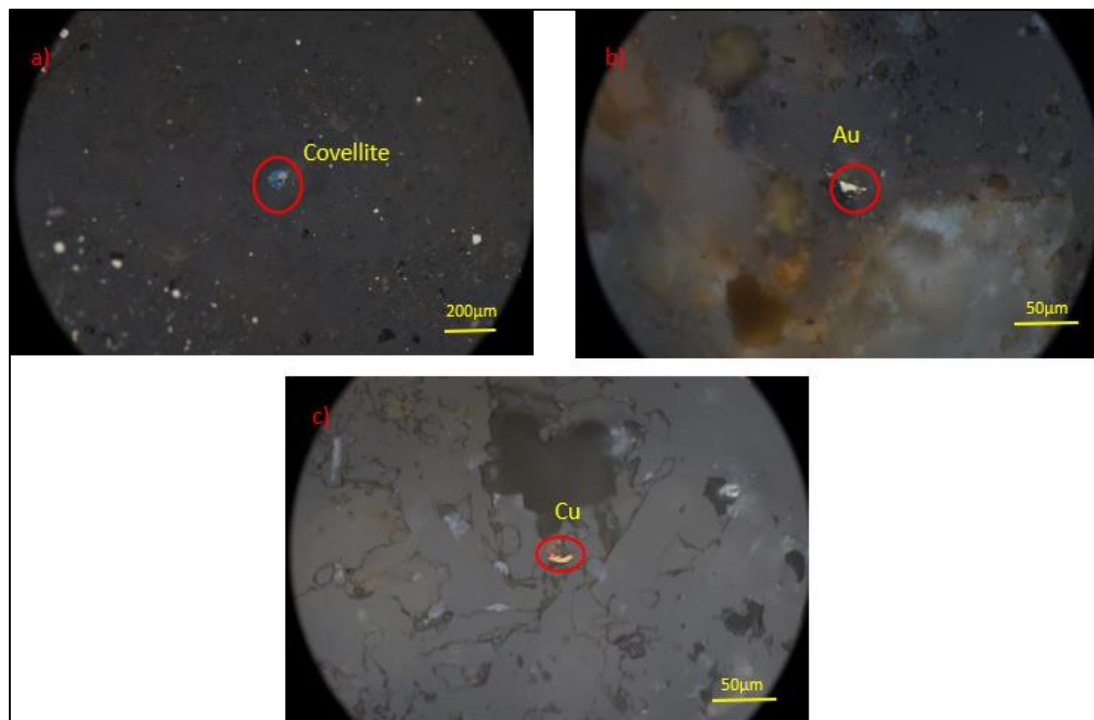


Figure 32:a) occurrences of covellite b) native gold and c) native copper in an ore sample

The sample of flotation concentrate mainly consists of pyrites and electrum as shown in Figure 33. Few graphite grains were also identified during the analysis. The only visible gangue in the tailing is goethite from the size range 50µm to less than 5µm as shown in Figure 34. According to the XRF result, about 4.92% of Iron oxide and 63.8% of silicon dioxide are available in the tailing sample.

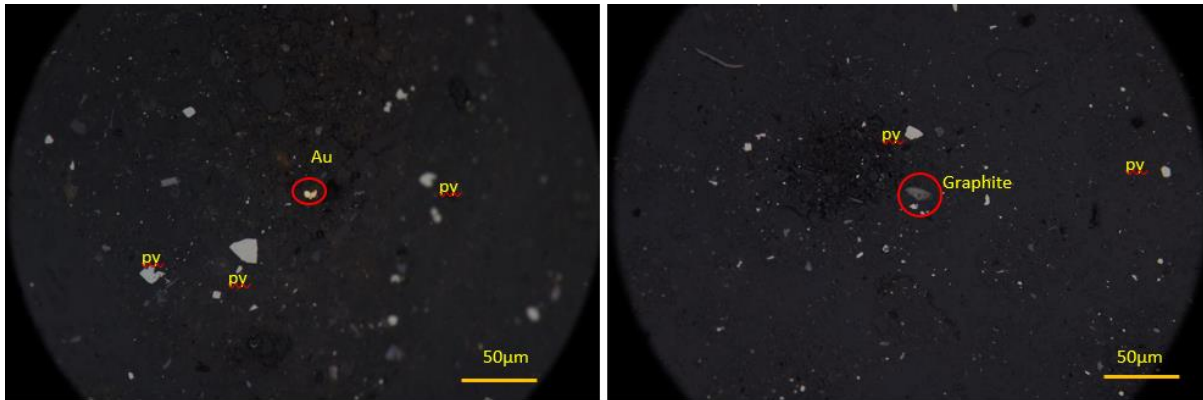


Figure 33:Microscopic view of flotation concentrate consists of pyrite, gold, and graphite

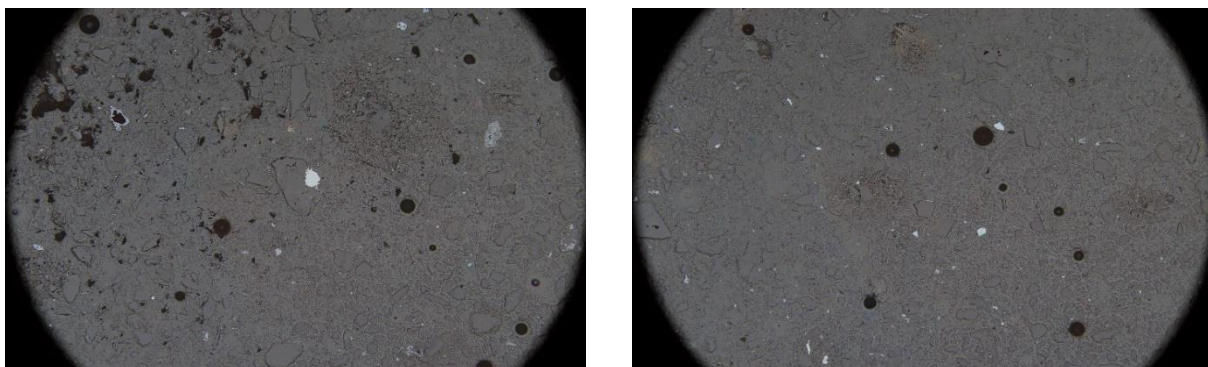


Figure 34:Microscopic view of flotation tailing

#### 4.1.2 XRD result

From Figure 35, Figure 36 and, Figure 37, it can be observed that all samples exhibit similar peaks attributable to quartz, muscovite, sanidine, kaolinite, and some calcite and pyrite.

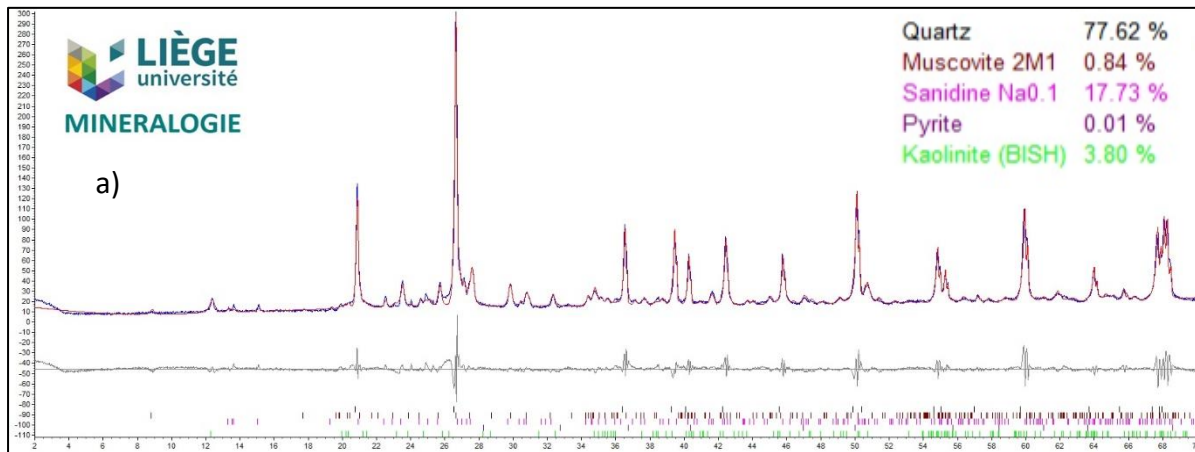


Figure 35: XRD analysis of Ada Tepe ore sample

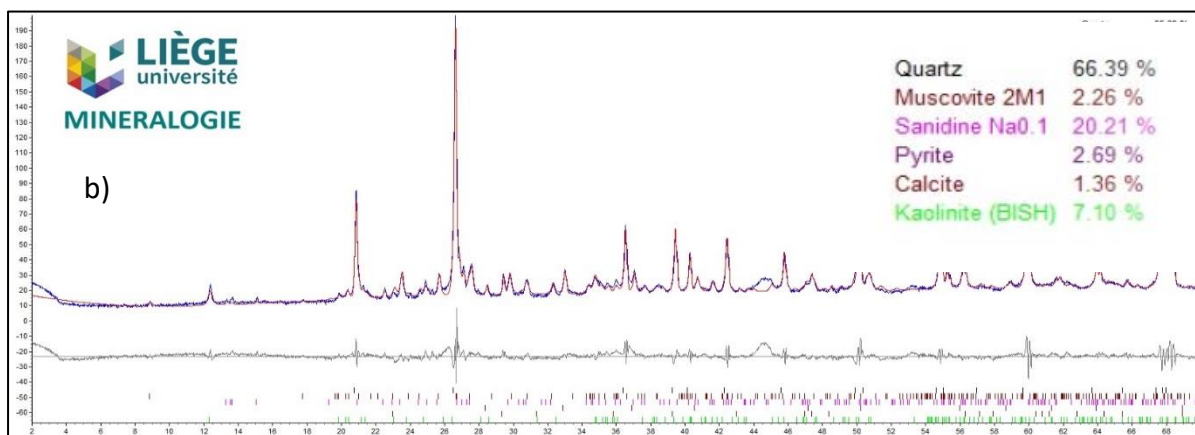


Figure 36: XRD analysis of concentrate sample

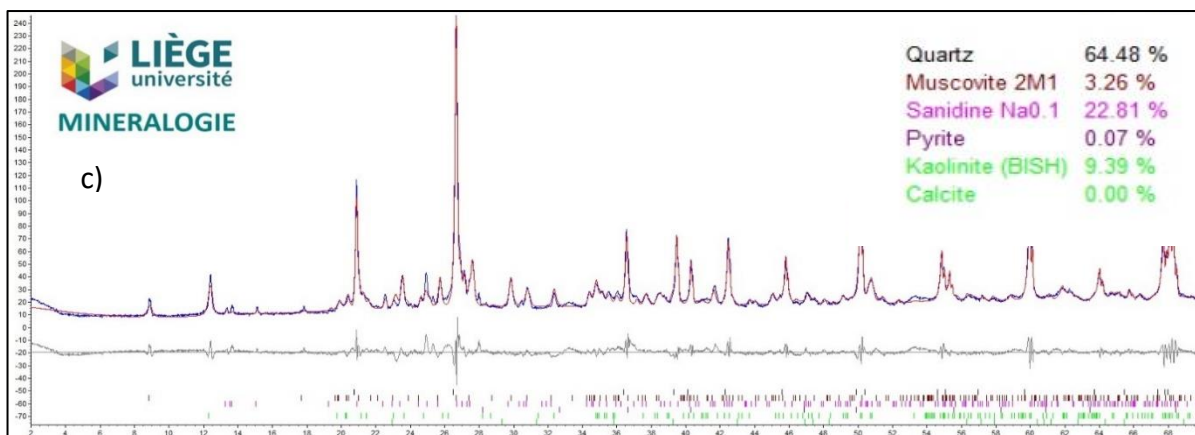


Figure 37: XRD analysis of tailing sample

#### 4.1.3 Particle size distribution

The particle size distribution of a tailing collected during the five consecutive days at the site is presented in Figure 38 below.

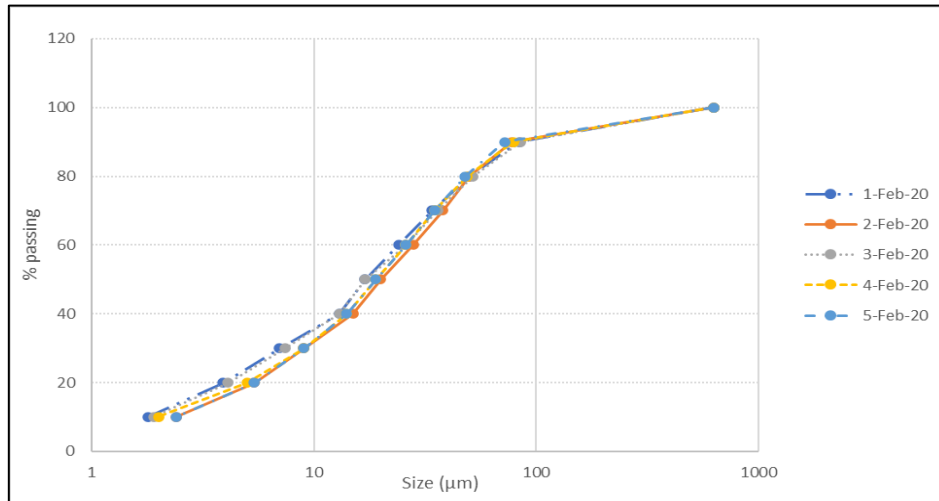


Figure 38: The granulometry of tailing sample

Observing the PSD result above, about 50% of particles are below 20μm which is considered as size that reduces the setting rate, thus sedimentation efficiency. Further investigations are required to identify the weight % of available minerals.



## 4.2 Modal mineralogy and liberation of the ore, concentrate, and tails

Figure 39 shows the modal mineralogy of the ore, concentrate +20 $\mu$ m tailing, -20 $\mu$ m tailing, and the reconstructed tailing samples. According to the graph, the quartz and orthoclase are the most abundant gangue minerals in each fraction. Also, a significant percentage of Fe-oxides can be seen in the concentrate as well as -20  $\mu$ m tailing fraction. Each of these minerals carries a variety of elements, including Al, K, Si, which influence the stability of fine solid in the tailing, thus the settling behavior of the particles. Altogether, those minerals occupied about 80-95 % w of the mineral composition of each fraction. Identification of most abundant gangue minerals in the -20  $\mu$ m tailing fraction is crucial to identify the fine generating minerals in the tailing as suspended fine solids cause high turbidity of the supernatant water. This because of negligible settling velocity and high stabilization period due to decreasing gravity with increasingly pronounced colloidal interaction and decreasing particle size (Chen Wang, 2014). Mainly quartz grains at 57.36% wt, orthoclase grains at 28.88 % wt, and 6.82 % wt Fe-oxide are presented in the -20  $\mu$ m tailing fraction.

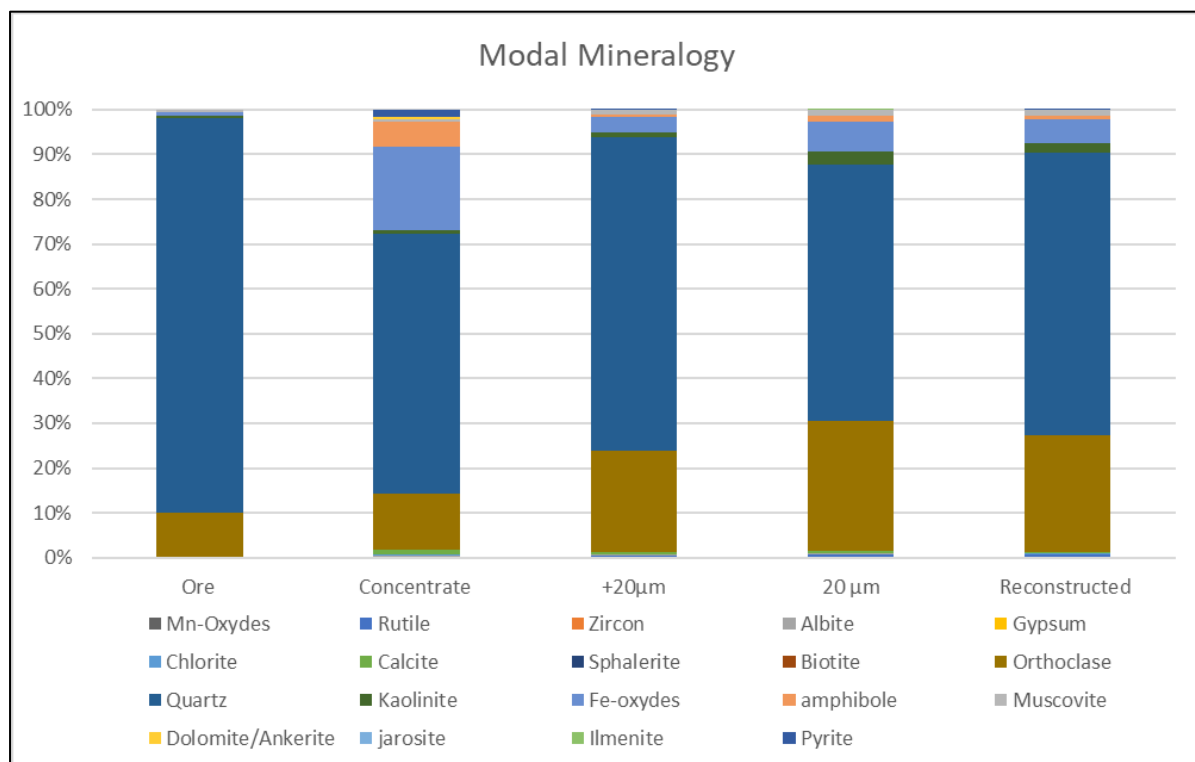


Figure 39: Modal mineralogy of ore, concentrate, and two size fractions of tailing

The liberation degree and the associated minerals with the native gold and electrum are important in view to investigate the flotation performance. Figures below show the SEM images of some selected samples from ore, concentrate, and the tailings. Figure 40 shows the

availability of native gold and electrum in the ore sample as marked. These grains are 100 % liberated. Also, the sizes of the grains are below 10  $\mu\text{m}$ .

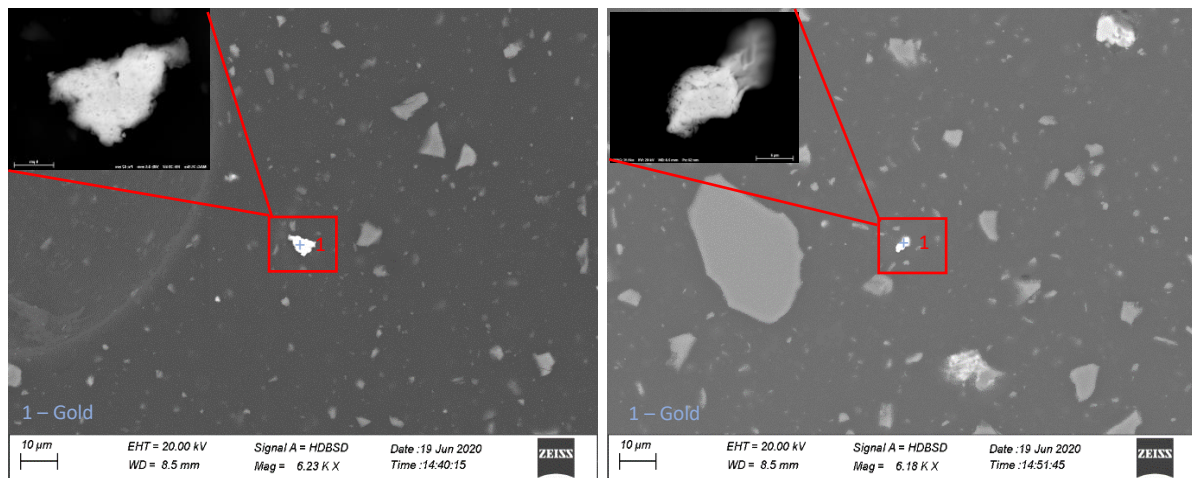


Figure 40: SEM image of the ore sample indicate the availability of gold (left) and electrum (right)

Figure 41 shows the electrum lost in the tailing associated with quartz and kaolinite. The grain size of this electrum is also below 10  $\mu\text{m}$  and they are 100 % locked. This result indicates that there are some gold and electrum associated with the quartz lost to the tailing reducing the recovery of the gold. The grain size of associated gangue minerals in the tailing is mostly above 100  $\mu\text{m}$  and it is close to P90 of the tailing.

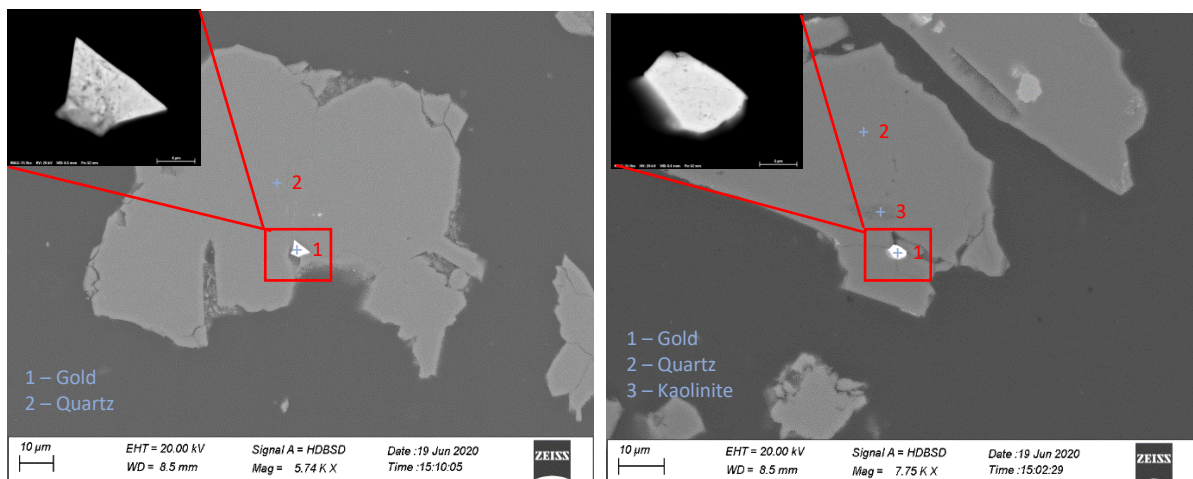


Figure 41: SEM image of tailing sample indicate the mode of occurrence of electrum and associate minerals.

Figure 42 below shows the gold and electrum grains available in the concentrate. About 86 of gold grains were identified and 12 % of total grains were associated with the quartz as seen in the figure. The size of the grains is below 10  $\mu\text{m}$ .

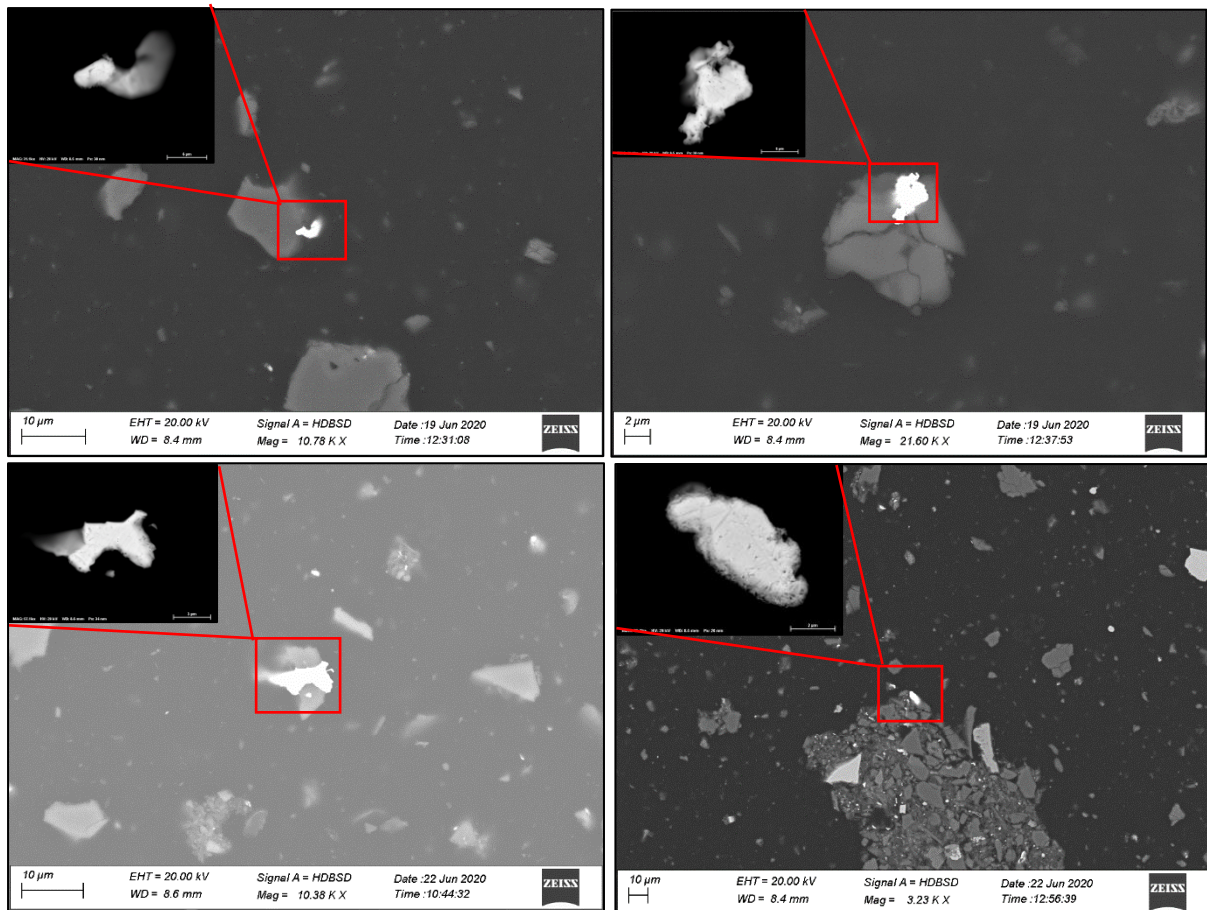


Figure 42: SEM image of concentrate sample indicate the mode of occurrence of gold and electrum grains.

The liberation analysis of minerals by a fraction is shown in Figure 43 below. These liberation curves show the percentage of the surface of certain grains exposed versus the cumulative percentage of grain mass meeting the certain liberation degree of those minerals ( L. Little et al., 2016). SEM-EDS commonly analyzes this result. According to the below figure, it can be observed that quartz is the mineral with the highest liberation degree in all fractions. At the same time, orthoclase and Fe-oxide have moderate liberation degree, but higher liberation in - 20 µm tailing fraction. The 100 % pure gold grain is 70 % liberated, while about 50 % of electrum grains are 60 % liberated in concentrate. They are associated with quartz and kaolinite as shown in the SEM images above. Another important information that we can observe is the increase in the liberation degree of kaolinite, orthoclase, and Fe-oxides in the tailing fraction. The liberation degree of 80 % of kaolinite has increased from about 20 % in the ore to 60 % in the tailing, while the liberation degree of 80 % of orthoclase has increased from about 35 % in the ore to 90 % in tailing.

Furthermore, the liberation degree of 80 % of Fe-oxide has increased from about 20 % in the ore to 60 % in the tailing. That suggests that those minerals are responsible for the generation

of most fine particles in the tailings which reduce the clarity of the recycled water. On the other hand, gold grains in the concentrate are moderately liberated while gold grains lost to the tailing are locked. Also, there are some locked silver grains found in the tailing.

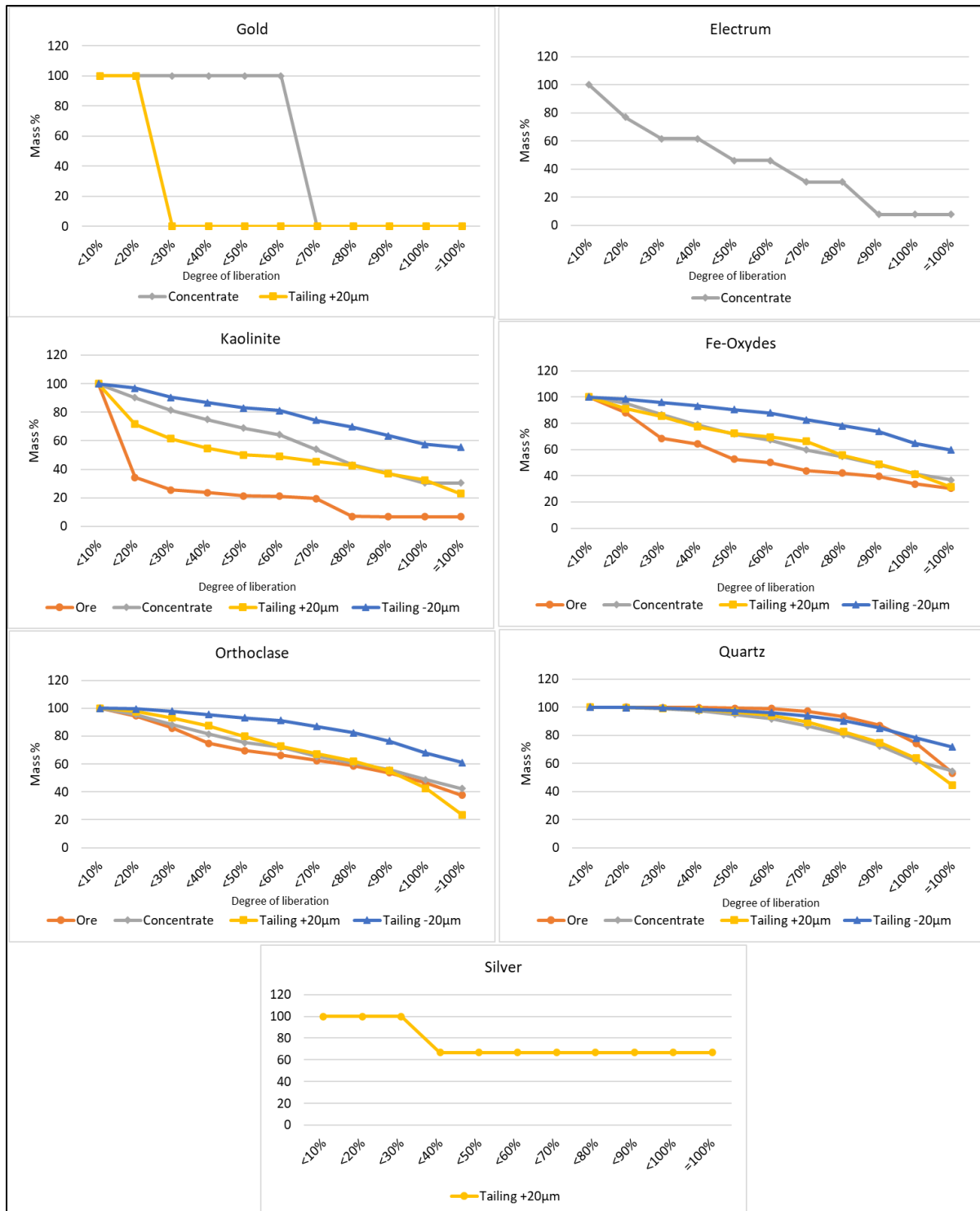


Figure 43: Cumulative liberation curves for gold, electrum, kaolinite, Fe-oxide, orthoclase, quartz, and silver by the fraction of ore, concentrate, tailing + 20 µm, and tailing -20 µm

#### 4.2.1 Optimization of coagulant and flocculant

The result obtained from the jar test is presented in tables and graphs below. Figure 44 shows the optimum dose of Magnafloc® 155 Ionic Polyacrylamide (PAM). The turbidity of water decreases with PAM dosages increase until reaching the optimum dosage of 32 mg/l and then turbidity increases. Overdosing causes the destabilization of the colloid particles. The turbidity at optimum dosage after 10 and 20 minutes is 22 and 19 FAU, respectively. This removal is a result of flocculation, which agglomerates colloidal particles by polymer bridging or charge neutralization, as previous studies have shown.

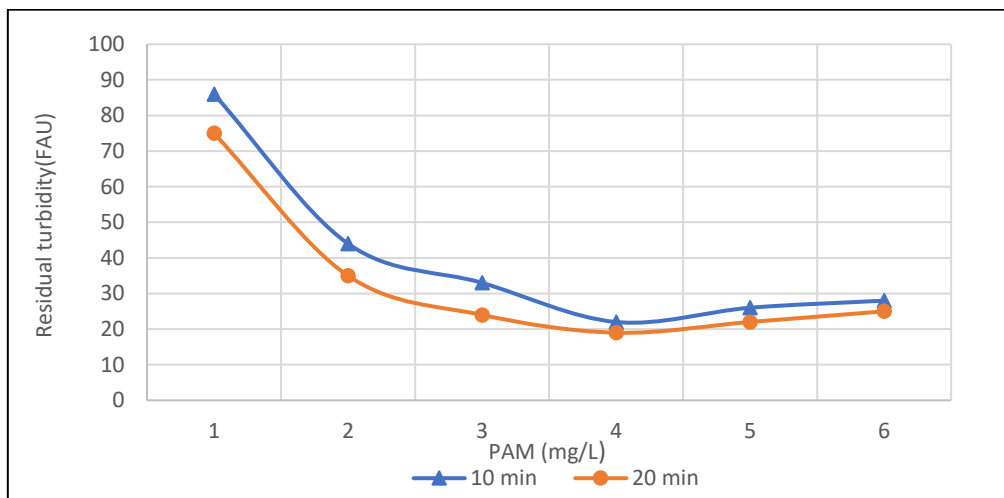


Figure 44: The effect of optimum dose of PAM on the removal of turbidity

Figure 45 shows the optimum dose of  $\text{FeSO}_4$  primary coagulant. The turbidity decreases with increasing dosages of  $\text{FeSO}_4$  until reaching to optimum dosage at 160-180 mg/l and then turbidity slightly increases with the addition of coagulant. The turbidity values at optimum dosage after 10 and 20 minutes are 79 and 17 FAU, respectively. This removal of particles is an effect of coagulation that neutralize the surface charge of the particles reducing the force of repulsion between colloidal particles and the distance between them to increase the attraction forces and Vander Vaal forces. This allows the particle to attach to each other, increasing the particle size, thus to settle fast. However, there is no significant difference in turbidity after 10 and 20 minutes.

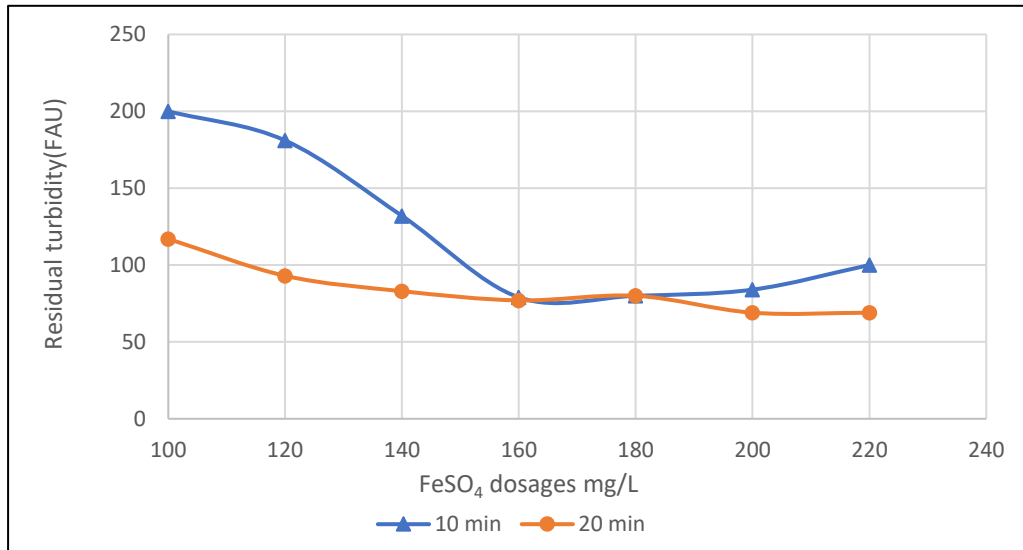


Figure 45: The effect of optimum dose of  $\text{FeSO}_4$  on the removal of turbidity

Figure 46 shows the effect from the optimum dose of  $\text{Al}_2(\text{SO}_4)_3$  primary coagulant. The turbidity decreases with increasing dosages of  $\text{FeSO}_4$  until it reaches the optimum dosage of 200 mg/l and then turbidity increases significantly with the addition of coagulant. The turbidity values at optimum dosage after 10 and 20 minutes are 41 and 27 FAU, respectively. Considering all coagulants,  $\text{Al}_2(\text{SO}_4)_3$  gives the lowest turbidity value at its optimum dosage. This might be due to the ionic value of the metal salt compared to other coagulants as stated in previous studies (Önel, Gocer, and Taner, 2018).

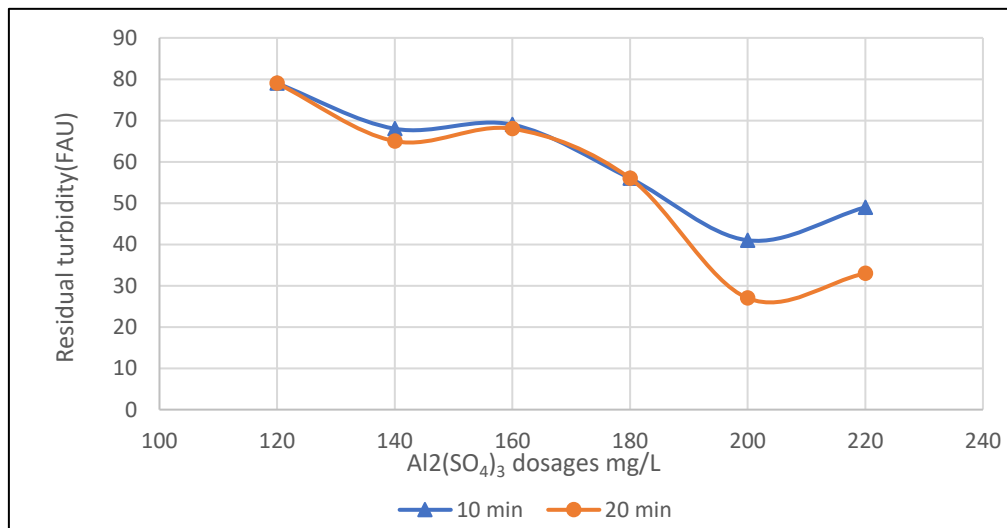


Figure 46: The effect of optimum dose of  $\text{Al}_2(\text{SO}_4)_3$  on the removal of turbidity

Figure 47 shows the effect from the optimum dose of  $\text{FeCl}_3$  primary coagulant. The turbidity decreases with increasing dosages of  $\text{FeCl}_3$  until it reaches an optimum dosage between 180 to 200 mg/l and then turbidity increases significantly with the addition of coagulant. The turbidity



values at optimum dosage after 10 and 20 minutes are 99 and 79 FAU, respectively. Even though the turbidity after a short time (10 minutes) increases with an excess coagulant, the turbidity after 20 minutes remains almost the same.

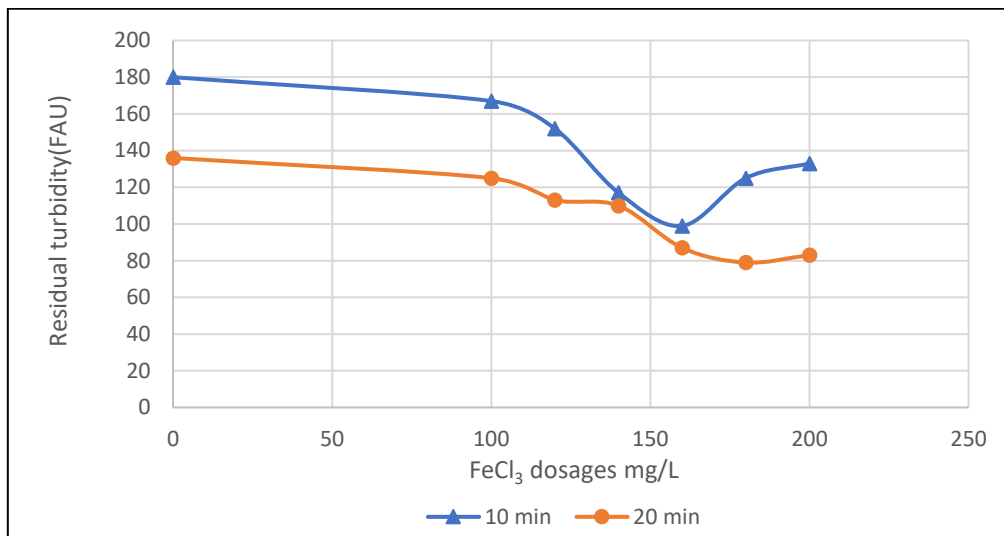


Figure 47: The effect of optimum dose of  $\text{FeCl}_3$  on the removal of turbidity.

Figure 48 shows the result on the effect from optimum dosages of PAM and  $\text{FeSO}_4$ . The turbidity of the supernatant considerably decreases with this combination compared to individual reagents. Also, it decreases the amount of PAM required to get the lowest turbidity value. Here, the lowest turbidity of 20 FAU is achieved with a combination of 160 mg/l coagulant and 28 mg/l flocculant, where optimum turbidity is higher even with 32 mg/l flocculant if the flocculant is used alone. That means that the coagulant helps to lower the flocculant requirement. This is because a combination of PAM with metal salt helps to remove some particles by neutralizing the surfaces which are not affected by the polymer. In contrast, other particles are agglomerated by polymer bridging.

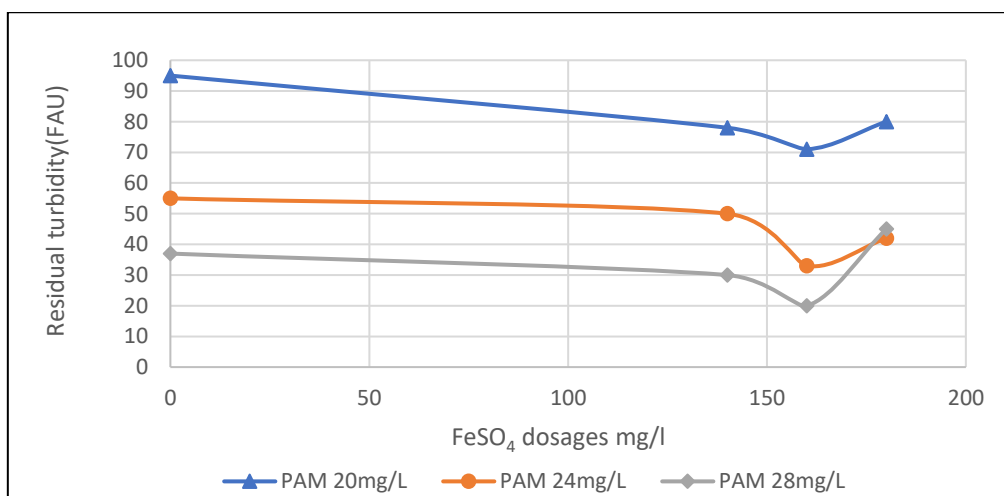


Figure 48: Effect of combining  $\text{FeSO}_4$  dose with the different doses of PAM on the turbidity.

Figure 49 shows the result using the optimum dosages of PAM and  $\text{Al}_2(\text{SO}_4)_3$ . In this combination also, the turbidity of the supernatant decreases compared to individual reagent performance. Also, it decreases the amount of PAM required to get the lowest turbidity result as other combinations. The optimum dosages of this combination are 180 mg/l and 28 mg/l for  $\text{Al}_2(\text{SO}_4)_3$  and PAM, respectively and the turbidity at optimum dosages is 25 FAU which is a bit high compared to the combination of PAM and  $\text{FeSO}_4$ .

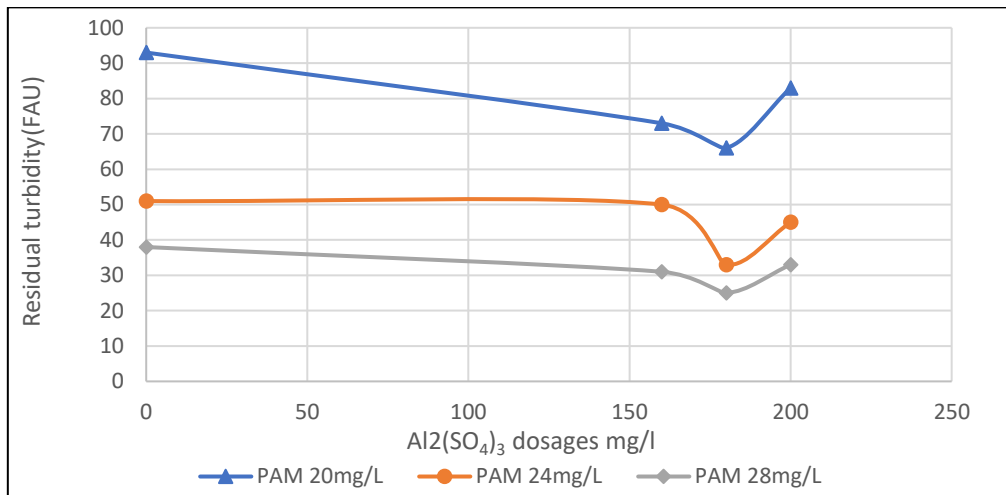


Figure 49: Effect of combining  $\text{Al}_2(\text{SO}_4)_3$  dose with the different doses of PAM on the turbidity

Figure 50 shows the result from optimum dosages of PAM and  $\text{Ca}(\text{OH})_2$  which give the lowest turbidity result out of all the settling aids but with higher dosages of coagulant compared to other coagulant dosages. The optimum dosage of  $\text{Ca}(\text{OH})_2$  is from 750-1000 mg/l, but the optimum turbidity values are almost the same with the different dosages of PAM. Also, it consumes the lowest dosage of PAM (24 mg/l) to achieve the lowest turbidity of all. Therefore, this combination can be used to reduce the number of polymers which are expensive compared to coagulant even though the dosage of  $\text{Ca}(\text{OH})_2$  is higher compared to other coagulants.

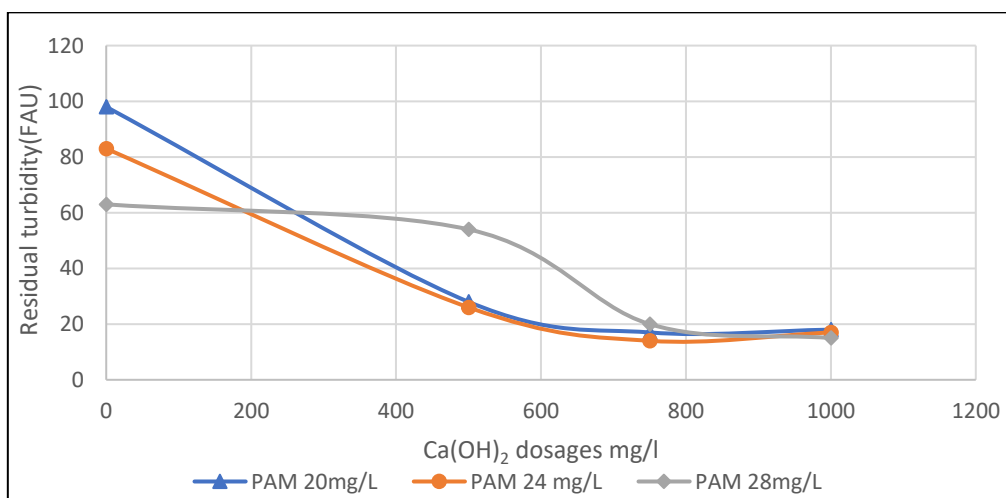


Figure 50: Effect of combining  $\text{Ca}(\text{OH})_2$  dose with the different doses of PAM



Table 4: Summary of settling aids optimization.

Coagulant/ Flocculant	Iron(II) sulphate	Aluminium sulphate	Iron(II) Chloride	PAM	PAM+ Al <sub>2</sub> (SO <sub>4</sub> ) <sub>3</sub>		PAM+ FeSO <sub>4</sub>		PAM+ Ca(OH) <sub>2</sub>	
					PAM	Al <sub>2</sub> (SO <sub>4</sub> ) <sub>3</sub>	PAM	FeSO <sub>4</sub>	PAM	Ca(OH) <sub>2</sub>
Opt. dosage (mg/l)	160	200	180	32	28	180	28	160	24	750
Turbidity (FAU)( after 20 min)	77	27	87	19	25		20		14	
pH	6.93	7.56	6.67	7.9	7.65		7.66		11.1	

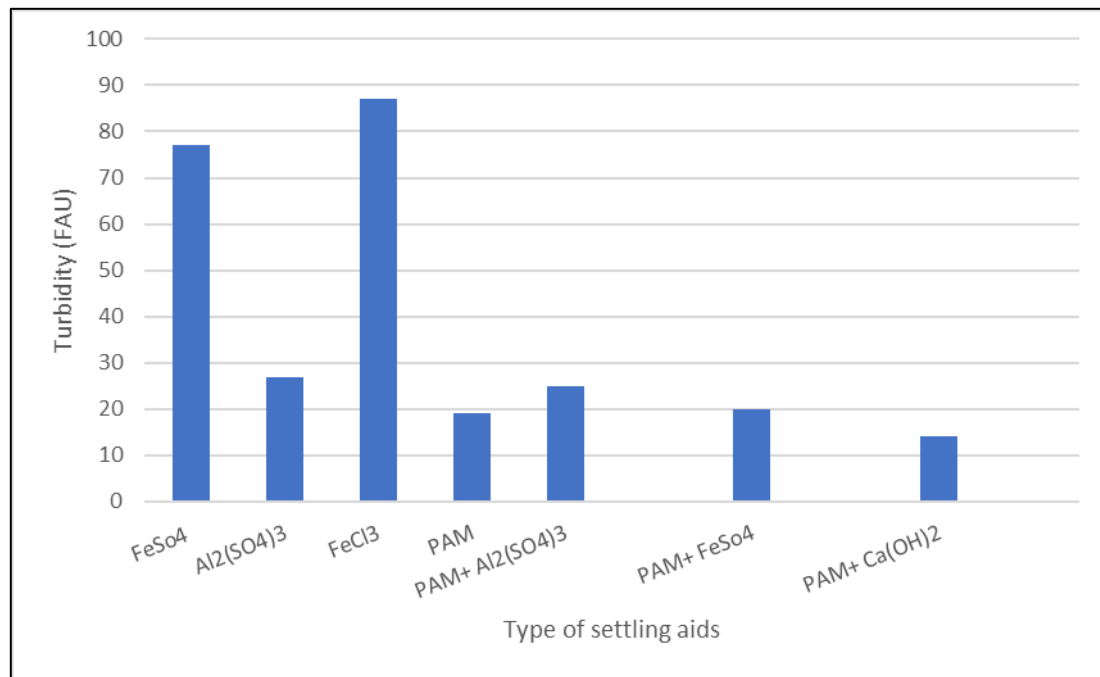


Figure 51: Graphical representation of settling aids optimization

Table 4 and Figure 51 present a summary of the test where the combination of PAM and Ca(OH)<sub>2</sub> has the lowest turbidity at all with the lowest dosage of PAM, but a higher dosage of Ca(OH)<sub>2</sub> compared to the other combinations. However, this combination could still be better considering not only the solid-liquid separation but also the economical perspective. Because flocculants are quite expensive compared to coagulant and reduction of flocculant dosage can reduce the operation cost even though the dosage of Ca(OH)<sub>2</sub> is higher compared to the other coagulant. Overall, these results imply that the combination of coagulant with flocculant could improve the efficiency of solid-liquid separation in thickeners rather than using a flocculant alone. Some previous studies by (Önen et al. 2018) and (Thamer J. Mohammed & Eman Shakir, 2018) have proved the high efficiency of the combination of coagulant and flocculant on solid-liquid separation. A recent literature review article concentrates on the use of PAM-based flocculants and/or cationic coagulants, as mentioned in (Soares, 2015).

#### 4.2.2 Effect of coagulant and flocculant on slurry pH

The natural pH value of tailing suspension is approximately 7.9. Due to the acidic behavior of  $\text{FeCl}_3$ ,  $\text{FeSO}_4$ , and  $\text{Al}_2(\text{SO}_4)_3$ , pH decreased by increasing coagulant concentrate (Figure 52). At optimum dosages, pH becomes 6.93, 7.56, 6.67 with  $\text{FeSO}_4$ ,  $\text{Al}_2(\text{SO}_4)_3$ ,  $\text{FeCl}_3$ , respectively. On the other hand, there is no significant change in pH when using anionic flocculant and the pH range is 7.9 to 8.2.

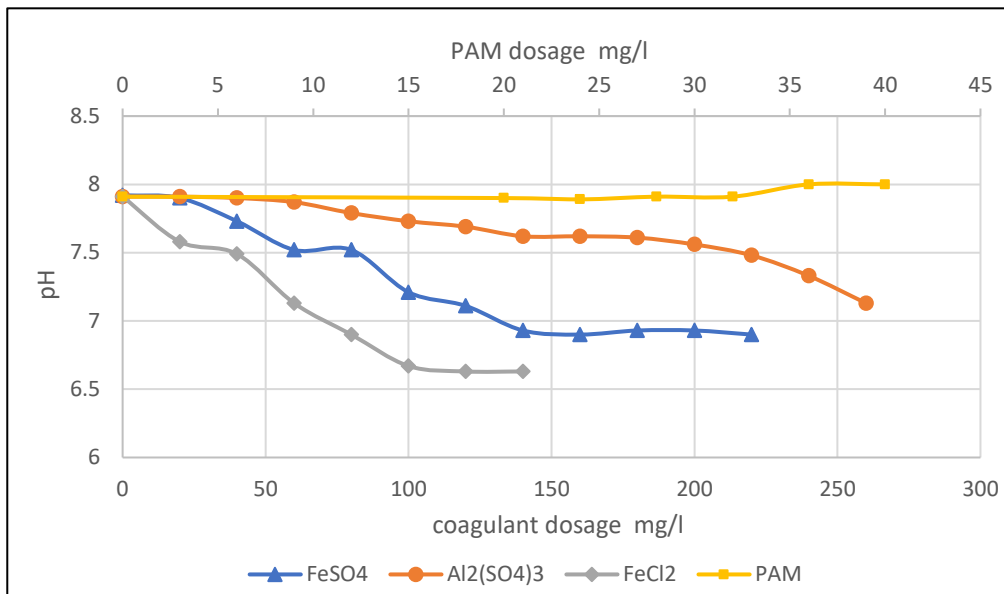


Figure 52: Effect of coagulant and flocculant on suspension pH

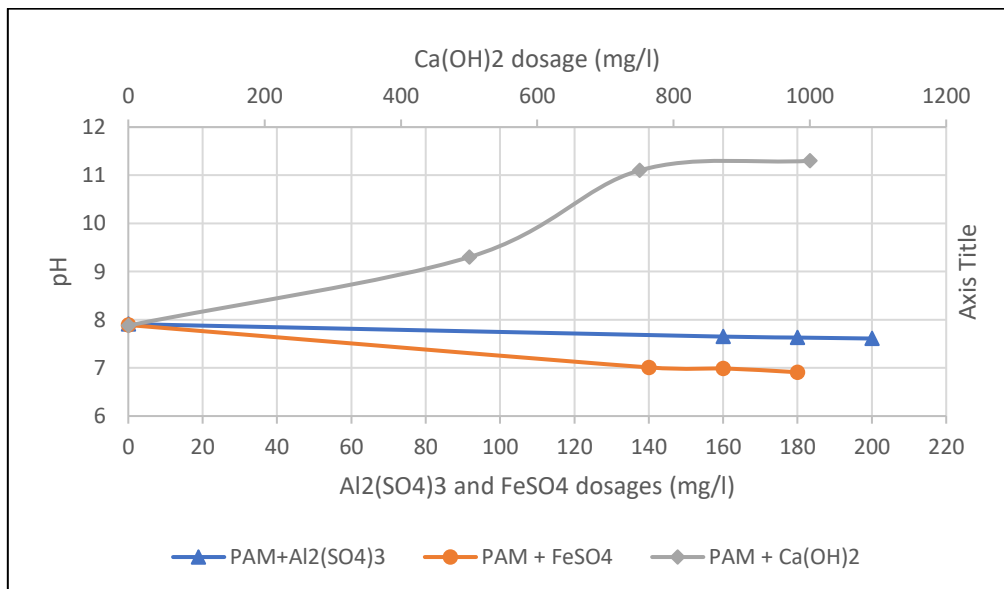


Figure 53: Effect of the combination of coagulant and flocculant on suspension pH

Furthermore, Figure 53 shows the effect of the combination of flocculant and coagulant on the pH of the suspension, and it can be seen that the results are slightly similar to the results obtained with coagulant alone. It concludes that the flocculation can be effective in a wide range of pH and does not provoke changes in the suspension pH value. However, the addition of  $\text{Ca(OH)}_2$  has increased the pH of the suspension up to 11.3 giving optimum 11.1 at optimum dosage of PAM (24mg/l) and  $\text{Ca(OH)}_2$  (750mg/l).

### 4.3 pH optimization

The turbidity of supernatant water from the jar test with certain settling aids at different pH range is illustrated in Figure 54 and Figure 55 below. Turbidity was measured after 10 and 20 minutes

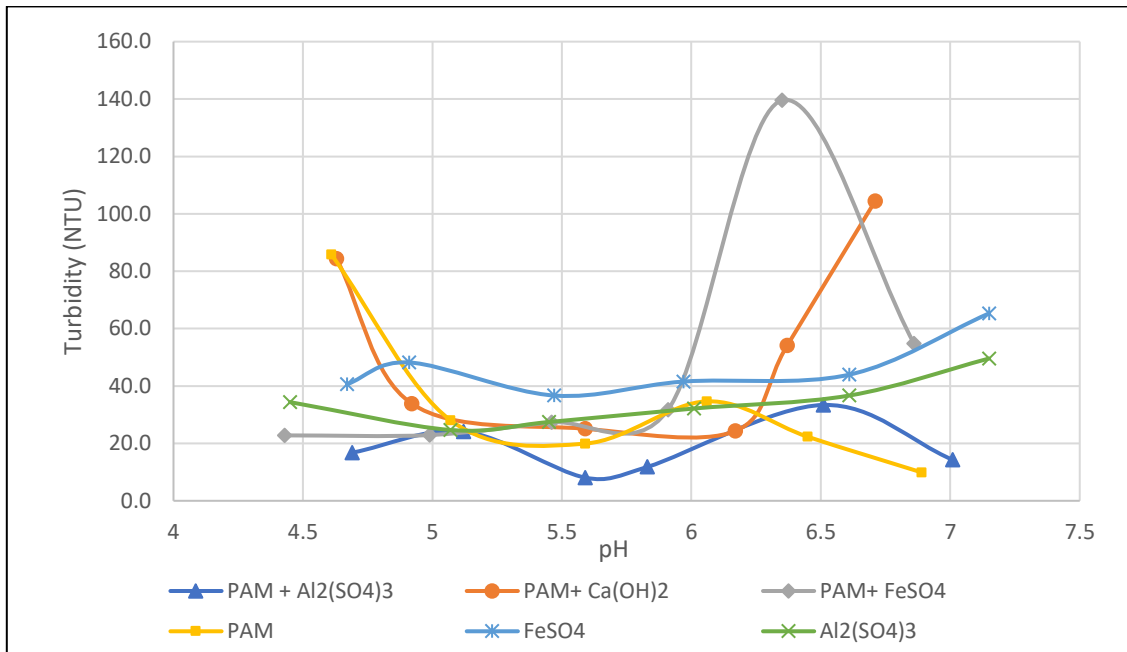


Figure 54: Effect of slurry pH on solid-liquid separation efficiency with different coagulant and flocculant (after 10 minutes)

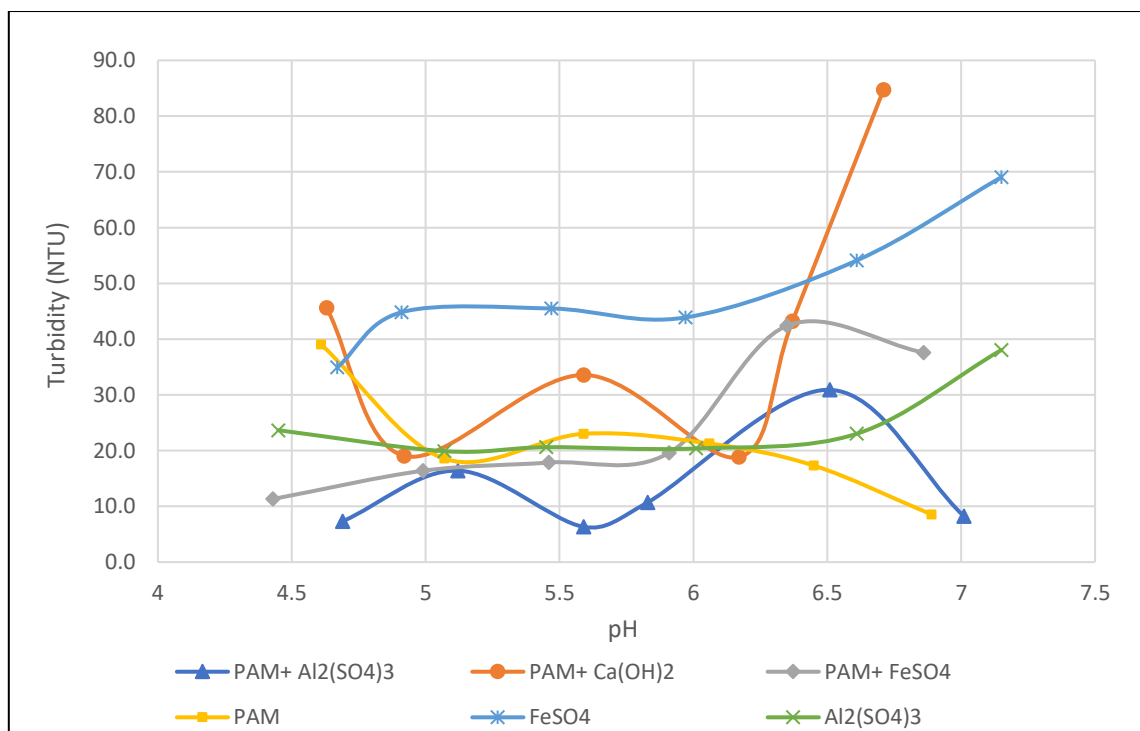


Figure 55: Effect of slurry pH on solid-liquid separation efficiency with different coagulant and flocculant (after 20 minutes)

According to the above figures, it is visible that all coagulants, flocculants, and their combination gave low turbidity within the range of pH 5.25 to pH 6. Therefore, this range could be considered as an optimum pH range for the effective solid-liquid separation. The natural pH of scavenger tailing at the DPM plant is 7.9. This value is quite close to the pH of natural kaolin suspension (7.86) (Önel, Gocer, and Taner, 2018). Therefore, characteristics of the scavenger slurry could be assumed as similar to the kaolin suspension, considering the availability of clay minerals such as kaolinite, orthoclase, and quartz. Furthermore, the typical pH at IEP of kaolin suspension within the range of 2.8 to 4.2 pH. (F. Miu et al. 2013; B. Ndlovu et al. .2015). The IEP of highly presence quartz is also about 2.2 (Besra, Sengupta, and Roy, 2000) That means; it can be assumed that the IEP of the scavenger tailing is also within this range. However, past studies have proved that the efficiency of coagulation is high when the suspension zeta potential is approaching the point of zero charges (IEP) as lower zeta potential reduces the repulsion forces particles allowing them to agglomerate. (Besra, Sengupta, and Roy, 2000).

Also, another past study has proved that the addition of coagulant decreases the zeta potential of the mineral surface due to the positive charge of the ions (Önel, Gocer, and Taner, 2018). As a result of this, the addition of coagulant to the slurry at 5-6 pH might reduce the pH of slurry up to IEP of the slurry resulting in higher efficiency and the settling of the suspended colloidal particles, but the addition of  $\text{Ca(OH)}_2$  increases turbidity at slurry pH above 6.25. The addition of flocculant does not significantly affect the zeta potential since the polymer bridging mechanism plays a significant role in flocculation.

Overall, these result shows that the turbidity of the supernatant water with  $\text{FeSO}_4$  is higher compared to the result from other coagulants and flocculants at any pH value. Also, the result obtained from the combination of flocculant and coagulant shows a little rise around pH 6.5 and then gradually decrease the turbidity. It might be due that the dominant mechanism of agglomeration of the particle is polymer bridging rather than neutralization. According to this result,  $\text{PAM} + \text{Al}_2(\text{SO}_4)_3$  can be considered as an optimum combination in terms of efficiency of the solid-liquid separation and the clarity of the recycled water at the natural pH of the tailing. But the combination of  $\text{PAM} + \text{Ca(OH)}_2$  would be effective in terms of cost due to lower dosage of PAM which is more expensive compare to the coagulant.

#### 4.4 Settling rate result.

The initial sedimentation rate of a suspension is an important parameter to evaluate the settling speed and stability of a colloidal system. The initial sedimentation rate was computed via a graphical procedure described by Ji et al. (2013). In this approach, mud-line height plots (e.g., Figure 23) were reproduced with elapsed time and a straight line was drawn from the origin (time = 0) that follows initial sedimentation behavior. The slope of the straight line represents the initial sedimentation rate (see annexes). The summary of the settling rate measurement is plotted in Figure 56. The calculated initial settling velocity (m/hrs) are shown in Table 5.

Table 5: Initial settling rates of flocs with different coagulant, flocculant and their combination

Type of settling aids	Initial setting velocity(m/hr )
PAM	3.36
FeSO <sub>4</sub>	0.18
Al <sub>2</sub> (SO <sub>4</sub> ) <sub>3</sub>	0.06
FeCl <sub>3</sub>	0.12
Ca(OH) <sub>2</sub>	0.48
PAM + FeSO <sub>4</sub>	5.04
PAM + Al <sub>2</sub> (SO <sub>4</sub> ) <sub>3</sub>	5.52
PAM + Ca(OH) <sub>2</sub>	5.52

It could be seen that the best sedimentation velocity provoked by individual coagulants was achieved with Ca(OH)<sub>2</sub>, which causes a settling rate of 0.48 m/hours. The second-best sedimentation velocity was calculated for FeSO<sub>4</sub>, which settled at 0.18 m/hours. All the combinations of PAM and salt have reached a significantly higher initial settling rate compared to the inorganic coagulants. Even though the combination of PAM with Al<sub>2</sub>(SO<sub>4</sub>)<sub>3</sub> and Ca(OH)<sub>2</sub> have reached approximately the same velocity (5.52 m/hours), this velocity with PAM + Ca(OH)<sub>2</sub> was achieved at a low dosage of PAM (24 mg/l) compared to PAM + Al<sub>2</sub>(SO<sub>4</sub>)<sub>3</sub>. However, rapid sedimentation may result in higher supernatant turbidity. But, a slower sedimentation velocity will result in more stable sedimentation, so supernatant turbidity may also be lower (e.g., settling velocity of tailing with Al<sub>2</sub>(SO<sub>4</sub>)<sub>3</sub> is slower compared to the other coagulant but still, the turbidity at optimum condition is higher compared to other coagulants). In other words, the conditions where the sedimentation velocities are optimum may not produce the same result for turbidity also. As a summary, the initial settling rate of the tailings with a single coagulant or flocculant is significantly slower compared to the settling rate with flocculant and coagulant together. The PAM+ Ca(OH)<sub>2</sub> can be considered as the optimum combination considering the dosages and turbidity results. The past study by (P. Mpofu, 2003) has also reported how prior addition of divalent cations (Mn<sup>2+</sup>, Ca<sup>2+</sup>) that undergo hydrolysis

to a monovalent complex ( $(\text{MnOH})^+$ ,  $\text{Ca}(\text{OH})^+$ ) resulted in increased settling rates for kaolinite flocculation by anionic PAM because adsorbed cations facilitated polymer bridging due to both electrical double-layer compression and zeta potential reduction

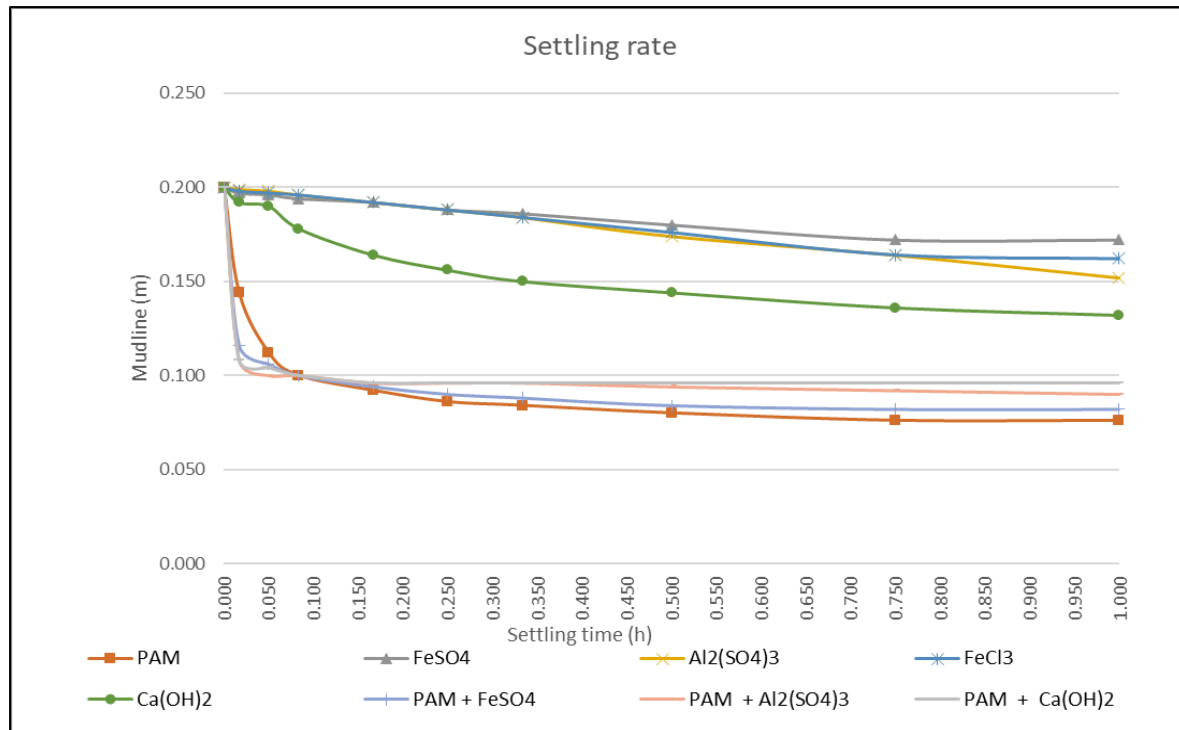


Figure 56: Summary of settling rate measurement

View of sedimented sludge with a flocculant (Figure 57) and a combination of both flocculant and coagulant (Figure 58) are presented below. Larger flocs sizes were obtained with polymers than coagulant due to the higher molecular weight of the polymers. This gives faster settling of particles than coagulation. In contrast, coagulation, or combination of coagulation with flocculation, gives smaller flocs, but high residual turbidity. These photos show that the compaction of sediment bed is better with a combination of coagulant and flocculant rather than a single flocculant.

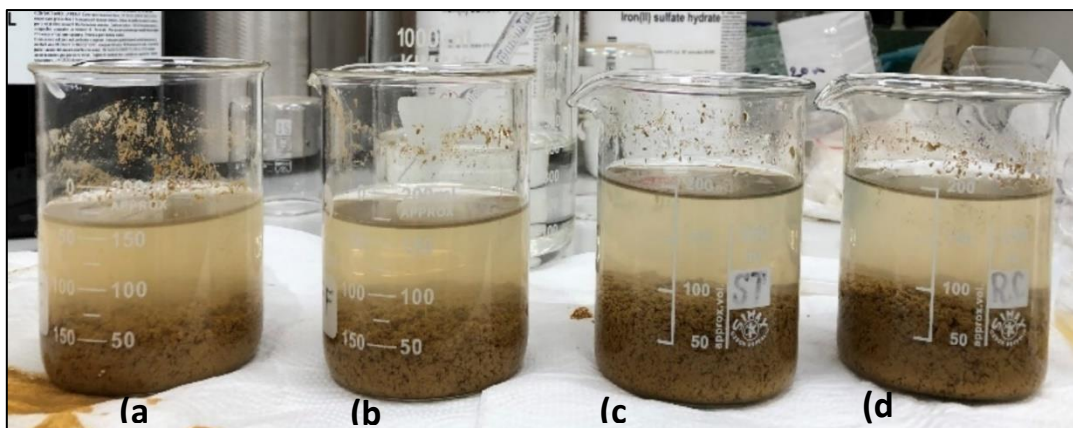


Figure 57: View of Sedimented Sludge with (a) 20 mg/ l (b) 24 mg/l (c) 28 mg/l (d) 32 mg/l of flocculant (PAM)

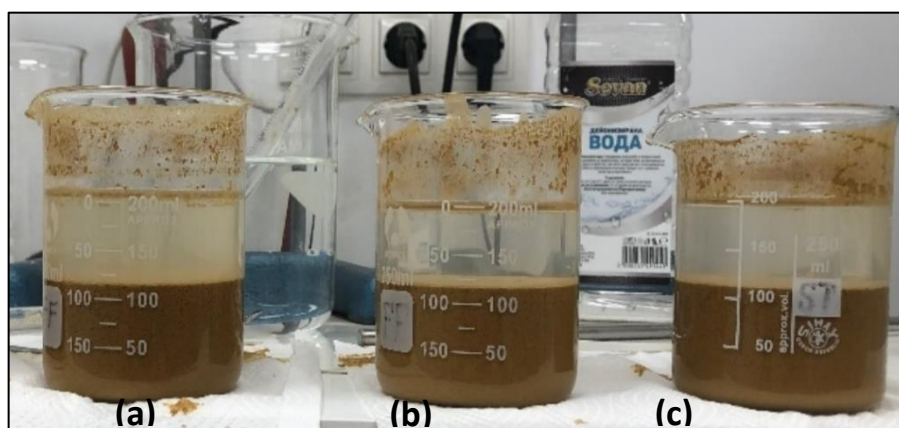


Figure 58: View of sedimented sludge with (a) 28mg/l of PAM + 500 mg/l of  $\text{Ca(OH)}_2$ ; (b) 28mg/l of PAM + 750 mg/l of  $\text{Ca(OH)}_2$ ; (c) 28mg/l of PAM + 1000 mg/l of  $\text{Ca(OH)}_2$

Figure 59 below shows the height of the sedimented sludge of the sediment with the use of different combinations between flocculant and coagulant. It shows that a combination of PAM +  $\text{FeSO}_4$  achieves better compaction of sediment bed compared to the other combination. Still, the settling rate with this combination is lower compared to the combination of PAM+ $\text{Ca(OH)}_2$ .

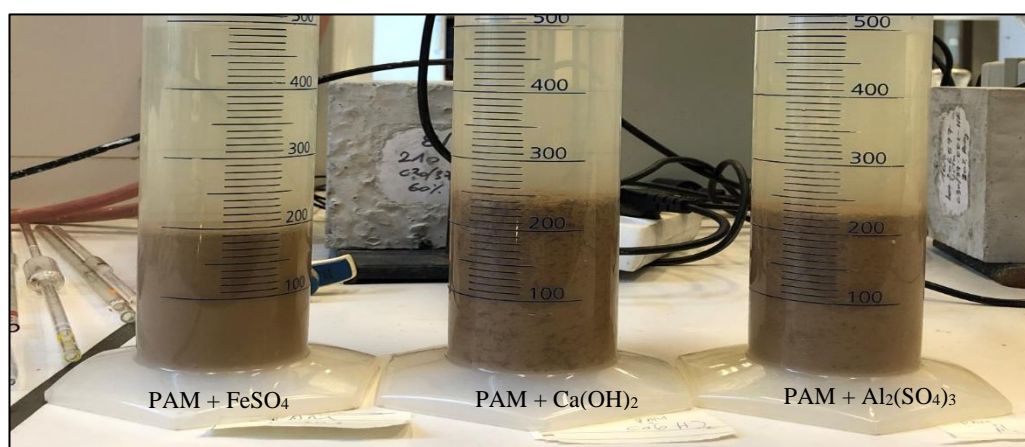


Figure 59: Height of sedimented sludge of tailing with PAM+ $\text{FeSO}_4$ , PAM+ $\text{Ca(OH)}_2$ , and PAM+  $\text{Al}_2(\text{SO}_4)_3$



#### 4.5 Process water characteristics

The chemical analysis of process water at the DPM plant is presented in Table 6 below. Considering the result, it can be observed that K, Ca, Na, and  $\text{SO}_4^{2-}$  have higher concentration compared to other ions, but it does not exceed too much the baseline concentration. Based on the concentration of the elements below, synthetic process water was made.

Table 6: Chemical analysis of Process water, Tailing thickener overflow, and concentrate thickener

Test Parameter	Unit	Process water	Tailing thickener O/F	Conc: thickner O/F
Metals				
Aluminium (Al)	µg/l	11.6±2.3	5.06±1.01	9.51±1.90
Iron (Fe)	µg/l	251±50	2.45±0.49	298±60
Potassium (K)	mg/l	55.4±11.1	52.7±10.5	50.7±10.1
Calcium (Ca)	mg/l	36.9±7.4	35.7±7.1	46.7±9.3
Magnesium (Mg)	mg/l	12.4±2.5	12.1±2.6	17.5±3.5
Manganese (Mn)	µg/l	1472±294	494±99	1538±308
Sodium (Na)	mg/l	119±24	113±23	110±22
Silicate ( $\text{SiO}_2$ )	mg/l	9.40±1.88	9.61±1.92	9.55±1.91
Anionic analysis				
Fluoride ( $\text{F}^-$ )	mg/l	1.53±0.15	1.52±0.15	1.55±0.16
Sulfate ( $\text{SO}_4^{2-}$ )	mg/l	264±13	263±13	231±12
Phosphate ( $\text{PO}_4^{3-}$ )	mg/l	0.789±0.039	0.353±0.018	0.182±0.009
Chloride ( $\text{Cl}^-$ )	mg/l	27.5±2.8	28.4±2.8	25.7±2.6
Nitrate ( $\text{NO}_3^-$ )	mg/l	3.00±0.15	2.77±0.14	2.80±0.14
Nitrite ( $\text{NO}_2^-$ )	mg/l	0.055±0.003	0.078±0.004	0.008±0.001
Total Dissolved Solids (TDS)	mg/l	572±29	522±26	412±21

## 4.6 Flotation trials

The grade and the recovery for Au and Ag achieved at bench flotation trials using actual process water ( Flot 1 and Flot 2), synthetic process water (Flot 3), and supernatant water obtained by two thickener water simulation (Flot 5 and Flot 6) are presented in Table 7 below. The thickener water simulation for the Flot 5 was done with a currently used flocculant (PAM). In contrast, the water simulation for Flot 6 was done using the optimal combination obtained by the jar test ( PAM+  $\text{Ca}(\text{OH})_2$ ). The result from the flotation trial no.3 was excluded from the discussion due to an unrealistic result obtained due to the degradation of collectors (PAX). However, trial number 4 was also carried out with the same conditions as trial no three but with freshly prepared PAX, and the result was realistic.

Table 7: Grade and Recovery of Au and Ag from the performed flotation trial

Trial Number	Au (g/t)	Au recovery (%)	Ag (g/t)	Ag recovery (%)
Flot 1	81.0	51.1	35.0	34.7
Flot 2	61.0	44.5	30.0	34.4
Flot 4	37.3	50.2	16.3	34.3
Flot 5	41.1	54.7	18.8	39.2
Flot 6	27.5	47.3	13.8	37.1

Figure 60 shows that higher grade and recovery are achieved with the process water obtained from the DPM plant than the synthetic process water or supernatant water. However, these performances are obtained only from the rougher floatation for comparative purposes. Therefore, expected recovery and grade were lower compared to the final grade and the recoveries for the precious metals at the plant. The high recovery and the grade in the first two trials could be due to the availability of residual flotation reagents in the process of water from the plant. At the same time, the other trials were conducted only with the newly added reagent. Several studies have discussed the favorable effect of residual reagents on flotation (Levay, 2001; Boujounoui, 2015). The lowest performance is shown by trial six, where  $\text{Ca}^{2+}$  concentration would be high due to the addition of  $\text{Ca}(\text{OH})_2$  as a coagulant. The result of early studies has shown the negative effect of  $\text{Ca}^{2+}$  and  $\text{Mg}^{2+}$  on flotation performance due to the precipitation of metal hydroxide on mineral surfaces. In contrast, some past studies have

discussed the positive effect of high metal ions concentration on froth stability(Bıçak et al, 2012).

According to the result shown in Figure 61, it can be observed that the results are relatively closed. But still, they have lower performance under optimum settling conditions. However, these trails were consisting of only a rougher flotation step due to the limitation of materials and time. Therefore, these results can not be directly related to the anticipated final grade and recovery at the plant. On the other hand, there were no real recovery and grade data for the rougher concentrate at the plant. Therefore, further flotation trails must be carried out following the actual plant flowsheet to be able to see the influence of newly tested optimal settling aids.

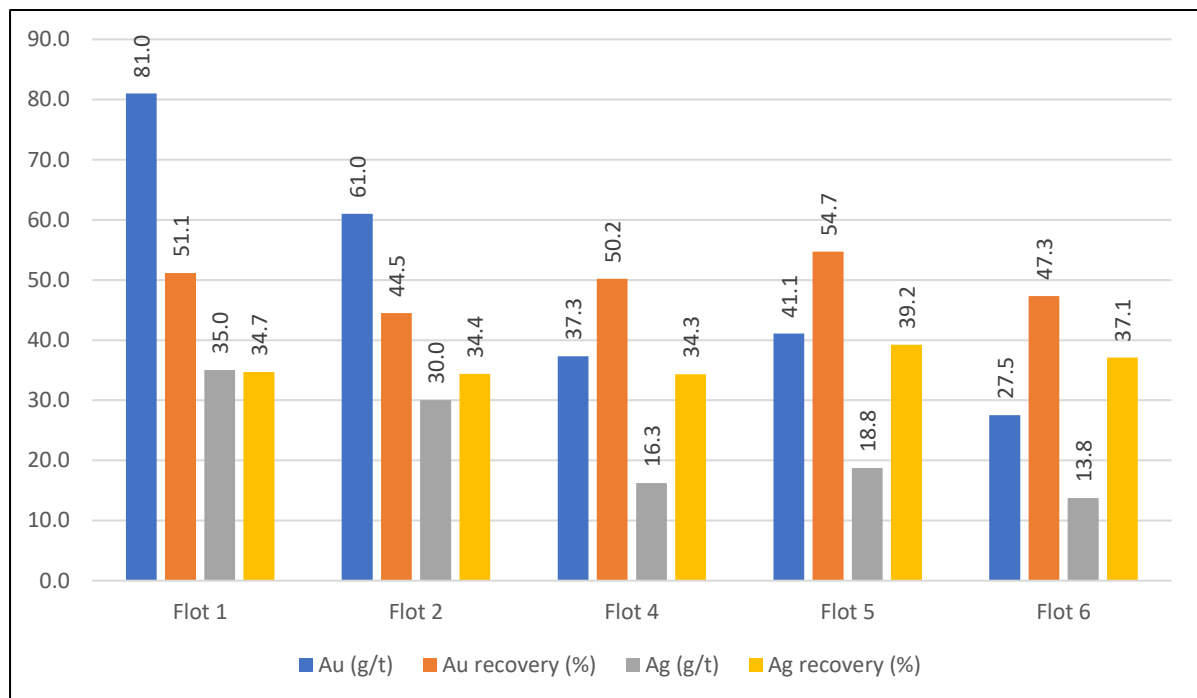


Figure 60: Grade recovery relationship for the precious metals in each flotation trial

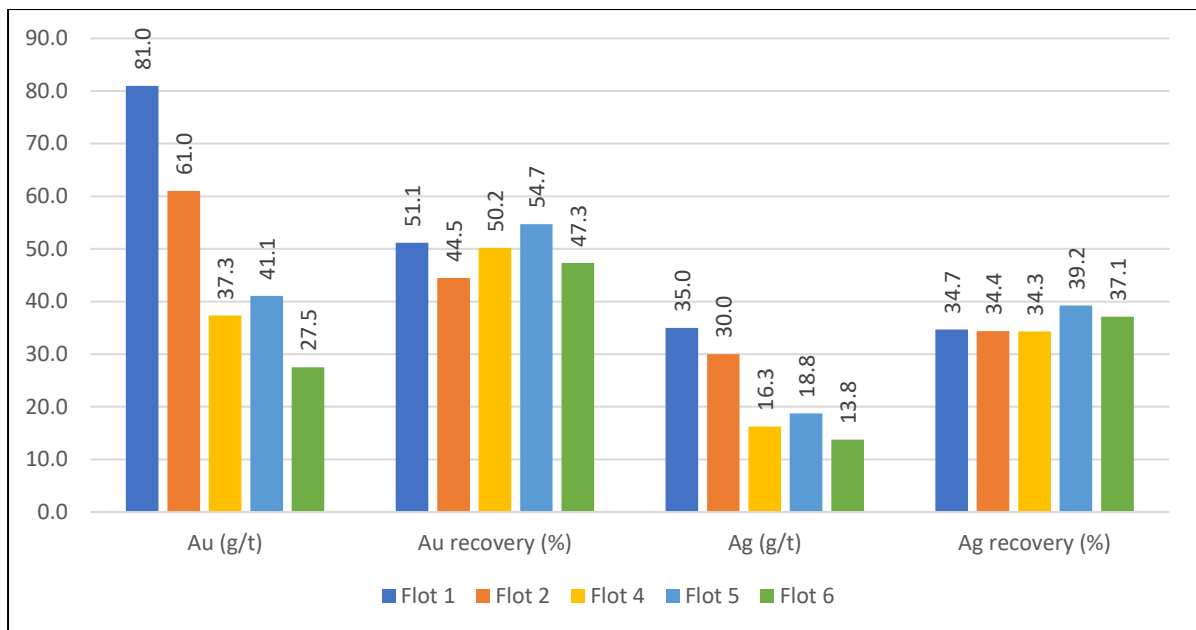


Figure 61: Comparison of grade and recovery of precious metals in five flotation trials.

## 5 Conclusions and recommendations

### 5.1 Conclusions

Based on the research objectives and the obtained results, the following conclusions could be made.

The mineralogical characterization results on the raw ore and -20 $\mu\text{m}$  fine fraction shows that the quartz, orthoclase, Fe-oxide, and kaolinite are the minerals that would introduce a significant number of fine particles to the tailing. This will adversely affect the efficiency of solid-liquid separation. On the other hand, some gold grains were associated with the quartz grains in the tailings and most of the gold grains in the concentrate are associated with gangue minerals. This could result in a reduction of recovery and grade of precious metals in the plant. In addition, the size of gold particles in the tail is approximately 15  $\mu\text{m}$  and the particle size of associated minerals are over 100  $\mu\text{m}$ , which is not a favorable size for floating. Therefore, finer grinding is required at SAG mill to avoid losing the precious metals. The gold particles in the concentrate are moderately liberated and most of the particles are associated with quartz particles which are roughly 15  $\mu\text{m}$ . Hence, a finer grinding at the VertiMill<sup>TM</sup> would also increase the grade of precious metals in the concentrate. In opposite, finer grinding would reduce the efficiency of the solid-liquid separation due to the high percentage of fine solids. Therefore, it can be suggested that the finer grinding and the use of optimal settling aids in a thickener can be both addressed at the same time.

The effect of the combination of metal salt and PAM on solid-liquid separation was investigated. The results suggested that the combination of  $\text{Ca}(\text{OH})_2$  and PAM than using single PAM could improve the clarity of the process water and the initial settling rate of sedimented bed. Also, the results show that the required dosage of PAM is relatively low (24 mg/l) when it uses in combination with  $\text{Ca}(\text{OH})_2$  than only PAM (32mg/l). This indicates that the polymer with high molecular weight is the primary characteristic that controls the settling rate, bed consolidation, and supernatant clarity. Having a faster initial settling rate does not always provide a faster consolidation of the sedimented bed.

In contrast, tailing with poor sedimentation could achieve better consolidation. Furthermore, results indicate that there is a direct influence of the pH on coagulation and flocculation and the efficiency of sedimentation is relatively high within the pH of 5.25-6. In this context, it should be noted that the pH in actual tailing at the plant is about 7.9.

The flotation result indicated that the recovery and grade are relatively lower with recycled water from a thickener water simulator. The lowest grade and recovery are obtained with water that is recovered with optimal dosages and reagent (PAM+  $\text{Ca}(\text{OH})_2$ ) obtained by the jar test. There are different roles of residual reagents dissolved in recycling water that affects on flotation. Some studies have shown that process water with an increased concentration of electrolyte results in better frothing ability. Calcium, copper, and sulfate ions have been found to enhance the adsorption of depressant onto gangue, improving the concentrate grade than other ions. Therefore, the expected result was to have a high grade by adding additional  $\text{Ca}^{2+}$ .

On the other hand, having a higher concentration of  $\text{Ca}^{2+}$  can also precipitate the metal hydroxide on the valuable minerals, thus depressing the minerals. Hence, the possible reason to get a low grade and recovery could be due to the precipitation effect. However, finer grinding and addition of raw water to dilute the concentration of impurity ions would improve the flotation performance by depressing more gangue minerals than the valuable minerals.

It should be noted that the lab-scale flotation test was realized only at a rougher stage due to the limitation of material and time, even though the flotation flowsheet of the plant consists of two cleaner stages and a cleaner scavenger stage. Therefore, the comparison of flotation result with actual plant data is not practical and simulation of the entire plant scheme must be carried out at the lab scale in a future project to outline practically relevant effects.

## 5.2 Recommendation for future work

Considering the past studies and all the outcomes of this project, several recommendations and suggestions can be provided for future works.

- Investigate the use of cationic polyelectrolyte than the anionic (PAM) one, which is currently being used in the plant since it could be more effective in both coagulation and flocculation than the use of metal salt only as a coagulant.
- Investigate an additional parameter such as mixing speed, mixing time, the zeta potential of the particle, and temperature on sedimentation efficiency.
- Investigate the possibility of a reduction of P80 to achieve better liberation by changing the milling parameters.
- Conduct a detailed study about the consolidation behavior of the tailing, with optimal coagulation and flocculation condition. There are several consolidation tests such as seepage induced test, relaxation test, continuous loading test, and constant rate of loading test, which could be envisaged in this context.

## 6 EIT Chapter

### 6.1 Environmentally sustainable mining: The case of integrated mine waste facility (IMWF)

Mining wastes, particularly in the form of waste rocks and tailings, can have major social and environmental impacts. There is a need for comprehensive long-term strategies for transforming the mining industry to move toward zero environmental footprints (Tayebi-Khorami, Edraki, Corder, and Golev, 2019). “How can the mining industry create new economic value, minimize its social and environmental impacts, and diminish liability from mining waste?” This would require cross-disciplinary skills, across the social, environmental, technical, legal, regulatory, and economic domains, to produce innovative solutions (Tayebi-Khorami, Edraki, Corder, & Golev, 2019). This chapter aims to explain current waste management frameworks and highlights the benefits of having an Integrated Mine Waste Facility (IMWF) at DMP Krumovgrad in social, environmental, and economic domains.

#### 6.1.1 Process and life cycle of the IMWF

The concept of the IMWF is to place thickened tailings into cells constructed from mine rock. The mined rock provides the strength required for overall stability and also internal drainage. Water reporting to the underdrain is pumped to the Raw and Process Water Reservoir (“RPWR”) located southwest of the open pit. The IMWF was constructed within two small valleys, being operated as two separate facilities early in the life of the project and later merging into a single facility as operations progress. Rehabilitation of the lower slopes of the IMWF is an ongoing process that started from the early stages of mining operations (AMEC Earth & Environmental UK Ltd, 2014).

The IMWF structures required for commencement of mining operations was constructed from the soil and rock excavated to create the platform for the process plant and the roads on the mine site. Once the mining operation started, the mine rock was trucked from the open pit to the IMWF, dumped, and spread to construct containment cells for the tailing. Tailings were thickened in the tailings thickening plant to the maximum practical amount and then conveyed by pump and pipeline to the containment cells. The IMWF is a fully drained facility and will not contain a water pond at any time during its operation. A system of under-drains is constructed along the axis of each small surface water channel in the footprint of the IMWF, and these drains will discharge to one of two sumps located at the toe of the facility.

It is estimated that 15.1 million tonnes of mined rock and 6.2 million tonnes of tailings will be stored within the IMWF over eight years during the life of the mine (AMEC Earth & Environmental UK Ltd, 2014).

#### 6.1.2 The social and environmental benefit of IMWF

The Project site and adjacent land are underlain by Palaeogene rocks that contain no significant aquifers. Local communities draw groundwater from shallow wells, the town of Krumovgrad sources its water from the Krumovitsa valley alluvial aquifer about 3km from Ada Tepe. Mining at Ada Tepe and abstraction of water for the project will have no significant impact on groundwater resources. The proposed mitigation measures, especially regarding watermanagement generally and management of wastes, in particular, are forecast to prevent groundwater contamination in the short and long term (post-closure).

A dual reservoir system has been developed, which has resulted in the mine being able to adopt a zero-discharge water management strategy. The two reservoirs are the RPWR and the Storm Water Overflow Reservoir (SWOR). These two reservoirs are adjacent to each other and have different functions about water management, these being the management of process water and storage of stormwater and pit inflows.

he Project presents a potential source of contamination of surface water and disturbance of surface water flows. The design of the Project mitigates against surface water impact using the following strategies:

- Thickening of the tailings before discharge to the IMWF and recycling of the supernatant water, which will reduce evaporation losses (compared to deposition of tailings in a TMF).
- Recycling of the mine and IMWF drainage waters back into the process.
- Adoption of a project water supply scheme that maximizes the use of recycling water and draws fresh water from the site area inflow.
- Maximizing recycling and minimizing environmental discharge towards “zero discharge”.
- Proposed Adoption of an environmental management plan that includes procedures for spill avoidance, containment, and treatment as well as various housekeeping measures that are regarded as international best practice.



- Progressive closure and rehabilitation of IMWF will protect erosion of the slopes and will reduce suspended solids in rainwater.

It is forecasted that the proposed mitigation will enable the Project to be constructed, operated, and closed without a significant impact on surface water flows and quality. As an example, other users of the surface water (including communities, businesses, and wildlife) will not be significantly affected. This forecast is based on assessment under normal and extreme (flood) events. The proposed closure strategy will include reinstatement of a permanent surface drainage system, including the closure of the Integrated Mine Waste facility and a pit lake in the final mine void.

#### 6.1.3 Contribution to the circular economy

Starting from the design phase of a mining site, the IMWF emphasizes the concept that effective design will reduce the generation of extractive waste, encourage its recovery, and minimize short- and long-term liabilities. Indeed, the ultimate goal would be to ensure that, where possible, a closed site can be left without the need for on-going monitoring. Therefore, keeping regular records of all the quantities and composition of extractive wastes generated at a site will aid decision-making on its fate and ensure its optimal management of mining waste.

Using the extracted waste rock as construction minerals – as far as it is technically feasible and environmentally sound – leads to less extractive waste being generated and offsets the primary production of construction minerals elsewhere.

#### 6.1.4 SWOT analysis of Ada Tepe project

The main goal of SWOT analysis is to evaluate the strengths and weaknesses, external opportunities, and threats for the organization or process. It allows defining internal resources and capabilities as well as market opportunities by evaluating the industry environment (T.Sammut-Bonnici and D. Galea, , 2015). This part summarizes the identified strengths and weaknesses, as well as the existing advantages and potential threats to the DPM Ada Tepe project based on the developed SWOT analysis on the state and development of the Bulgarian mining sector.

##### Strength

- DMP Krumovgrad mine is located in an environment rich in biodiversity with a low level of air, water, and soil pollution. The area stands out for having a vast ecologically clean land area and a large number of potential deposits.
- Great potential for finding new mineral deposits ( Au and Ag) and a large number of clean areas for exploration works.
- It has an already established infrastructure and processing plant for gold extraction.
- Well-developed environmental monitoring system, the regulatory framework established, and programs adopted for the implementation of environmental policies.
- The project is directly related to the political and financial stability of Bulgaria.

##### Weakness

- High transportation costs due to limited access and remote location.
- A significant part of the area belongs to Natura 2000, which creates limitations and requires additional procedures.
- Unsolved waste-related problems.
- Create risk ( deterioration of working environment parameters, negative social effect, visual impact on the surrounding landscape to their re-cultivation), which can be managed by achieving the quality of the environment, and working conditions.

##### Opportunities

- Constantly growing global and national consumption of raw materials and energy.
- High demand for precious metals in the market.
- Development of non-traditional raw materials.
- The rapid development of production technologies, mining, and processing equipment

- Development of equipment and technologies, creating opportunities for ecological and healthy production.
- Public attributes to support efforts to protect the environment.
- Effective collection and recycling of the waste throughout the technological chain of processing of metals.

#### Treats

- The global climate is change and fall of the country into the drought zone.
- The high costs of implementing European environmental legislation.
- Ineffective communications with a potential investor who has expressed interest in search and research.
- Ineffective dialogue on discussion with non-governmental environmental organizations.
- High market risk, especially for exchange products due to cyclical periods at a lower and higher price with large amplitudes.
- Significant investment in environmental protection and reclamation.

## 6.2 An economical benefit analysis

Highly efficient dewatering and thickening of the whole tailing with ultrafine particles are one of the most important processes for the preparation of IMWF, which will benefit the mine operation in both environmentally and economically. The objective of this chapter is to make a rough estimation of the benefit of using optimal conditions in DPM's plant. The comparison of daily operation costs between the current method and new method considering only a reagent cost. The estimated result is presented in Table 8 below. Current prices are obtained from [www.kemcore.com](http://www.kemcore.com) and [www.alibaba.com](http://www.alibaba.com).

Table 8: Daily operational cost comparison between two methods.

Method	Chemical reagent	Quantity (t/d)	Price (USD/t)	Total (USD)
Original method	PAM	0.28	2500	700
	Total (USD)			700
New method	PAM	0.2	2500	500
	Ca(OH) <sub>2</sub>	6.2	17	105.4
	Total (USD)			605.4

Daily operational costs for the current method is roughly 700 USD and 605 USD for the new method. Therefore considering the efficiency and the economy, the new process is more efficient and reduces the daily cost for the chemical at the plant by approximately 95 USD.

## 7 Bibliography

- L. Little et al. (2016). Using mineralogical and particle shape analysis to investigate enhanced mineral liberation through phase boundary fracture. *Powder Technology*, 794-804.
- A. Mierczynska-Vasilev, M.Kor, and J. Addai-Mensah. (2013). The influence of polymer chemistry on adsorption and flocculation of talc suspensions. *Chemical Engineering Journal* 220, 375-382.
- Allan Costine, J. C. (2018). Variations in the molecular weight response of anionic polyacrylamides under different flocculation conditions. *Chemical Engineering Science* 176, 127-138.
- AMEC Earth & Environmental UK Ltd. (2014). *Evaluation of Liner Requirement – Integrated Mine Waste Facility Dundee Precious Metals Krumovgrad Ada Tepe Gold Project, Bulgaria*.
- American Water Works Association. (2011). *Operational Control of Coagulation and Filtration Processes*. American Water Work Association .
- B. Ndlovu, S. Farrokhpay, and E. Forbes,. (2015). Characterisation of Kaolinite Colloidal and Flow Behaviour Via Crystallinity Measurements. *Powder Technology*, 269, 505–512.
- B. Wills and Napier-Munn. (2006). *Will's Mineral Processing Technology*. Elsevier Science & Technology Books.
- Besra, Sengupta, and Roy. (2000). Particle characteristics and their influence on dewatering of kaolin, calcite and quartz suspensions. *International Journal of Mineral Processing*, 89-112.
- Bıçak et al. (2012). The effect of water chemistry on froth stability and surface chemistry of the flotation of a Cu-Zn sulfide ore. *International Journal of Mineral Processing*, 32-37.
- Boujounoui, A. B. (2015). The influence of water quality on the flotation performance of complex sulphide ores: Case study at Hajar Mine, Morocco. *Journal of the Southern African Institute of Mining and Metallurgy*, 1243-1251.
- C. Wang, D. Harbottle, Q Liu et al. (2014). Current state of fine mineral tailings treatment: A critical review on theory and practice. *Minerals Engineering* 58, 113-131.
- Corin & Manono. (2020). Considering the Impact of Water Quality on Flotation Response. *Corin*, 18-22.
- D. Liu, M. Edraki, P. Fawell, and L. Berry. (2020). Improved water recovery: A review of clay-rich tailings and saline water interactions. *Powder Technology* 364, 604-621.
- D.Fornasiero, and J. Ralston,. (2006). Effect of surface oxide/hydroxide products on the collectorless flotation of copper-activated sphalerite. *International Journal of Mineral Processing*, vol.78., 231–237.
- Dunne, R. (2005). Flotation of gold and gold bearing ores. *Development of Mineral Processing*, 309-344.
- European Commission. (2020, May 01). *Extractive Waste*. Retrieved from European Commission: <https://ec.europa.eu/environment/waste/mining/index.htm>
- F. Miu, Q. Zhao, and L. Lui,. (2013). Experimental Study on the Electrokinetics of Kaolinite Particles in Aqueous Suspension. *Physicochemical Problems of Mineral Processing*, 49, 659–672.

- Fernando and Carvalho. (2017). Mining industry and sustainable development: Time for change. *Food and energy security*, 61-77.
- Gregory, J. (2013). Flocculation Fundamental. London: Department of Civil, Environment & Geomatic Engineering, University College London.
- H. Garrick, F.Stewart, Hayes, et al. (2016). *Adaptive, integrated water management designs and probabilistic modelling for mine waste facility closure and restoration*. Perth: Australian Centre for Geomechanics.
- J. Mohammed, and E. Shakir. (2018). Effect of settling time, velocity gradient, and camp number on turbidity removal for oilfield produced water. *Egyptian Journal of Petroleum*, 31-36.
- Jeongsook Kim, L. K. (1998). Investigation of Coagulation mechanism with Fe(III) Salt Using Jar Tests Flocculation Dynamics. *Korean Society of Environmental Engineering, Vol 3* , 11-19.
- Ji, Lu, Liu et al. (2013). Effect of solution salinity on settling of mineral tailings by polymer flocculants. *Colloids and Surfaces A: Physicochemical and Engineering Aspects*, 29-38.
- Levay, G. S. (2001). The impact of water quality on performance . *Journal of the Southern African Institute of Mining and Metallurgy*, 101, 69-75.
- M. Deng, Q. Liu, and Z. Xu , . (2013). Impact of gypsum supersaturated water on the uptake of copper and xanthate on sphalerite. *Minerals Engineering vol.49*, 165-171.
- M. Grigorova, and I. Koprev. ( 2020). MINING AND TECHNICAL CONDITIONS IN OPEN PIT “KHAN KRUM” GOLD MINE IN SOUTHEASTERN BULGARIA. *International Scientific Conference GEOBALCANICA*.
- Muzenda, and Edison. (2010). An Investigation into the Effect of Water Quality on Flotation Performance. *World Academy of Science, Engineering and Technology*.
- N. Moss, and B. Dymond,. (1978). . Flocculation: theory and application. *Mine and Quarry Journal* 5, 1-8.
- Önel, Gocer, and Taner. (2018). EFFECT OF COAGULANTS AND FLOCCULANTS ON DEWATERING OF KAOLIN SUSPENSIONS. *Ömer Halisdemir Üniversitesi Mühendislik Bilimleri Dergisi*, 297-305.
- Outotec. (2017). *Description of 20m paste thickener*. Outotec.
- P. Marchev, B.Singer, S. Hasson , and R. Mortiz. (2004). The Ada Tepe deposit: A sediment-hosted, detachment fault-controlled, low-sulfidation gold deposit in the Eastern Rhodopes, SE Bulgaria. *Schweizerische Mineralogische und Petrographische Mitteilungen*, 59-78.
- P. Mpofu, J. A.-M. (2003). Influence of hydrolyzable metal ions on the interfacial chemistry, particle interactions, and dewatering behavior of kaolinite. *Colloid Interface Science*. 261 , 349-359.
- P. Mukheled and D. Al-Sameraiy,. (2017). A new pproach using coagulation rate constant for evaluation of turbidity removal. *Applied Water Science*, 1439-1448.
- Prestidge, C. S. (1997). Copper (II) activation and cyanide deactivation of zinc sulphide under mildly alkaline conditions vol.108. *Applied Surface Science*,, 333-344.
- Reichl et al. (2016). World Mining Data. *In Minerals Production; International Organizing Committee for the World Mining Congresses*.

- S. Ahmed, and S. Siddiqua. (2014). A review on consolidation behavior of tailings. *International Journal of Geotechnical Engineering*, 102-111.
- S. Williams, and J. Phelan,. (1985). Process development at Woodlawn Mines,” in *Complex Sulphides. the AIME*, 293-304.
- Saari, Jansson, and Musuku. (2020). *The effect of plant process water quality on the flotation of sulphide ore*. Outotec (Finland) Oy, Boliden Kevitsa Mining Oy.
- Sharma, D. a. (2006). Flocculants - An ecofriendly approach. *Journal of Polymers and the Environment*, 195-202.
- Soares, L. B. (2015). The Influence of Tailings Composition on Flocculation. *THE CANADIAN JOURNAL OF CHEMICAL ENGINEERING*.
- T.Sammut-Bonnici and D. Galea, . (2015). SWOT Analysis. *Wiley Encyclopedia of Management*, 1-8. doi:10.1002/9781118785317.weom120103
- T.Tadros. (2011). Interparticle interactions in concentrated suspensions and their bulk (rheological) properties. . *Advance Colloid Interface Science*. 168, 263–277.
- Tayebi-Khorami, M., Edraki, M., Corder, G., & Golev, A. (2019). Re-Thinking Mining Waste through an Integrative Approach Led by Circular Economy Aspirations. *Minerals* 9, , 286.
- White,Bennett,Meik, & Corrigan. (2014). *Dundee Precious Metals Inc- Revised NI 43-101 Technical Report- Ada Tepe Deposit, Krumovgrad project, Bulagaria*. CSA Global (UK) Ltd.
- X. Kang, Z. Xia, R.Chen, H.Sun, and W. Yang. (2019). Effects of inorganic ions, organic polymers, and fly ashes on the sedimentation characteristics of kaolinite suspensions. *Applied Clay Science* 181.
- Yin Zhi-gang, Sultan Ahmed, Sun Wei, Hu Yue-hua, Zhai Ji-hua and Gao Yue-sheng. (2018). Flocculation of flotation tailings in presence of silicate gel and polymer. *Journal of Central South University*, 1928-1937.

## 8 Appendices

### 8.1 Appendix 1: Optimization of settling aids

Table 9: Jar test result using PAM as a flocculant

<b>PAM (mg/l)</b>	<b>20</b>	<b>24</b>	<b>28</b>	<b>32</b>	<b>36</b>	<b>40</b>
<b>Turbidity (FAU)</b>						
<b>10 min</b>	86	44	33	22	26	28
<b>20 min</b>	75	35	24	19	22	25
<b>pH</b>	7.91	7.89	7.91	7.91	8.01	8.2

Table 10: Jar test result using FeSO<sub>4</sub> as a coagulant

<b>FeSO mg/L</b>	<b>0</b>	<b>20</b>	<b>40</b>	<b>60</b>	<b>80</b>	<b>100</b>	<b>120</b>	<b>140</b>	<b>160</b>	<b>180</b>	<b>200</b>	<b>220</b>
<b>Turbidity (FAU)</b>												
<b>10 minutes</b>	265	250	207	127	210	200	181	132	79	80	84	100
<b>20 minutes</b>	223	134	124	120	162	117	93	83	77	80	69	69
<b>pH</b>	7.92	7.9	7.73	7.52	7.52	7.21	7.11	6.93	6.9	6.93	6.93	6.9

Table 11: Jar test result using Al<sub>2</sub>(SO<sub>4</sub>)<sub>3</sub> as a coagulant

<b>Al<sub>2</sub>(SO<sub>4</sub>)<sub>3</sub> mg/l</b>	<b>0</b>	<b>20</b>	<b>40</b>	<b>60</b>	<b>80</b>	<b>100</b>	<b>120</b>	<b>140</b>	<b>160</b>	<b>180</b>	<b>200</b>	<b>220</b>	<b>240</b>	<b>260</b>
<b>Turbidity (FAU)</b>														
<b>10 minutes</b>	163	153	143	102	120	127	79	68	69	56	41	49	49	53
<b>20 minutes</b>	136	65	65	56	61	95	79	65	68	56	27	33	28	32
<b>pH</b>	7.91	7.91	7.9	7.87	7.79	7.73	7.69	7.62	7.62	7.61	7.56	7.48	7.33	7.13

Table 12: Jar test result Using FeCl<sub>3</sub> as a coagulant

<b>Dosage mg/L</b>	<b>100</b>	<b>120</b>	<b>140</b>	<b>160</b>	<b>180</b>	<b>200</b>	<b>220</b>
<b>Turbidity</b>							
<b>10 minutes</b>	180	167	152	117	99	125	133
<b>20 minutes</b>	136	125	113	110	87	79	83
<b>pH</b>	7.58	7.49	7.13	6.9	6.67	6.63	6.63

Table 13: Jar test result using combination of PAM and Al<sub>2</sub>(SO<sub>4</sub>)<sub>3</sub>

<b>PAM (mg/l)</b>	<b>20</b>	<b>20</b>	<b>20</b>	<b>20</b>	<b>24</b>	<b>24</b>	<b>24</b>	<b>24</b>	<b>28</b>	<b>28</b>	<b>28</b>	<b>28</b>
<b>Al<sub>2</sub>(SO<sub>4</sub>)<sub>3</sub></b>	<b>0</b>	<b>160</b>	<b>180</b>	<b>200</b>	<b>0</b>	<b>160</b>	<b>180</b>	<b>200</b>	<b>0</b>	<b>160</b>	<b>180</b>	<b>200</b>
<b>Turbidity (FAU)</b>	93	73	66	83	51	50	33	45	38	31	25	33
<b>pH</b>	7.91	7.65	7.63	7.63	7.9	7.68	7.65	7.61	7.91	7.65	7.63	7.61



Table 14: Jar test result using combination of PAM and FeSO<sub>4</sub>

PAM (mg/l)	20	20	20	20	24	24	24	24	28	28	28	28
FeSO <sub>4</sub>	0	140	160	180	0	140	160	180	0	140	160	180
Turbidity (FAU)	95	78	71	80	55	50	33	42	37	30	20	45
pH	7.91	7.01	6.99	9.93	7.9	7.13	6.93	6.91	7.89	7.01	6.99	6.91

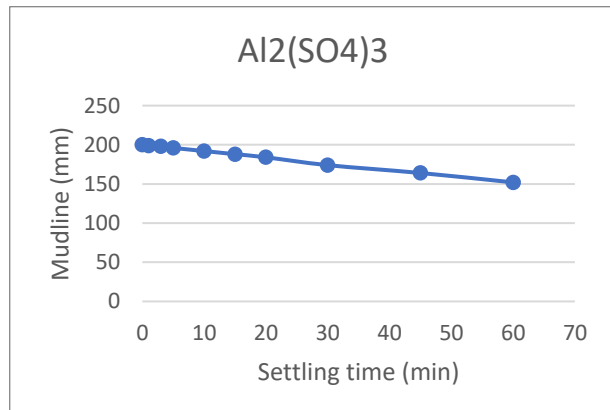
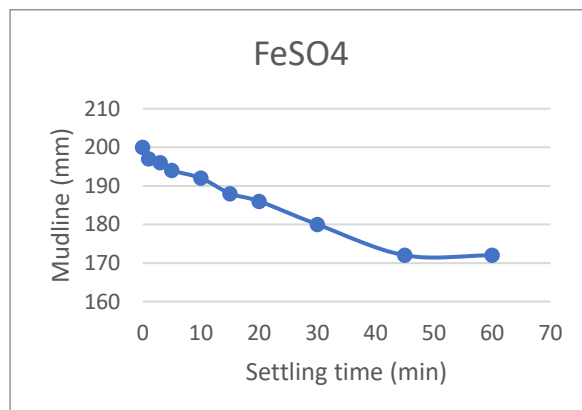
Table 15: Jar test result using combination of PAM and Ca(OH)<sub>2</sub>

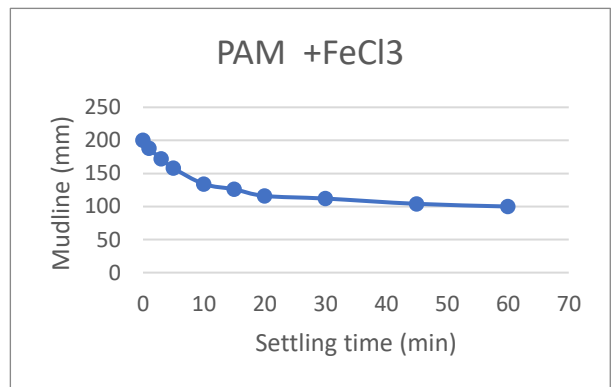
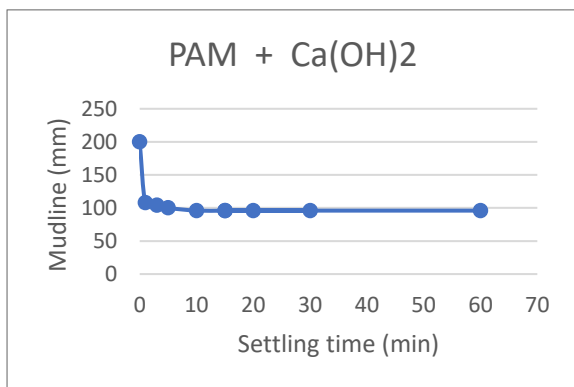
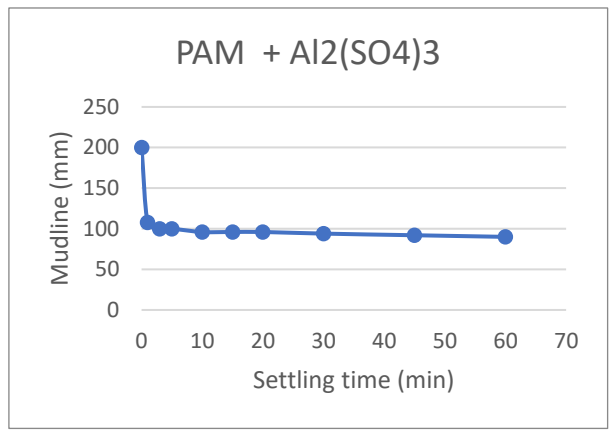
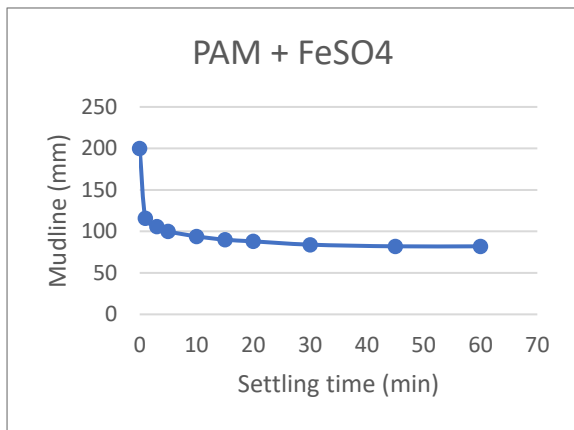
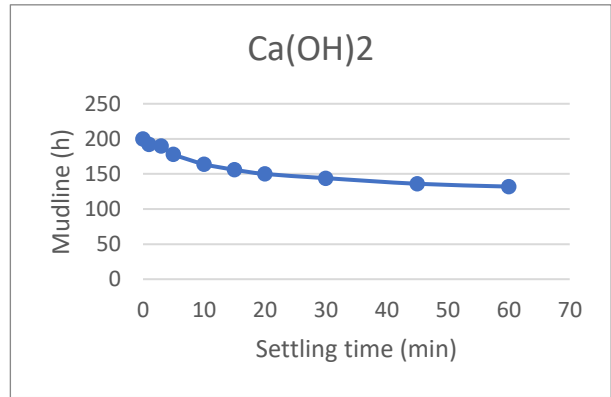
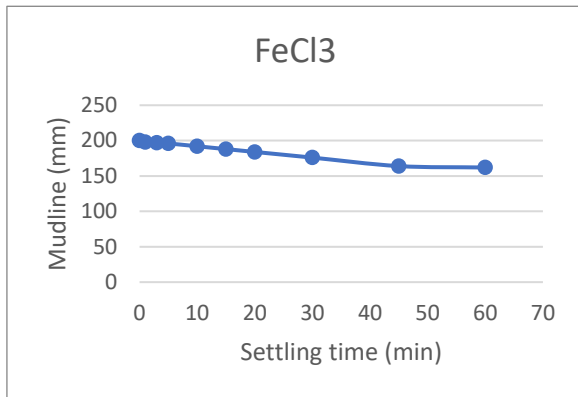
PAM (mg/l)	20	20	20	20	24	24	24	24	28	28	28	28
Ca (OH) <sub>2</sub> mg/l	0	500	750	1000	0	500	750	1000	0	500	750	1000
turbidity	98	28	17	18	83	26	14	17	63	54	20	15
pH	7.91	10.3	11.2	11.3	7.9	9.3	11.03	11.53	7.88	9.3	11.1	11.3

## 8.2 Appendix 2: Measurement of settling rate

Table 16: Mudline height measurement result

Mudline height (m)									
Time (h)	PAM	PAM+FeSO4	PAM+Al2(SO4)3	PAM+Ca(OH)2	PAM+FeCl3	FeSO4	Al2(SO4)3	FeCl3	Ca(OH)2
0.000	0.200	0.200	0.200	0.200	0.200	0.200	0.200	0.200	0.200
0.017	0.144	0.116	0.108	0.108	0.188	0.197	0.199	0.198	0.192
0.050	0.112	0.106	0.100	0.104	0.172	0.196	0.198	0.197	0.190
0.083	0.100	0.100	0.100	0.100	0.158	0.194	0.196	0.196	0.178
0.167	0.092	0.094	0.096	0.096	0.134	0.192	0.192	0.192	0.164
0.250	0.086	0.090	0.096	0.096	0.126	0.188	0.188	0.188	0.156
0.333	0.084	0.088	0.096	0.096	0.116	0.186	0.184	0.184	0.150
0.500	0.080	0.084	0.094	0.096	0.112	0.180	0.174	0.176	0.144
0.750	0.076	0.082	0.092	0.096	0.104	0.172	0.164	0.164	0.136
1.000	0.076	0.082	0.090	0.096	0.100	0.172	0.152	0.162	0.132





### 8.3 Appendix 3: pH optimization

Table 17: pH optimization result with PAM+  $\text{Ca(OH)}_2$

PAM+ $\text{Ca(OH)}_2$					
pH	Measurement at 10	Turbidity (NTU)	Measurement at 20	Turbidity (NTU)	
4.63	576.165	84.38	337.09	45.63	
4.92	264.575	33.87	173.195	19.06	
5.59	210.5	25.11	262.715	33.57	
6.17	205.78	24.34	171.87	18.85	
6.37	389.23	54.08	322.28	43.23	
6.71	699.96	104.45	578.24	84.72	

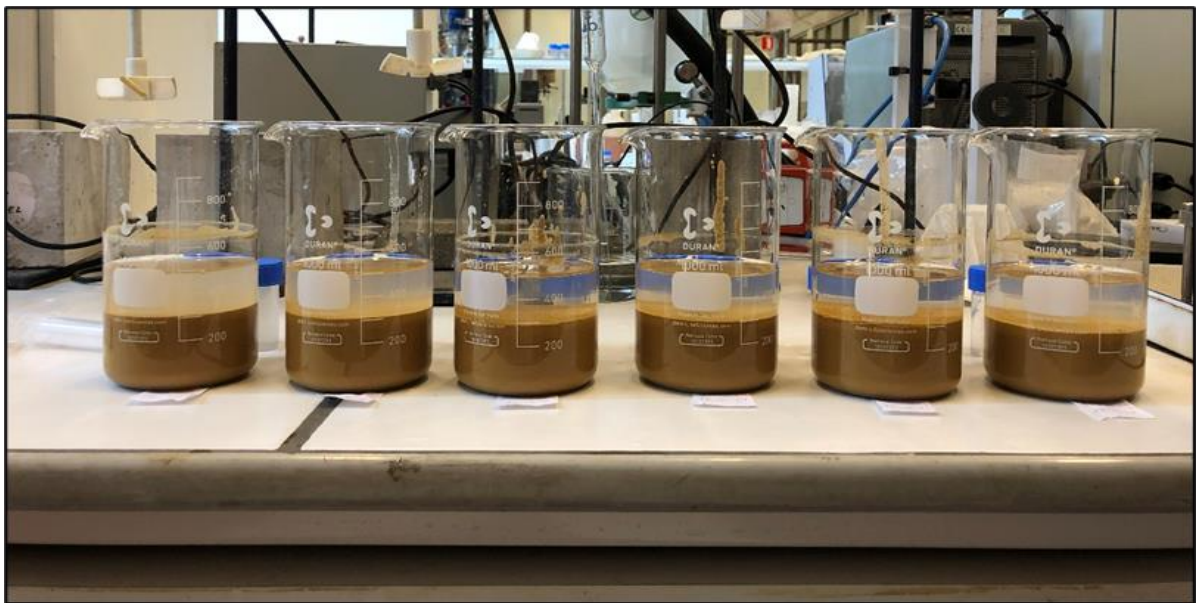


Figure 62: View of sedimented sludge after pH optimization with PAM+  $\text{Ca(OH)}_2$  at pH 4.63 , 4.92, 5.59, 6.17, 6.37 , 6.71 in order

Table 18:pH optimization result with PAM+ $\text{FeSO}_4$

PAM+ $\text{FeSO}_4$					
pH	Measurement at 10	Turbidity (NTU)	Measurement at 20	Turbidity (NTU)	
4.43	196.215	22.79	125.465	11.32	
4.99	196.99	22.92	156.68	16.38	
5.46	224.275	27.34	165.79	17.86	
5.91	251.375	31.73	176.62	19.62	
6.35	916.525	139.56	317.225	42.41	
6.86	393.68	54.80	287.455	37.58	

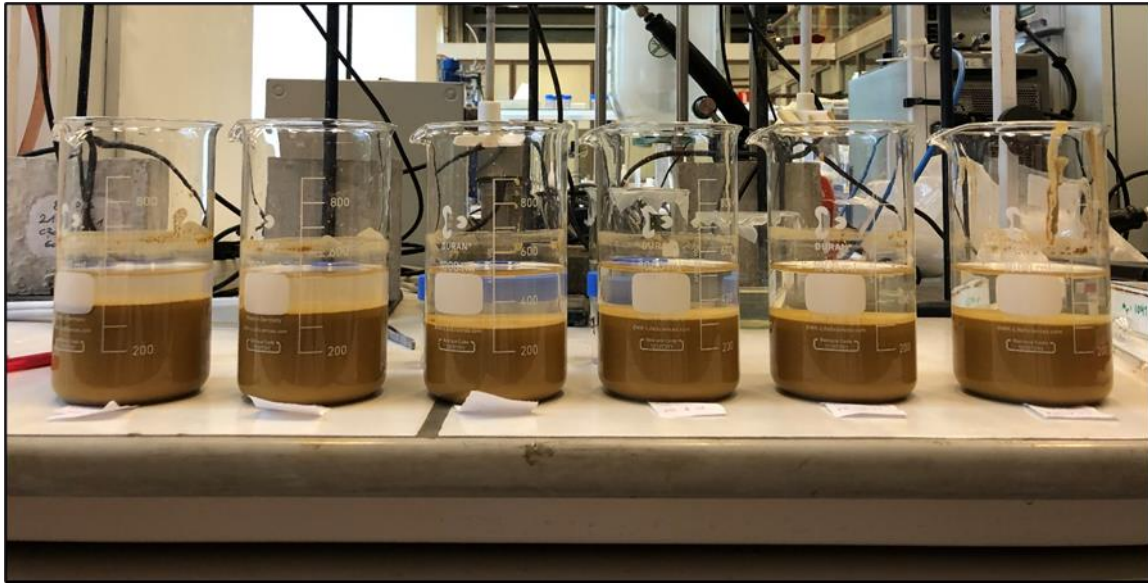


Figure 63: : View of sedimented sludge after pH optimization with PAM+ FeSO<sub>4</sub> at pH 4.43 , 4.99, 5.46, 5.91, 6.35 , 6.86 in order

Table 19: pH optimization result with PAM

pH	PAM			
	Measurement at 10	Turbidity (NTU)	Measurement at 20	Turbidity (NTU)
4.61	584.85	85.79	296.435	39.04
5.07	228.675	28.06	170.04	18.55
5.59	178.54	19.93	197.62	23.02
6.06	269.395	34.66	186.865	21.28
6.45	193.19	22.30	162.4	17.31
6.89	116.535	9.88	108.275	8.54

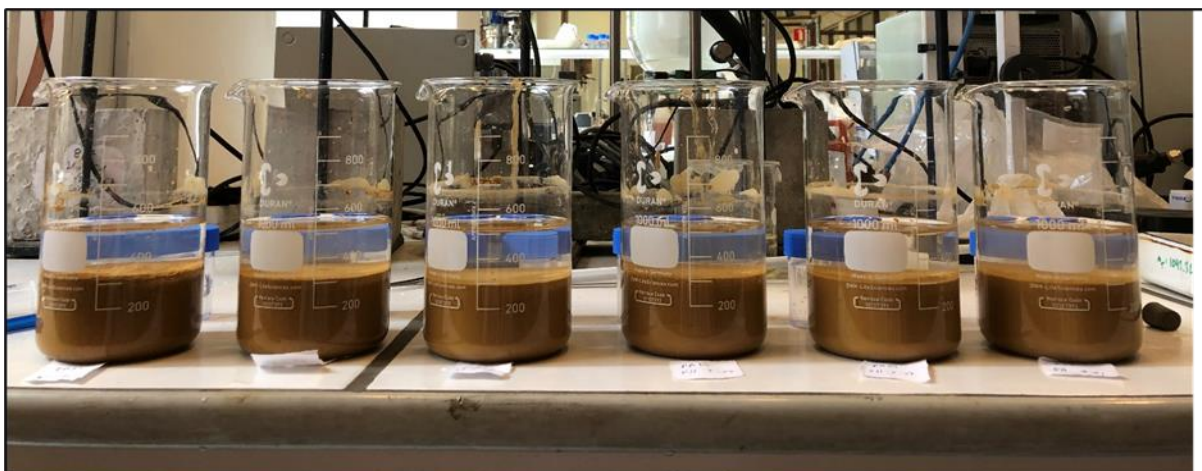


Figure 64: : View of sedimented sludge after pH optimization with PAM at pH 4.61 , 5.07, 5.59, 6.06, 6.45 , 6.89 in order

Table 20: pH optimization result with  $\text{FeSO}_4$

pH	FeSO <sub>4</sub>			
	Measurement at 10	Turbidity (NTU)	Measurement at 20	Turbidity (NTU)
4.67	306.135	40.61	271.085	34.93
4.91	353.01	48.21	332.125	44.82
5.47	281.905	36.68	336.235	45.49
5.97	311.95	41.55	326.325	43.88
6.61	326.82	43.96	389.415	54.11
7.15	458.5	65.31	481.555	69.05

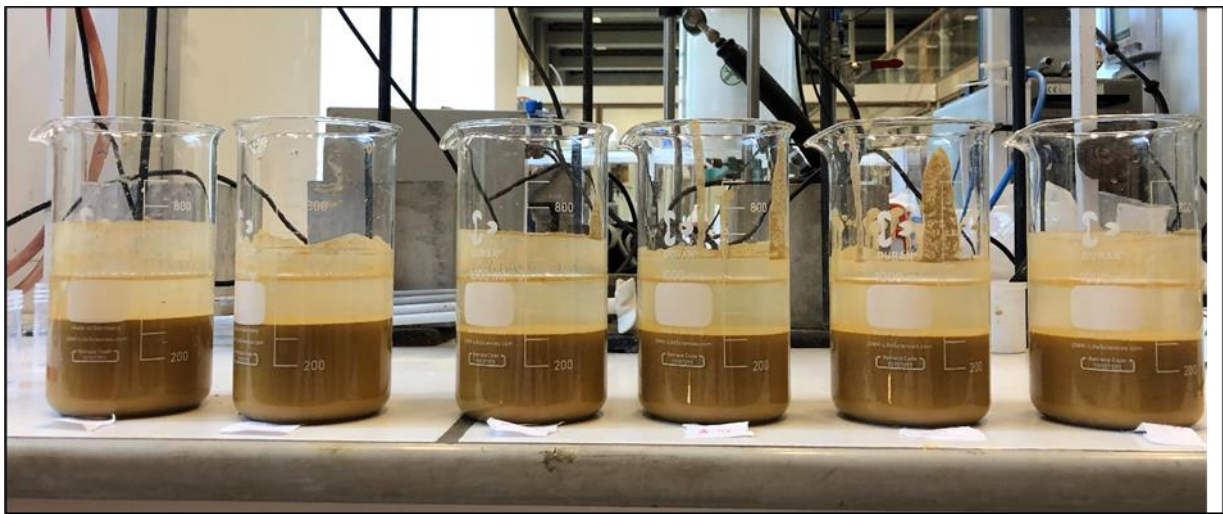


Figure 65: : View of sedimented sludge after pH optimization with  $\text{FeSO}_4$  at pH 4.67 , 4.91, 5.47, 5.97, 6.61 , 7.15 in order

Table 21: pH optimization result with  $\text{Al}_2(\text{SO}_4)_3$

pH	$\text{Al}_2(\text{SO}_4)_3$			
	Measurement at 10	Turbidity (NTU)	Measurement at 20	Turbidity (NTU)
4.45	267.74	34.39	201.545	23.66
5.07	207.835	24.68	178.38	19.90
5.45	224.945	27.45	182.79	20.62
6.01	254.02	32.16	181.405	20.39
6.61	281.92	36.69	197.66	23.03
7.15	361.57	49.60	290.38	38.06



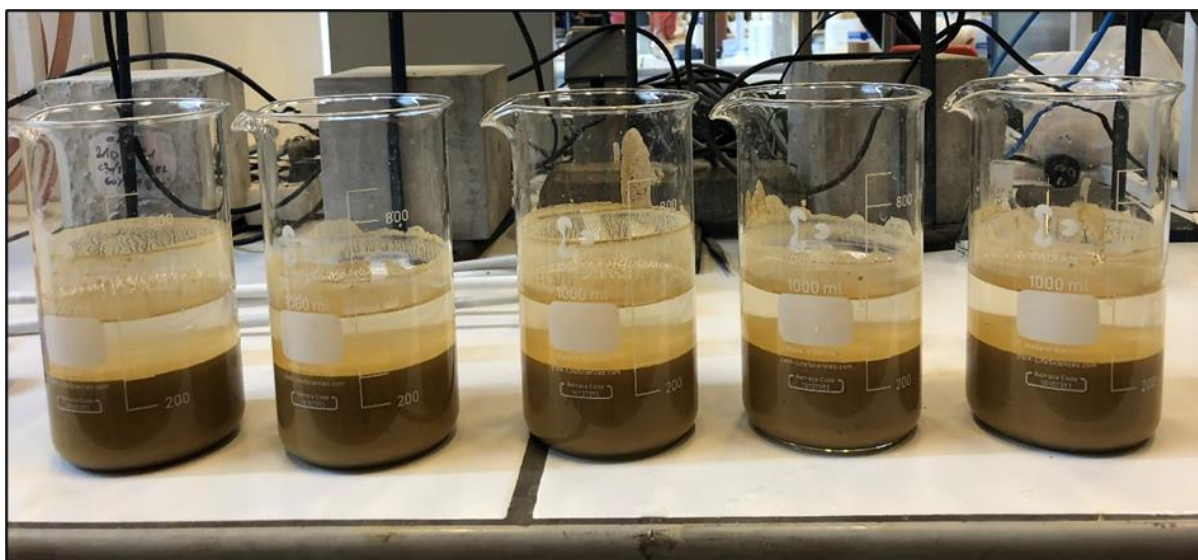


Figure 66: View of sedimented sludge after pH optimization with  $\text{Al}_2(\text{SO}_4)_3$  at pH 4.45 , 5.07, 5.45, 6.01, 6.61 , 7.15 in order

Table 22: pH optimization result with PAM+ $\text{Al}_2(\text{SO}_4)_3$

pH	PAM+ $\text{Al}_2(\text{SO}_4)_3$			
	Measurement at 10	Turbidity (NTU)	Measurement at 20	Turbidity (NTU)
4.69	159.075	16.77	100.775	7.32
5.12	204.725	24.17	156.845	16.41
5.59	105.375	8.07	94.63	6.33
5.83	128.395	11.80	121.845	10.74
6.51	261.64	33.40	246.24	30.90
7.01	143.545	14.26	106.48	8.25

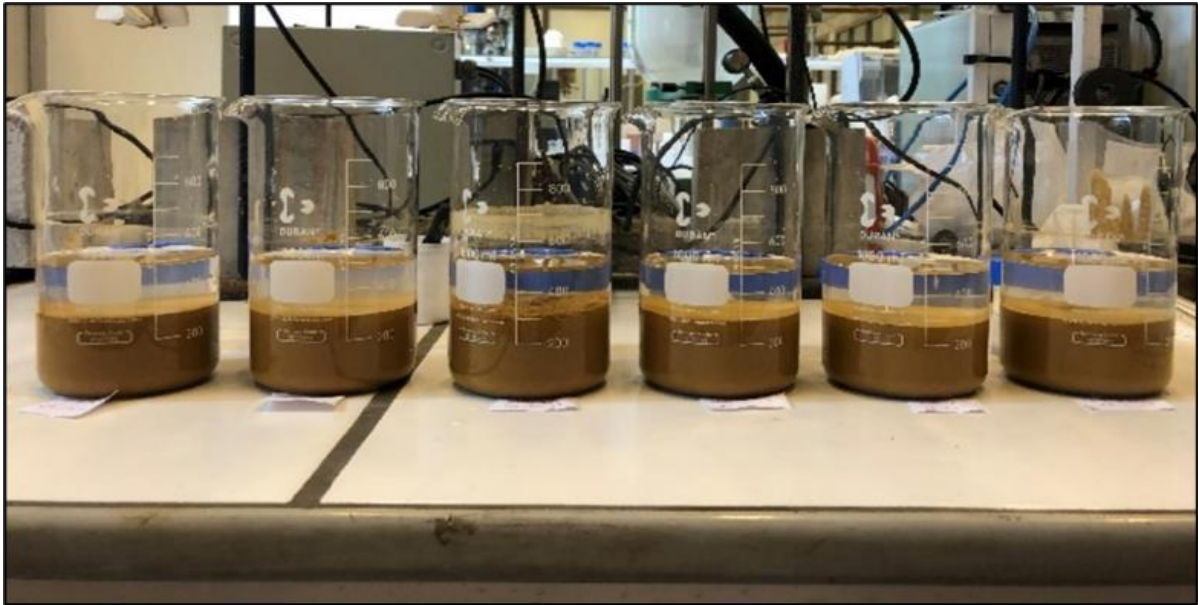


Figure 67: View of sedimented sludge after pH optimization with PAM+Al<sub>2</sub>(SO<sub>4</sub>)<sub>3</sub> at pH 4.69 , 5.12, 5.59, 5.83, 6.51 , 7.01 in order

## 8.4 Appendix 4: Flotation trial

Flotation test 1 with Process water								
Fraction	Mass (g)	Recalculated mass (g)	Au (g/t)	Au Mass (g)	Au recovery %	Ag (g/t)	Ag Mass (g)	Ag recovery %
Feed	1780.00	1701.75	4.21	0.0072	100.00	2.68	0.0046	100.00
concentrate	45.23	45.23	81.00	0.0037	51.14	35	0.0016	34.71
Tailing	1656.52	1656.52	2.11	0.0035	48.86	1.80	0.0030	65.29
Loss	78.25							
Error	4.40							

Flotation test 2 with Process water								
Fraction	Mass (g)	Recalculated mass (g)	Au (g/t)	Au Mass (g)	Au recovery %	Ag (g/t)	Ag Mass (g)	Ag recovery %
Feed	1780.00	1685.00	4.21	0.0071	100.00	2.68	0.0045	100.00
concentrate	51.75	51.75	61.00	0.0032	44.50	30	0.0016	34.38
Tailing	1633.25	1633.25	2.41	0.0039	55.50	1.81	0.0030	65.62
Loss	95.00							
Error	5.34							

Flotation test 3 with synthetic water								
Fraction	Mass (g)	Recalculated mass (g)	Au (g/t)	Au Mass (g)	Au recovery %	Ag (g/t)	Ag Mass (g)	Ag recovery %
Feed	1780.00	1666.53	4.21	0.0070	100.00	2.68	0.0045	100.00
concentrate	93.48	93.48	41.07	0.0038	54.72	18.75	0.0018	39.24
Tailing	1573.05	1573.05	2.02	0.0032	45.28	1.73	0.0027	60.76
Loss	113.47							
Error	6.37							

Flotation test 4 with synthetic water								
Fraction	Mass (g)	Recalculated mass (g)	Au (g/t)	Au Mass (g)	Au recovery %	Ag (g/t)	Ag Mass (g)	Ag recovery %
Feed	1780.00	1683.33	4.21	0.0071	100.00	2.68	0.0045	100.00
concentrate	95.28	95.28	37.33	0.0036	50.19	16.25	0.0015	34.32
Tailing	1588.05	1588.05	2.22	0.0035	49.81	1.87	0.0030	65.68
Loss	96.67							
Error	5.43							

Flotation test 6 with recycled water from test 3 & 4								
Fraction	Mass (g)	Recalculated mass (g)	Au (g/t)	Au Mass (g)	Au recovery %	Ag (g/t)	Ag Mass (g)	Ag recovery %
Feed	1780.00	1714.02	4.21	0.0072	100.00	2.68	0.0046	100.00
concentrate	124.02	124.02	27.53	0.0034	47.32	13.75	0.0017	37.12
Tailing	1590.00	1590.00	2.39	0.0038	52.68	1.82	0.0029	62.88
Loss	65.98							
Error	3.71							